Aqueous Two-Phase Systems for Next-Generation Biotechnological Assays

by

Joshua B. White

A dissertation submitted in partial fulfillment
of the requirements for the degree of
Doctor of Philosophy
(Biomedical Engineering)
in the University of Michigan
2013

Doctoral Committee:

Professor Shuichi Takayama, Chair
Associate Professor Paul J. Christensen
Assistant Professor Jeffrey C. Horowitz
Professor James B. Grotberg
Associate Professor Jan P. Stegemann

To my parents, Brad and Lynnda White, for continuously supporting my dreams, allowing me to fail, and always encouraging me to get back up. To my sister, Emily, for your never-ending love and unwavering belief in my abilities. To the rest of my family, friends, and colleagues, for your unbelievable support and incredible memories.

Acknowledgements

I would like to acknowledge my advisor, Professor Shuichi Takayama, for many valuable lessons that have helped me develop as a scientist, critical thinker, and dreamer. He has shown and inspired in me a great deal of enthusiasm for science with his big picture ideation, continual brainstorming, and encouragement to think outside the box. Thank you for allowing me the freedom to work in your lab, to continually experiment and pursue a variety of projects, and to pursue professional development outside of the lab.

I would like to thank the rest of my committee members, Jeff Horowitz, Paul Christensen, Jan Stegemann, and James Grotberg, who have each mentored me and encouraged me in different ways. Your collaboration and willingness to help develop me as a researcher and scientist have been invaluable and I thank you all for your unique insights and perspectives.

I would also like to recognize members of the Takayama lab and collaborators. It has been a privilege to work with such a dynamic group of people that continually impress me with their ingenuity and kindness: Arlyne Simon, John Frampton, David Lai, Sasha Cai Lesher-Perez, Byoung Choul Kim, Chris Moraes, Sung Jin Kim, Taisuke Kojima, Joe Labuz, Brendan Leung, Steve Cavnar, Madhuresh Sumit, Toshiki Matsuoka, Jason Kuo, Joong Yull Park, Hossein Tavana, Andreja Jovic, Bobak Mosadegh, Minsub Han, Amy Hsiao, Nick Douville, and Poorna Ramamurthy.

Finally, I would like to express my love and gratitude to my parents, Brad and Lynnda White, and my sister, Emily, who have constantly supported me and provided me with opportunities to achieve success.

Table of Contents

List of Figures

List of Tables

ABSTRACT

Aqueous Two-Phase Systems for Next-Generation Biotechnological Assays

by

Joshua B. White

Next-generation biotechnological assays, described here as those that increase throughput, improve upon physiological relevance, accomplish previously impossible biological and/or engineering tasks, or some combination thereof, will play increasingly crucial roles in the healthcare, biotechnology, and pharmaceutical industries in the next several decades. Unfortunately, although many of the recent technological innovations that have been achieved accomplish these goals, they are also commonly burdensome, technologically challenging, and perform highly niche tasks, thereby making them difficult and sometimes impossible to adopt into the healthcare, biotechnology, and pharmaceutical industries that would benefit most from them. This dissertation has four chapters, each of which describes the application of an aqueous two-phase system (ATPS) for next-generation biotechnological assays. The importance and relevance of these assays is discussed in the context of drug development in the pharmaceutical industry, where there has been decreasing return-on-investment despite the influx of billions of dollars in research and development. First, ATPS-immunocytochemistry was used to stain for multiple biomarkers from a single cell monolayer and do so more rapidly and with higher signal intensity than traditional cell staining. An ATPS of 5% polyethylene glycol (PEG) and 12.8% dextran (DEX) was then determined to be the optimal system with which to perform cell monoculture patterning for high-throughput screening analysis of cell migration and to perform co-culture patterning to achieve more physiologically relevant cell behavior that can be used as a toxicological and/or functional screening assay. ATPS was further used to create an assay that localizes trypsin to achieve reproducible and high-throughput *in vitro* wounding on transwell inserts. Finally, an ATPS-enzyme-linked immunosorbent assay (ELISA) was developed to pattern detection antibodies and quantify 4 biomarkers of graft-versus-host-disease without antibody cross-reactivity and with greater sensitivity compared to traditional ELISA. Such next-generation technologies will provide a launching point for the development of user-friendly, easily adoptable, and scalable assays that can be utilized by both basic science researchers and for-profit biotechnology industries to better characterize diseases and develop therapeutics.

Chapter 1

Introduction and Thesis Overview

1.1 Drug Discovery and the Pharmaceutical Industry

Since the 1990s, a decade when pharmaceutical companies experienced incredible success in the development of blockbuster drugs that translated into billions of dollars of revenue, there has been a significant decline in the creation of breakthrough medicines despite increasing investments in pharmaceutical research and development (R&D) (Munos, 2009). In fact, it was estimated that there was a 50% reduction in the approval of new molecular entities by the FDA and other regulatory bodies from 2005-2010 compared to 2000-2005 (Mathieu, 2008). This decline in productivity can be thought of in terms of reduced efficiency, the decline in the number of drugs produced from a library of potential compounds, and reduced effectiveness, the inability to translate drug candidates into revenue-producing pharmaceuticals (Paul et al., 2010). A recent industry-wide analysis outlined several factors that have contributed to this decline: lags between the introduction of technological innovations and the ability to translate those innovations into successful drugs, the pursuit of projects with lower probabilities of success, and increased attrition rates in clinical trials (Pammolli et al., 2011).

Biotechnological innovations like mapping the human genome and microbiome, epigenetics, and stem cell therapy have shown promise in the development of targeted and/or personalized medications. Although these breakthroughs have attracted interest for their potential to help understand and treat molecular mechanisms of disease on a personal level, they have yet to be successfully translated into therapies on a large scale. The disconnect between these

technologies' promise and their apparent lack of efficacy are likely due to the fact that they were discovered in the last 10-20 years and are still not fully understood. The human genome project, for example, was started in 1990 (Human Genome Project Information) and has provided incredible amounts of information regarding gene expression, regulation, and dysregulation. However, through this research, it has become apparent that the molecular mechanisms regulating various diseases are often very complex and cannot be traced to a single specific genetic abnormality. Even cystic fibrosis, a disease often caused by a single mutation in the cystic fibrosis transmembrane conductance regulator (CFTR) protein, has several different subtypes that result in different phenotypic outputs (O'Sullivan and Freedman, 2009). Although mutation-specific treatments are available, they generally only alleviate symptoms instead of curing the underlying problem. With diseases that are more complicated, such as cancer, it becomes apparent that treatment of these disorders with multiple underlying mutations and complex regulatory networks will require a better understanding of the biomolecular pathways that regulate these diseases and the development of multi-faceted approaches for treating these disorders.

The pursuit of projects with low probabilities of success is due to a combination of technical and market-based challenges. For example, it has been hypothesized that many of the easily-targeted diseases already have drugs to treat them and the remaining diseases without therapeutics are mechanistically more complex and difficult to treat (Scannell et al., 2012). Furthermore, changes in the way targets are selected may also contribute to the decline in drug development efficiency. Early screening approaches relied more on phenotypic screens that "cast a wide net" for potential therapeutic targets (Swinney and Anthony, 2011) as well as iterative screening that made small modifications to potential compounds in a stepwise manner to slowly

but surely approach a robust final product. Conversely, current drug development often uses genomics and proteomics to find a specific treatable target, and in doing so, may decrease the likelihood of finding a compound with which to treat it. Furthermore, high-throughput screening approaches that simultaneously analyze thousands of compounds for potency often disregard other critical factors such as drug absorption, bodily distribution, metabolism, and excretion (Scannell et al., 2012). In doing so, researchers are prone to missing potentially efficacious compounds while also including potent drugs that possess negative pharmacokinetic behavior that could limit a compound's potential for success in later trials. Not only do technical challenges plague the drug discovery process, but market-based forces have also led to a decline in productivity. There has been a shift in pharmaceutical R&D spending toward high risk and high potential reward compounds such as those to treat cancer, Alzheimer's, obesity, and rheumatoid arthritis (Pammolli et al., 2011). Although the likelihood of creating compounds to treat these complex diseases is low, there is also the potential for a significantly higher return on investment due to a higher likelihood for medical reimbursement from insurance companies, fewer competitors in the landscape, and patent protection. Therefore, improving the likelihood of success in drug development will require companies to not only develop more effective technical approaches but also strategic business plans to optimize the return on investment.

Finally, the most costly and crippling aspect of drug development, the failure of drugs in clinical trials, is partially a byproduct of the challenges mentioned above regarding new technology and selecting the appropriate targets and compounds. By selecting inefficacious compounds or high risk drug profiles, there is inherently a higher likelihood of failing at later stages in the drug development process. This is reflected in the startlingly high clinical attrition rates in both Phase II and Phase III; from 2008-2010, 51% of Phase II compounds failed due to

lack of efficacy and another 19% failed due to safety concerns, similarly, from 2007-2010, 66% and 21% of Phase III compounds failed due to lack of efficacy and safety, respectively (Khanna 2012). Improvements in early-stage discovery processes could increase the likelihood for success during clinical trials; these improvements might come from comprehensive biostatistical analysis and epidemiological studies of patient populations, computational models, and novel screening and diagnostic technologies. Unfortunately, with regards to new and/or enabling technologies, many of the technologies that are developed in academic settings are overly-complicated, require highly specialized instrumentation and workers, and are not scalable, thereby making them difficult or impossible to implement on a large scale. Therefore, next-generation technology will not only need to be able to better predict compound efficacy, but it will also need to seamlessly interface with existing infrastructure. In this regard, aqueous two-phase systems (ATPSs) may provide an easily scalable and adoptable approach with which to create more physiologically relevant *in vitro* assays and high-throughput screening for early-stage drug development, pre-clinical compound testing, and testing at the clinical stage of development.

1.2 Aqueous Two-Phase Systems

An ATPS forms when two aqueous solutions that are enriched with different polymers or a polymer and a salt are mixed at sufficiently high concentrations. The solubilized polymers and salts cause the solutions to become incompatible, and as a result, the individual aqueous phases remain immiscible. This phenomenon was first recognized in 1896 by Martinus Beijerinck, who discovered that aqueous solutions of agar were immiscible with other aqueous solutions of starch or gelatin (Beijerinck, 1896). Since this initial discovery, the investigation of ATPSs has become a field of study unto itself and researchers have even extended the application to multiphase

systems with upwards of 18 distinct phases (Albertsson, 1960). Although enthalpic and entropic theoretical considerations have been used to predict and/or explain the formation of ATPSs based on Flory-Huggins theory for polymer solutions (Baskir et al., 1989a; Baskir et al., 1989b; Sjöberg and Karlström, 1989), oftentimes an empirical approach is required to determine if an ATPS will form based on the following parameters: polymer molecular weights, salt concentration, temperature, and solution pH. The resulting output of these experiments is a binodal curve, which delineates the concentrations of each polymer and/or salt in solution that lead to the formation of a single or two-phase system.

Once a two-phase system has been characterized, it can be utilized for various interesting applications. One area that has been heavily investigated is the use of ATPSs in separation and purification techniques in industrial-scale biological processes (Asenjo and Andrews, 2011). Two characteristics of ATPSs make them especially useful for purifying and/or extracting specific biomolecules from solution: low interfacial tension and biomolecule partitioning. First, unlike oil/water systems that have high surface tensions that lead to the denaturation of proteins and other biomolecules, ATPSs have low surface tensions and are highly biocompatible, thereby preserving the structure and function of active biological material. Second, passive partitioning of certain biomolecules can generate highly purified and/or concentrated solutions. Furthermore, partitioning behavior is dependent, to a degree, on the physicochemical properties of the ATPS. Therefore, by altering the hydrophobicity, concentrations, and molecular weights of polymers in the ATPS, as well as pH and concentrations of various salts in solution, one can modify partition behavior (Albertsson, 1986). This is especially useful for protein purification due to the diverse range of protein conformations, charges, sizes, and hydrophobicities. For example, Tubío et al. used different concentrations and molecular weights of polyethylene glycol (PEG) and sodium

citrate, as well as salt enrichment with NaCl, to enhance trypsin and α-chymotrypsin localization to the citrate phase of the ATPS (Tubío et al., 2007).

Although ATPSs have been effectively utilized for biomolecule purification, our lab has continued to investigate their use for biotechnological applications. Using an ATPS of PEG and dextran (DEX), it was demonstrated that lipofectamine and lentiviruses could be partitioned to the DEX phase; using the ATPS, these transfection reagents were then patterned over a monolayer of cells in an array format to promote the expression of fluorescent proteins (Tavana et al., 2009). Since this initial work was performed, numerous other applications and methods have been developed to take advantage of the ability to easily and discretely pattern biomaterials and cells. Cell patterning of individual or multiple cell types using PEG/DEX ATPSs has been accomplished in a variety of formats including pipetting (Tavana et al., 2010; Tavana et al., 2011, Frampton et al., 2013b), acoustics (Fang et al., 2012), and microfluidics (Frampton et al., 2011). It was also demonstrated that PEG/DEX ATPSs could be combined with microbubble technology to localize sonoporation of cells (Frampton et al., 2013a) and with picoliter dispensing systems to achieve single cell or subcellular delivery of proteases and other biomolecules (Frampton et al., 2013c).

ATPS-based assays, therefore, may be especially useful and interesting in biotechnology and potentially drug discovery and development for several reasons. First, the core technology is extremely easy to implement and therefore more amenable to adoption in biology-based labs and other research settings that are averse to adopting new and complex technology (Berthier et al., 2012). Second, ATPSs can create more physiologically relevant *in vitro* settings that may be better able to predict cellular or organ-level responses and therefore be a better early indicator of drug success (Neužil et al., 2012). Finally, the ability to pattern small arrays of cells and/or

biomolecules enables high throughput screening that can generate more reliable data. These types of next-generation assays will be crucial to enable researchers and clinicians to develop more efficacious treatments and thereby curb the rising costs associated with drug development and health care.

1.3 Dissertation Overview

This work is divided into four separate chapters, each describing a way in which ATPSs are applied to pattern cells and/or biomolecules and can be utilized to improve the drug development process. Chapter 2 describes the application of ATPS-based localization of antibodies for high throughput and multiplexed biomarker detection from cell monolayers. Chapter 3 describes single cell and co-culture cell patterning and provides examples of several basic functional readouts that can be performed. Chapter 4 demonstrates a method by which an ATPS can be utilized to locally deliver trypsin to generate an *in vitro* wound on transwell inserts. Chapter 5 discusses the application of an ATPS to localize antibodies in an enzyme-linked immunosorbent assay (ELISA) for crosstalk-free and multiplexed detection of patient proteins as a way to better characterize disease state in patients with graft-versus-host disease.

1.4 References

Albertsson, P.-A. Partition of Cell Particles and Macromolecules, 2nd Ed. Wiley (1960).

Albertsson, P.-A. Partition of Cell Particles and Macromolecules, 3rd Ed. Wiley (1986).

Asenjo, J.A. and B.A. Andrews. Aqueous two-phase systems for protein separation: A perspective. *J. Chromatogr. A.* **1218**, 8826-8835 (2011).

Baskir, J.N., T.A. Hatton, and U.W. Suter. Protein Partitioning in Two-Phase Aqueous Polymer Systems. *Biotechnol. Bioeng.* **34**, 541-558 (1989a).

Baskir, J.N., T.A. Hatton, and U.W. Suter. Thermodynamics of the Partitioning of Biomaterials in Two-Phase Aqueous Polymer Systems: Comparison of Lattice Model to Experimental Data. *J. Phys. Chem.* **93**, 2111-2122 (1989b).

Beijerinck, M.W. *Zentralblatt fur Bakteriologie, Parasiten und Infektionskrankenheiten*. **2**, 697–699 (1896).

Berthier, E., E.W. Young, and D.J. Beebe. Engineers are from PDMS-land, Biologists are from Polystyrenia. *Lab Chip* **12**, 1224-1237 (2012).

Fang, Y., J.P. Frampton, S. Raghavan, R. Savahi-Kaviani, G. Luker, C.X. Deng, and S. Takayama. Rapid Generation of Multiplexed Cell Cocultures Using Acoustic Droplet Ejection Followed by Aqueous Two-Phase Exclusion Patterning. *Tiss. Eng. C* **18**, 647-657 (2012).

Frampton, J. P., H. Shi, A. Kao, J.M. Parent, and S. Takayama. Delivery of Proteases in Aqueous Two-Phase Systems Enables Direct Purification of Stem Cell Colonies from Feeder Cell Co-Cultures for Differentiation into Functional Cardiomyocytes. *Adv. Healthcare Mat*. DOI: 10.1002/adhm.201300049 (2013c).

Frampton, J. P., J.B. White, A.T. Abraham, and S. Takayama. Cell Co-culture Patterning Using Aqueous Two-phase Systems. *J. Vis. Exp*. **73**, e50304 (2013b).

Frampton, J.P., D. Lai, H. Sriram, and S. Takayama. Precisely targeted delivery of cells and biomolecules within microchannels using aqueous two-phase systems. *Biomed. Microdev*. **13**, 1043-1051 (2011).

Frampton, J.P., Z. Fan, A. Simon, D. Chen, C.X. Deng, and S. Takayama. Aqueous Two-Phase System Patterning of Microbubbles: Localized Induction of Apoptosis in Sonoporated Cells. *Adv. Func. Mat.* DOI: 10.1002/adfm.201203321 (2013a).

Human Genome Project Information. http://genomics.energy.gov

Khanna, I. Drug discovery in pharmaceutical industry: productivity challenges and trends. *Drug Discov. Today* **17**, 1088-1102 (2012).

Mathieu, M.P. *Parexel's Bio/Pharmaceutical*R&*D Statistical Sourcebook*. Parexel International Corporation, 2008.

Munos, B. Lessons for 60 years of pharmaceutical innovation. *Nat. Rev. Drug Discov.* **8**, 959–968 (2009).

Neužil, P., S. Giselbrecht, K. Lange, T.J. Huang, and A. Manz. Revisiting lab-on-a-chip technology for drug discovery. *Nat. Rev. Drug Discov.* **11**, 620-632 (2012).

O'Sullivan, B.P and S.D. Freedman. Cystic Fibrosis. *Lancet* **373**, 1891-1904 (2009).

Pammolli, F., L. Magazzini, and M. Riccaboni. The productivity crisis in pharmaceutical R&D. *Nat. Rev. Drug Discov.* **10**, 428-438 (2011).

Paul, S.M., D.S. Mytelka, C.T. Dunwiddie, C.C. Persinger, B.H. Munos, S.R. Lindborg, and A.L. Schacht. How to improve R&D productivity: the pharmaceutical industry's grand challenge. *Nat. Rev. Drug Discov.* **9**, 203-214 (2010).

Scannell, J.W., A. Blanckley, H. Boldon, and B. Warrington. Diagnosing the decline in pharmaceutical R&D efficiency. *Nat. Rev. Drug Discov.* **11**, 191-200 (2012).

Sjöberg, Å. and G. Karlström. Temperature Dependence of the Phase Equilibria for the System Poly(ethy1ene glycol)/Dextran/Water. A Theoretical and Experimental Study. *Macromol*. **22**, 1325-1330 (1989).

Swinney, D.C. and J. Anthony. How were new medicines discovered? *Nat. Rev. Drug Discov.* **10**, 507-519 (2011).

Tavana, H., A. Jovic, B. Mosadegh, L.Q. Yi, X. Liu, K.E. Luker, G.D. Luker, S.J. Weiss, and S. Takayama. Nanolitre liquid patterning in aqueous environments for spatially defined reagent delivery to mammalian cells. *Nat. Mat*. **8**, 736-741 (2009).

Tavana, H., B. Mosadegh, and S. Takayama. Polymeric Aqueous Biphasic Systems for Non-Contact Cell Printing on Cells: Engineering Heterocellular Embryonic Stem Cell Niches. *Adv. Mater*. **22**, 2628-2631 (2010).

Tavana, H., B. Mosadegh, P. Zamankha, J.B. Grotberg, and S. Takayama. Microprinted Feeder cells guide embryonic stem cell fate. *Biotech. Bioeng.* **108**, 2509-2516 (2011).

Tubío, G., B. Nerli, and G. Picó. Partitioning features of bovine trypsin and alpha-chymotrypsin in polyethyleneglycol-sodium citrate aqueous two-phase systems. *J. Chromatogr. B.* **852**, 244-249 (2007).

Chapter 2

Aqueous Two-Phase Localized Immunocytochemistry for Multiplexed Protein Detection

This chapter describes the use of a PEG/DEX ATPS for localizing antibodies on a monolayer of cells. Antibody partitioning was first demonstrated by equilibrating an antibody-enriched ATPS and then reading signals produced from aliquots of each phase by dot blot. After demonstrating antibody partitioning, staining characteristics of the system were characterized based on polymer concentrations of the ATPS, droplet volumes of the dispensed DEX, and incubation times. The versatility of the technique was highlighted by using ATPS to localize primary and/or secondary antibodies, as well as by producing signals in colorimetric, fluorescent, and chemiluminescent formats. Finally, multiplexed protein detection was performed in a single dish by applying an array of DEX droplets containing different primary antibodies. ATPS-immunocytochemistry can be further adapted to perform multiplex ATPS-immunohistochemistry to aid in biomarker discovery and patient stratification, as well as to screen for antibody quality, perform high-throughput screening of antibody therapeutics, and perform in-cell ELISA.

2.1 Introduction

Immunohistochemistry (IHC) is a common research technique that uses antibodies to detect the presence and localization of specific proteins. The process is used by both basic research scientists and clinicians to investigate prognostic factors and predict therapeutic outcomes of diseases, as well as to differentially diagnose patients based on the presence (or lack thereof) of specific cell morphologies and/or protein expression by the cells of interest (Luongo de Matos et al., 2010). Although IHC is readily used, there is a lack of standardization in sample processing and interpretation across labs, which makes it difficult to make universally accepted conclusions from results. Furthermore, as research and medicine shifts to personalized treatments, newer technologies that aid in the above processes will be necessary to achieve this paradigm shift (Dietel and Sers, 2006; Wang and Vo-Dinh, 2009).

One of the ways researchers are advancing such technologies is to implement multiplexing, or the ability to detect multiple biomarkers of interest from a single sample. For example, DNA microarrays and other genomic prolifers are increasingly being used to characterize the genomic status of patients (Shen and Wu, 2009). However, changes in DNA are not always replicated at the protein level, which is a more relevant readout since it reflects cell behavior and overall physiological response. Therefore, sensitive and accurate multiplex protein-based assays, such as multiplex IHC, will be even more relevant to the advancement of the field. To this end, several research groups have implemented methods with which to perform multiplex IHC; multiple antibody labeling (Xing et al., 2007), membrane layering (Gannot et al., 2005), microchannels (Kim et al., 2010), and microfluidic probes (Lovchik et al., 2012) have all demonstrated the capacity to detect multiple antigens from a single sample. These technologies can be applied to early biomarker discovery and validation, where there is a need to analyze

large numbers of samples and biomarkers in parallel to identify potential therapeutic targets (Sauter et al., 2003), and later in clinical trials, where it is useful to analyze multiple biomarkers to stratify patients and analyze their responses to therapeutics, especially when samples are limited.

The multiplex IHC approaches listed above, however, are not without their own limitations. Multiple antibody labeling requires highly specific combinations of antibodies to prevent their cross-reactivity, and in the case of fluorescent readouts also requires complex combinations of fluorophores and filter cubes to distinguish signals; therefore, with this approach it becomes exceedingly difficult to detect more than 2 proteins from the same sample. Membrane layering utilizes a stack of functionalized membranes to transfer different individual proteins from the sample to each membrane. Unfortunately this approach consumes large amounts of reagent and does not provide very detailed transfer features. Finally, although microfluidics consume small amounts of expensive reagents and can achieve extremely small sample areas, it requires highly specialized equipment and requires technical expertise to operate, making it burdensome to adopt into many labs and scale commercially.

The use of aqueous two-phase systems (ATPSs) to pattern reagents, on the other hand, only requires handheld pipettes, consumes microliter volumes of reagents, can be readily scaled, and can be easily modified to accommodate various biologics such as transfection reagents (Tavana et al., 2009), multiple cell types (Frampton et al., 2013b), and microbubbles (Frampton et al., 2013a), among other reagents. This technique was further modified here to spatially pattern antibodies over a monolayer of cells to achieve rapid and robust localized detection of proteins. Sizes of staining areas and spacing between them can be tailored by selecting the appropriate molecular weights and concentrations of polyethylene glycol (PEG) and dextran

(DEX) dissolved in solution. Furthermore, because this technique confines antibodies to microliter droplets of DEX on the surface of cells and decreases the available void volume, it reduces the diffusion distance for antibodies to bind their respective proteins, thereby increasing signal intensity and decreasing the incubation time required to stain cells. ATPS-based staining is also highly versatile and can be used to pattern primary and/or secondary antibodies and can be used with colorimetric, fluorescent, or chemiluminescent readouts. Due to the ease with which ATPS-ICC is performed and the versatility of the assay, we envision the technique could be a powerful tool in drug development for multiplex protein detection for biomarker discovery, patient diagnosis, and to explain patient response to therapeutic protocols.

2.2 Materials and Methods

2.2.1 Antibody partitioning in PEG/DEX ATPSs

Partitioning of primary IgG antibodies (cytokeratin 7 (CK7), 18-0234, Life Technologies; cytokeratin 8 (CK8), 18-0185Z, Life Technologies; leukocyte common antigen (LCA), 180367, Life Technologies) and a biotinylated detection antibody (B-2763, Life Technologies) was determined by dot blot. Briefly, 1:500 dilutions of antibodies were added to Eppendorf tubes containing 10% w/w PEG 35 kDa (81310, Sigma) and 10% w/w DEX 500 kDa (DEXT500, Pharmacosmos) (total volume, 1 ml). Control tubes contained only PEG and DEX and were not enriched with antibodies. The contents of each Eppendorf tube were thoroughly mixed by rocking at room temperature for 10 min. The tubes were then centrifuged at 400 rcf at 4° C for 15 min, which facilitated the complete phase separation and equilibration of the PEG and DEX phases. Polyvinylidene fluoride (PVDF) membranes (10413052, Whatman) were soaked in methanol for 15 s, water for 2 min and finally PBS for 5 min. Six 0.5 µl samples each of the PEG

and DEX phases were dispensed onto the PVDF membranes, which were then blocked in 1% BSA for 1 h and washed 4 times with PBS containing 0.05% Tween-20. In the case of membranes spotted with solutions containing primary antibodies, membranes were further incubated for 1 h with biotinylated goat anti-mouse antibody (1:1000 dilution) in PBS. Following another 4 washes, both membranes were incubated with streptavidin-conjugated horseradish peroxidase for 1 h, washed 4 times, and incubated with SuperSignal ELISA Femto Maximum Sensitivity Substrate (37074, Thermo Scientific). Chemiluminescent signal was detected using a FluorChem M (Protein Simple) imaging system. Partition coefficients, defined as the reagent concentration in the PEG phase divided by the reagent concentration in the DEX phase, were calculated by taking the ratios of chemiluminescent signals from the PEG and DEX spots on the PVDF membranes.

2.2.2 Staining characteristics

A549, H2170, and SK-MES-1 pulmonary epithelial cell lines (CCL-185, CRL-5928, HTB-58; ATCC) were maintained in F12, RPMI, and MEM-alpha media, respectively, supplemented with 10% FBS (12306C, Sigma) and 1% anti-anti (15240-062, Gibco). To demonstrate staining capabilities, cells were plated into 35- or 60-mm dishes and grown to confluence over the course of 24 h. Cells were fixed with 4% paraformaldehyde (PFA) for 15 min, rinsed with PBS, permeabilized with 0.1% Triton X-100 (T-9284, Sigma), and rinsed and stored in PBS for future use.

To demonstrate how staining size was dependent on ATPS characteristics, the following ATPSs were formulated from PEG 35 kDa and DEX 500 kDa: 5% DEX and 5% PEG, 10% DEX and 10% PEG, and 20% DEX and 20% PEG. Immunocytochemistry (ICC) was performed on fixed and permeabilized cells that were treated for 1 h with 1% H_2O_2 to neutralize intrinsic

peroxidase activity, washed with PBS containing 0.05% Tween 20, blocked for 1 h with 1% BSA (810683, Millipore), and washed. Localized staining of cells was then performed using ATPSs; briefly, DEX phases were enriched with a 1:200 dilution of mouse anti-CK 7 and PEG phases enriched to a final BSA concentration of 0.1%, confluent dishes of cells were filled with PEG solution, and antibody-enriched DEX droplets were dispensed into dishes using a Matrix MultiChannel Equalizer Pipette (Thermo Scientific). Cells were incubated with primary antibodies in ATPS for 1 h, washed, incubated for 1 h with 1:400 biotinylated goat anti-mouse antibody (B2763, Molecular Probes) in PBS, washed, incubated for 1 h with streptavidin-conjugated horseradish peroxidase (Strep-HRP), washed, and developed using diaminobenzidine (DAB) (750118, Invitrogen). Staining areas were analyzed using ImageJ.

Time-dependent staining was performed with a similar, but slightly modified protocol. Following treatment with H_2O_2 and blocking with BSA as before, dishes were filled with PEG containing 0.1% BSA. Then 0.5 µl droplets of DEX containing 1:200 anti-CK 7 were dispensed into dishes and incubated for the following lengths of time: 120, 60, 30, 20, 10, 5, 2.5, and 1 min. Dishes were washed, incubated with secondary antibody, washed, incubated with Strep-HRP, and washed as before. Finally, signal was developed using SuperSignal ELISA Femto Maximum Sensitivity Substrate (PI37074, Fisher Scientific), read on a FluorChem M Digital Imager, and images were analyzed for signal intensity using ImageJ. Time-dependent staining characteristics were also analyzed for cells incubated with antibodies in the absence of ATPS. In this format, cells were fixed and permeabilized in a 96-well dish. The staining protocol was the same as that outlined above for ATPS-treated cells in dishes, except with the following modifications: individual wells with cells were incubated with 1:200 primary mouse anti-CK 7 in PBS containing 0.1% BSA for the prescribed times, and signal was developed by incubating wells

with 100 µl ABTS (00-2024, Invitrogen) and read at 415 nm on a Synergy Neo HTS Multi-Mode Microplate Reader (Biotek).

2.2.3 Multiplex staining of epithelial cells

Multiplex staining of epithelial cells was performed with 3 different readout formats: colorimetric (with DAB), chemiluminescent, and fluorescent. Following fixation, permeabilization, incubation with H_2O_2, and blocking, dishes were filled with 10% PEG containing 0.1% BSA. Mouse anti-human CK 7, anti-human CK 8, and anti-human leukocyte common antigen were diluted 1:200 in 10% DEX solutions, which were then dispensed into PEG in array format and incubated for 1 h. Dishes were washed and incubated with the appropriate secondary antibodies for 1 h. For colorimetric and chemiluminescent readouts, dishes were incubated with 1:400 biotinylated goat anti-mouse antibodies, and for fluorescent readouts, dishes were incubated with 1:200 FITC-conjugated rabbit anti-mouse antibodies (sc-358916, Santa Cruz Biotechnology). For the fluorescent readout, dishes were then washed and imaged using an Eclipse TE300 microscope (Nikon), while for colorimetric and chemiluminscent readouts, dishes were washed, incubated with Strep-HRP, washed, and developed as previously.

2.3 Results and Discussion

2.3.1 Antibody partitioning in PEG/DEX ATPSs

During ATPS equilibration, antibodies naturally partition based on molecular characteristics and phase system properties. After solutions were fully equilibrated, sample aliquots were taken from each phase, applied to PVDF membranes, and detected via chemiluminescent signals from the aliquots on a FluorChem M Digital Imager. In this format,

chemiluminescent signal intensity is proportional to the amount of antibody in solution. By dividing signal intensity of the PEG phase by that of the DEX phase, we obtained partition coefficients for several different antibodies (Figure 2.1). As can be seen, qualitatively there is no visually detectable signal arising from the region of the PVDF membrane where PEG was spotted, while there are distinct chemiluminescent signals arising from the regions were DEX was incubated. Quantitatively, partition coefficients are <0.072, i.e., virtually 100% of antibodies partition to the DEX phase.

Because antibodies naturally partition to the DEX phase, we can use ATPS technology to spot small droplets of DEX containing antibodies on a monolayer of cells to perform localized staining (Figure 2.2). In this format, the workflow for ATPS-ICC or ATPS-IHC is very similar to traditional non-ATPS methods, but with slight modifications to the antibody incubation steps. Therefore, all initial processing steps including fixation, permeabilization, incubation with H_2O_2, and blocking are identical. In the traditional approach, cells are incubated with a bath solution of primary antibodies; to perform staining of multiple proteins, different primary antibodies are included in solution (Figure 2.2 A, i). Primary antibodies bind uniformly across the cell monolayer, and after washing away excess primary antibodies (Figure 2.2 A, ii), cells are incubated with secondary antibodies, which bind to their respective primary antibodies, and then washed to remove unbound secondary antibodies (Figure 2.2 A, iii). This approach is limited, however, because each capture and detection antibody pair must have a distinct species of origin and reactivity to prevent antibody cross-reactions. For example, if one wanted to stain for protein A and protein B, one could use a mouse anti-protein A and rabbit anti-protein B as the primary antibodies, then apply goat anti-mouse and donkey anti-rabbit secondary antibodies. If, however, a mouse anti-protein A and mouse anti-protein B were used, the secondary antibody wound bind

to both primary antibodies and it would be impossible to distinguish signals produced by the individual proteins.

ATPS-ICC and ATPS-IHC, on the other hand, confine different primary antibodies to their respective DEX droplets (Figure 2.2 B, i). In this format, because antibodies partition to DEX and cannot diffuse outward, they only bind to proteins in the area over which the DEX droplet spreads (Figure 2.2 B, ii). Therefore, even when a bath solution of secondary antibody is applied (and subsequently washed away), signal is only produced in the regions where primary antibodies are spotted (Figure 2.2 B, iii). Unlike the traditional format, this approach enables the use of a single species of primary antibodies and a single detection antibody to detect multiple proteins at different locations, i.e., one could use mouse anti-protein A, mouse anti-protein B… mouse anti-protein Z and a goat anti-mouse secondary antibody. This is the case because even though the secondary antibody binds to all primary antibodies, because each primary antibody is localized, signals are spatially resolved.

2.3.2 Staining characteristics

Using the ATPS-based approach described above, we characterized staining properties based on ATPS concentrations, droplet volumes, and incubation times. ATPSs of PEG 35 kDa and DEX 500 kDa were formulated at concentrations of 5, 10, and 20%, and PEG and DEX were further enriched with 0.1% BSA and primary antibody, respectively. During the primary antibody incubation step, 0.5, 1, and 2 μl drops of antibody-containing DEX were dispensed into PEG solutions, followed by washing and development (Figure 2.3 A). As expected, higher concentrations of polymers (due to greater interfacial tensions between the solutions) and smaller droplet volumes led to smaller staining areas (Figure 2.3 B). For the 10% and 20% ATPSs at the

lower volumes, however, differences in staining areas were marginal, and because the 20% solutions are much more viscous and can be more difficult to pipette and wash from dishes, 10% solutions may be more ideal for some applications. Furthermore, although ATPSs with other molecular weights of PEG and DEX were not investigated, results would be expected to follow a similar pattern; for the same concentrations tested here, lower molecular weights would be expected to have larger staining areas due to lower surface tensions between the solutions that would facilitate greater droplet spreading.

ATPSs also seem to facilitate more complete binding of antibodies to proteins (Figure 2.4). Antibodies were incubated with cells for times ranging from 1 to 120 min; for the ATPS format, signal was developed with chemiluminescent substrate and read on a digital imager, while for the non-ATPS format, signal was developed with ABTS and read on a plate reader. Because the readout formats were different, raw signal intensities varied by several orders of magnitude. Therefore, to compare binding kinetics, signal intensities were normalized against the signal intensity produced at the 120 min time point. Data were then fit with Michaelis-Menten-like equations, whose corresponding curves were also plotted. Based on these fits, maximum normalized signal intensities at $t=\infty$ were 1.08 and 0.92 for ATPS and non-ATPS staining, and the times to reach 50% and 90% of maximal signal intensity occurred at approximately 2 and 19 min and 3.5 and 32 min for the ATPS and non-ATPS formats, respectively. This seems to indicate that the microdroplet confinement causes more antibodies to bind cells and to do so more rapidly, which can be attributed to a shift in equilibrium binding kinetics and a restriction to diffusion caused by antibody partitioning to the small DEX droplets.

Finally, several non-traditional staining proofs-of-concept were performed to demonstrate the versatility and fidelity of this approach. First, ATPS-localization of secondary antibodies was

performed. In the previous formats, ATPS was used to localize primary antibodies to distinct regions and secondary antibodies were bath-applied; in this "reverse" format, primary mouse antibody was applied uniformly in PBS, followed by ATPS spotting of biotinylated goat anti-mouse secondary antibody. Washing and signal development occurred as before to produce colorimetric signals (Figure 2.5 A). This idea was taken a step further to spot both the primary and secondary antibodies using ATPS. Here, we first spotted and incubated primary antibody (Figure 2.5 B, i). Following the necessary washing, ATPS was then used to spot secondary antibody so that the DEX droplet containing secondary antibody partially overlapped the area where primary antibody was spotted (Figure 2.5 B, ii), much like a Venn diagram. When signal was finally developed, it was only localized to the central region where both primary and secondary antibodies were incubated (Figure 2.5 B, iii). These proofs-of-concept are important because they highlight the need to have both primary and secondary antibodies present to produce signal and that antibody binding is specific. Finally, ATPS-based spotting of antibodies enables spatial control that can be used to selectively localize antibodies in discrete patterns (here droplets spell "IHC") with various readout formats (Figure 2.5 C).

As can be seen, ATPS-ICC offers several advantages over traditional approaches. Discrete localization of antibody spots enables researchers and scientists to conserve precious and expensive antibodies. Whereas traditional staining may require > 1 ml antibody solution, this approach can apply antibodies in < 1 µl droplets, thereby conserving antibodies by 1000-fold. Furthermore, ATPS enables greater amounts of antibody binding and more rapid binding of antibodies than traditional approaches, thereby reducing the time required to perform the assay. Finally, the ability to pattern primary and secondary antibodies, as well as to combine the assay with various readout formats, enables researchers to tailor the system to suit their needs. For

example, in the development of antibodies to detect a protein of interest, researchers could use ATPS to spot several different types of antibodies side-by-side to compare binding efficiency and/or signal production (while simultaneously conserving antibodies) to select the most optimal antibodies for their purposes. Furthermore, by combining this approach with various signal formats such as fluorescence or chemiluminescence, it may be easier to quantitatively analyze expression levels instead of relying on qualitative and arbitrary analyses that are typical of traditional ICC and IHC.

2.3.3 Multiplex staining of epithelial cells

Multiplex staining is performed in the same manner as single staining, except DEX droplets are enriched with different primary antibodies. Epithelial cells were stained for CK 7, CK 8, and LCA, which were chosen as positive (cytokeratins) and negative stains (LCA) (Figure 2.6). As can be seen, signal was localized and only produced for CK7 and CK8, while no signal was produced at LCA spots, which is expected because LCA is a marker of leukocytes and hematopoietic progenitor cells and should not be expressed in epithelial cells. Side-by-side analysis with immunofluorescently-labeled secondary antibodies confirmed the staining patterns produced with DAB.

Multiplex staining could be especially interesting in the context of biomarker discovery and patient stratification. Side-by-side staining of cells with known and potential biomarkers of disease would enable researchers, clinicians, and drug developers to catalog larger panels with which to identify diseases and gauge their progression. During the clinical trials stage, once a panel of biomarkers has been identified for a disease, multiplex ATPS-IHC would be a useful method that would enable researchers to better stratify patients and predict patient responses to treatments. For example, panels of biomarkers that include p63, CK5/6, and TTF-1 have been

shown to be useful in differentiating between squamous cell carcinoma and small cell lung cancer. In this case, p63 and CK5/6 are highly expressed in squamous cell carcinomas, while TTF-1 is rarely expressed (and vice-versa for small cell lung cancer) (Mani and Zander, 2012). These types of multiplexed biomarker detection methods are growing increasingly useful in differential patient diagnosis and will be especially useful in identifying subsets of patients that respond best to different types of treatment protocols, especially when there are limited and precious samples.

2.4 Conclusions

ICC and IHC are well-established techniques, and IHC is commonly used in biomarker discovery and to diagnose patients. These techniques, however, are limited by their lack of standardization, qualitative nature of the readouts, and limited ability to detect multiple biomarkers from a single sample. Many techniques have been developed to perform multiplex protein detection from immunohistochemical samples, but they often require highly technical operation of specialized equipment and/or extensive validation of antibody specificity.

ATPS-ICC, demonstrated here, should be easy to translate to ATPS-IHC. Unlike previously developed multiplex techniques, this approach only requires polymer-enriched solutions and pipettes to be performed; therefore, due to the low technical skill required it should be readily adoptable into many laboratory settings. Furthermore, in the context of clinical labs that require rapid and automated staining of samples, ATPS-based multiplex staining could also be implemented due to its easy interfacing with automated plate handlers and liquid dispensers. Interfacing the ATPS-based approach with liquid handlers could also enable even greater precision in staining; we demonstrated that we were able to achieve staining areas of

approximately 2 mm^2 with a handheld multichannel pipette, but liquid handlers capable of delivering <0.5 µl of fluid could produce even smaller staining areas that enable higher degrees of multiplexing. We further demonstrated here that ATPS-ICC can reduce assay time and increase signal intensity; whereas traditional staining required longer than 30 min to reach 90% of the maximum signal intensity, the ATPS approach, which confines antibodies to the surface, reduced this time to less than 20 min.

ATPS-ICC and ATPS-IHC could be valuable tools in the drug development process. During the biomarker discovery stage, these approaches could be used to perform side-by-side analysis of validated biomarkers with potential new biomarkers of interest. Similarly, as new antibodies are generated to detect biomarkers, a similar side-by-side analysis could be used to compare antibody selectivity and signal generation capabilities to select the highest affinity and highest-signal producing antibodies. Furthermore, during clinical trials, it would be beneficial to have multiple biomarker analysis methods to more definitively stratify patients and predict and/or explain patient response to therapeutic regimes. As a potential future avenue, with the appropriate liquid dispensing tools, this approach could be used to deliver antibodies to a single cell or small groups of cells to perform in-cell ELISA to directly quantify protein expression. This will be an important area of basic and translational research in drug development because it is now apparent that single cells within a larger population (even if they are the same cell type) can differ dramatically, and therefore it will be crucial to characterize and understand these differences to better understand (patho)physiology and to develop efficacious therapeutics. Finally, as the industry shifts from small pharmaceutical compounds to biological therapeutics, one could envision implementing this approach as a high-throughput and/or multiplexed *in vitro* screening approach for recombinant antibodies. After plating a monolayer of cells (cell lines or

primary cells), an array of antibody-containing DEX droplets could be spotted onto the dish against the desired target proteins; droplets could contain either a single antibody or a combination of antibodies, and subsequent cell responses could be studied.

The immediate applications for ATPS-ICC and ATPS-IHC in biomarker discovery and validation and patient stratification will require further technical validation and the development of scoring systems to be implemented in clinical settings, but these applications, as well as other potentially exciting screening uses make it especially promising as a next-generation technology in the drug development and biotechnology industries.

Antibody Partition

CK7: 0.026

CK8: 0.050

LCA: 0.072

2^{o}: 0.032

Figure 2.1: Antibody partitioning in a PEG and DEX ATPS. A representative chemiluminescent image of a PVDF membrane spotted with CK8 antibodies is shown. Qualitatively there is no signal arising from the regions of the membrane where PEG aliquots were spotted, while there are clearly signals arising from the regions where DEX was dispensed. After subtracting background signal from the regions of interest, partition coefficients were calculated for CK7, CK8, LCA, and biotinylated goat-anti mouse secondary (2^{0}) antibodies by averaging the signal intensities from six individual spots from each phase and taking the ratios of these averages.

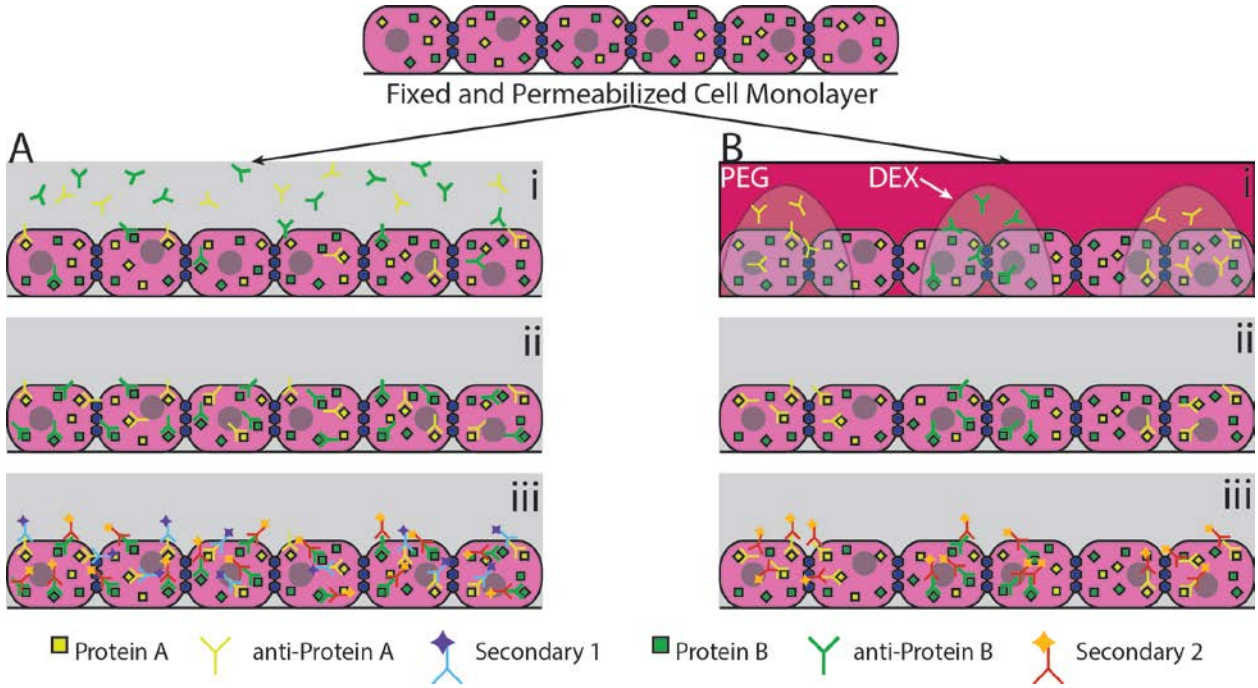

Figure 2.2: Comparison of workflows of ICC and IHC with ATPS-ICC and ATPS-IHC. A) Traditional staining format. i) multiplex protein detection is performed by incubating a fixed and permeabilized monolayer of cells with a homogeneous bath solution containing the primary antibodies of interest; ii) after rinsing unbound antibodies, primary antibodies are bound across the entire monolayer of cells; iii) following a wash, secondary antibodies are applied and bind to their respective primary antibodies. In this format, each primary/secondary antibody pair must be raised with different species reactivity to prevent antibody cross-reactions from occurring and each must have a different signal-producing readout so as to be able to distinguish between the proteins. B) ATPS-ICC or ATPS-IHC format. i) multiplex protein detection is performed by incubating a fixed and permeabilized monolayer of cells with an ATPS that localizes the primary antibodies of interest to specific regions; ii) after rinsing, primary antibodies are bound only to areas over which DEX spread; iii) following a wash, a single secondary antibody can be applied to produce signal. In this format, primary antibodies can all be raised in the same species and a single secondary antibody can be applied (with a single enzyme conjugation) because antibody areas are spatially resolved.

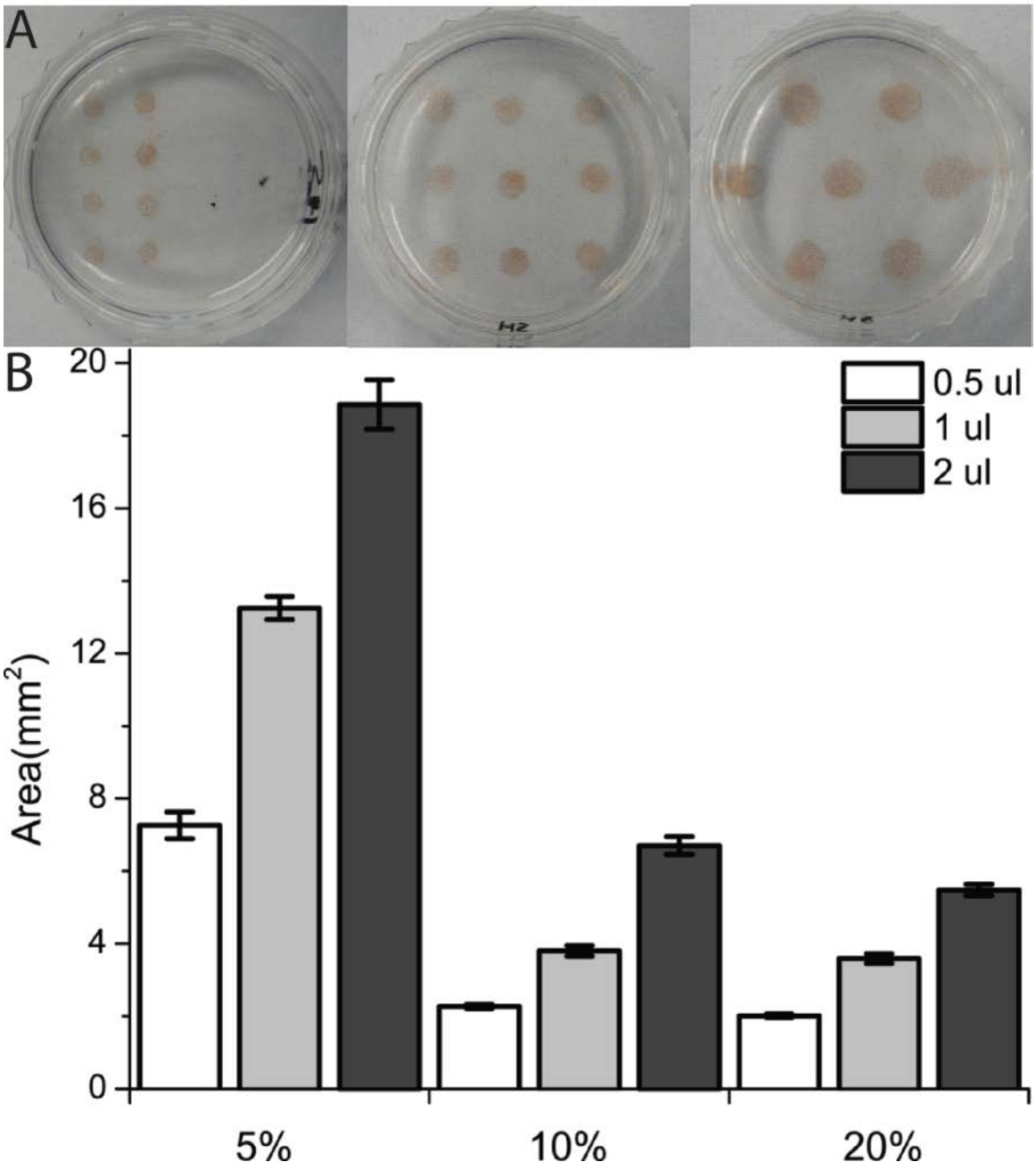

Figure 2.3: Droplet volume- and polymer concentration-dependent staining areas. A) Representative images of monolayers of SK-MES-1 cells in 35 mm dishes stained with 0.5 µl CK7 antibody-containing DEX droplets from ATPSs of PEG 35 kDa and DEX 500 kDa at concentrations of 20 (left), 10 (middle), and 5% (right). B) Signal areas were quantified using ImageJ; as expected, signal areas were smaller for higher concentrations of polymers and smaller volumes of DEX.

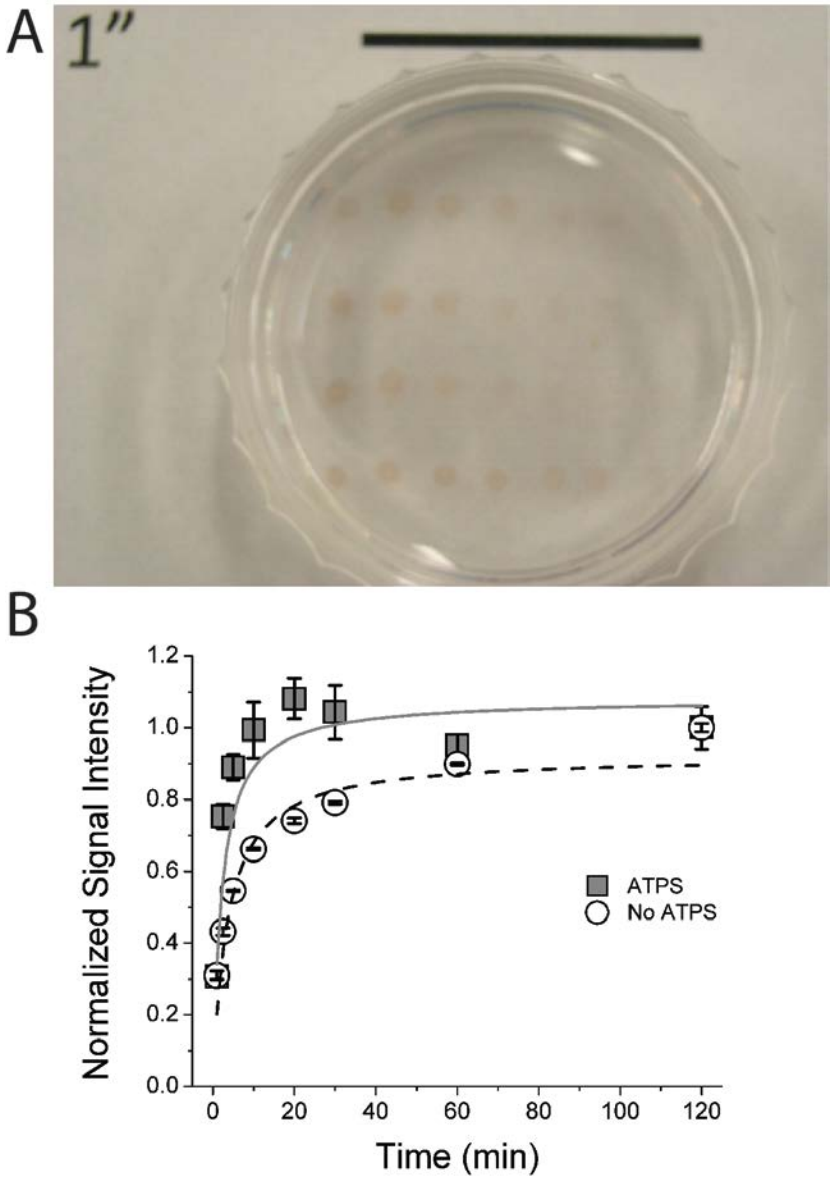

Figure 2.4: Time-dependent staining intensity of A549 cells. A) Representative image of a 35-mm dish of epithelial cells stained with DEX droplets containing CK7 for 120, 60, 30, 20, 10, 5, 2.5, and 1 min (left to right), respectively. B) Signal intensities were normalized against the intensity at 120 min so as to be able to compare kinetics of the ATPS- and non-ATPS-based systems. Points were fit with Michaelis-Menten-like curves, which show that ATPS-based staining causes higher maximum signal intensity and causes those maximum signals to be reached more rapidly than non-ATPS-based staining.

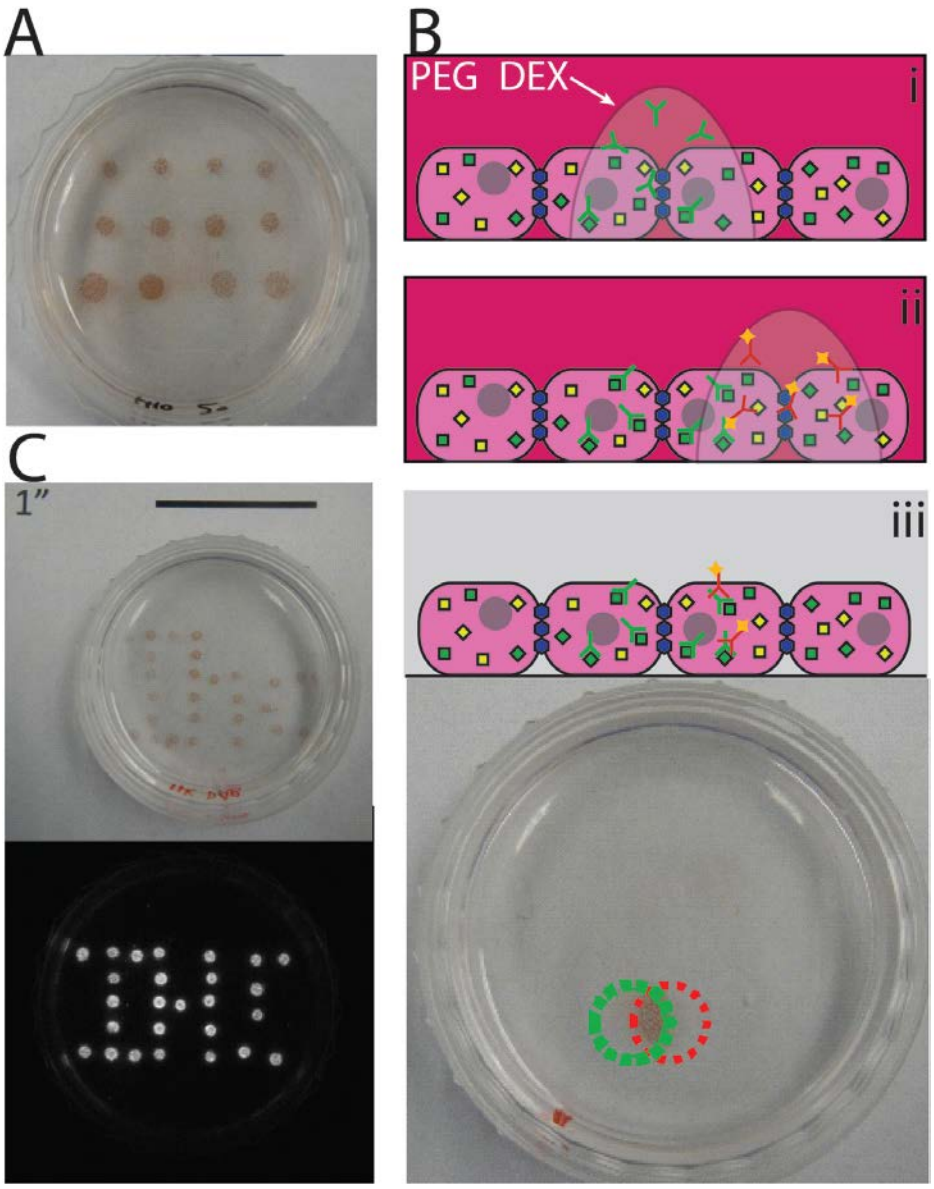

Figure 2.5: Other staining capabilities with ATPS-ICC. A) After applying a uniform solution of primary antibody, ATPS can be used to spot DEX droplets of secondary antibodies, which also results in localized staining. B) Both primary (i) and secondary (ii) antibodies can be spotted sequentially, which produces signal that is localized to the interior and overlapping region where both antibodies were localized in a Venn diagram format (iii). C) ATPS-based staining can be applied with high degrees of spatial control, as demonstrated by the spelling of "IHC," and can also be used with various signal output formats, including chemiluminescence.

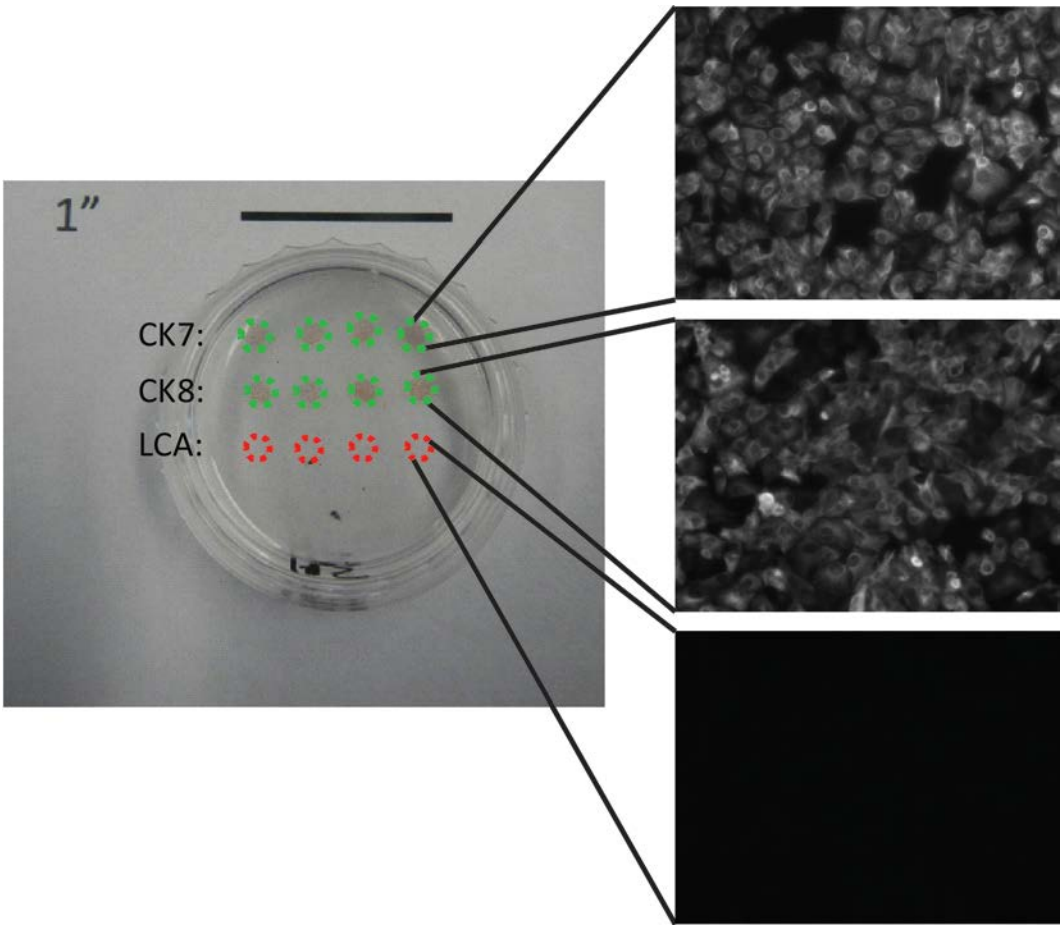

Figure 2.6: Multiplex staining of epithelial cells. Epithelial cells were stained for CK7, CK8, and LCA. As expected, signal was produced in regions where cytokeratins were localized (green dashed circles), while no signal was generated at regions where LCA was spotted (red dashed circles). Fluorescent staining from another dish confirmed the stain was specific for cytoskeletal proteins and was not due to non-specific binding of the antibody to the dish or other cellular domains.

2.5 References

Dietel M., and C. Sers. Personalized medicine and development of targeted therapies: The upcoming challenge for diagnostic molecular pathology. A review. *Virchows Arch.* **448**, 744-755 (2006).

Frampton, J.P., J.B. White, A.T. Abraham, and S. Takayama. Cell co-culture patterning using aqueous two-phase systems. *J. Vis. Exp*. DOI: 10.3791/50304 (2013b).

Frampton, J.P., Z. Fan, A. Simon, D. Chen, C.X. Deng, and S. Takayama. Aqueous two-phase system patterning of microbubbles: localized induction and apoptosis in sonoporated cells. *Adv. Func. Mat.* DOI: 10.1002/adfm.201203321 (2013a).

Gannot, G., M.A. Tangrea, J.W. Gillespie, H.S. Erickson, B.S. Wallis, R.A. Leakan, V. Knezevic, D.P. Hartmann, R.F. Chuaqui and M.R. Emmert-Buck. Layered peptide arrays: high-throughput antibody screening of clinical samples. *J. Mol. Diagn*. **7**, 427 (2005).

Kim, M.S., T. Kim, S.Y. Kong, S. Kwon, C.Y. Bae, J. Choi, C.H. Kim, E.S. Lee and J.K. Park. Breast Cancer Diagnosis Using a Microfluidic Multiplexed Immunohistochemistry Platform. *PLoS One*, 2010, 5, 12.

Lovchik, R.D., G.V. Kaigala, M. Georgiadis, and E. Delamarche. Micro-immunohistochemistry using a microfluidic probe. *Lab Chip* **12**, 1040-1043 (2012).

Luongo de Matos, L., D.C. Trufelli, M.G. Luongo de Matos, and M. Aparecida da Silva Pinhal. Immunohistochemistry as an important tool in biomarkers detection and clinical practice. *Biomark. Insights* **5**, 9-20 (2010).

Mani, H. and D.S. Zander. Immunohistochemistry: applications to the evaluation of lung and pleural neoplasms: part 1. *Chest* **142**, 1316-1323 (2012).

Sauter, G., R. Simon, and K. Hillan. Tissue microarrays in drug discovery. *Nat. Rev. Drug Discov.* **2**, 962-972 (2003).

Shen, Y. and B.-L. Wu. Microarray-based genomic DNA profiling technologies in clinical molecular diagnostics. *Clin. Chem.* **55**, 659-669 (2009).

Tavana, H., A. Jovic, B. Mosadegh, L.Q. Yi, X. Liu, K.E. Luker, G.D. Luker, S.J. Weiss, and S. Takayama. Nanolitre liquid patterning in aqueous environments for spatially defined reagent delivery to mammalian cells. *Nat. Mat.* **8**, 736-741 (2009).

Wang H.N., and T. Vo-Dinh. Multiplex detection of breast cancer biomarkers using plasmonic molecular sentinel nanoprobes. *Nanotechnology* **20**, 065101 (2009).

Xing, Y., Q. Chaudry, C. Shen, K.Y. Kong, H.E. Zhau, L.W. Chung, J.A. Petros, R.M. O'Regan, M.V. Yezhelyev, J.W. Simons, M.D. Wang and S.Nie. Bioconjugated quantum dots for multiplexed and quantitative immunohistochemistry. *Nat. Protoc*. **2**, 1152-1165 (2007).

Chapter 3

Cell Co-Culture Patterning Using Aqueous Two-Phase Systems

This chapter describes the use of a PEG/DEX ATPS for patterning monocultures and co-cultures of cells. The cloud-point method was used to construct binodal curves for several types of serum-free and 10% serum-enriched media. PEG 35 kDa and DEX 500 kDa were then tested at 1x, 2x, and 3x their critical concentrations, the concentrations below which two phases do not form, to determine the conditions that enabled effective cell patterning, that did not adversely affect cell morphology, and that did not facilitate serum precipitation from solution. Cells were exclusion- and island-patterned in monoculture and monitored for proliferation and migration over the course of 72 h. Exclusion and island patterning were combined to pattern hepatocytes and fibroblasts in co-culture, and hepatocytes were then qualitatively analyzed for albumin production over 96 h. These techniques demonstrate a simple and scalable method with which cells can be patterned for high-throughput cell migration analysis and/or patterned to achieve more physiologically relevant cell behavior for compound screening applications.

3.1 Introduction

The human body is made up of billions of cells that have arisen from a single cell in a complex and orchestrated series of steps including cell division, growth, migration, and differentiation. Cells are organized into a series of organ systems that each performs a set of specific functions. Within a specific organ, cell-cell, cell-extracellular matrix, and cell-environment interactions are finely orchestrated to ensure the organ functions properly (Astashkina et al., 2012); furthermore, each organ system interacts with others via mechanical, chemical, and electrical signals to maintain the body in homeostasis. However, when signaling becomes aberrant, or when the body is assaulted with damaging external stimuli and the body cannot return itself to homeostasis, disease results. To better understand human physiology and pathophysiology, and to develop therapeutics directed against pathophysiological targets, researchers and clinicians use a range of *in vitro* and *in vivo* approaches.

Although *in vivo* testing is conducted on whole living organisms, and is therefore thought to more accurately reflect physiological responses, there are many problems and drawbacks associated with this approach including ethical challenges, prohibitive costs (Perkel, 2012), and lack of translatable results from animals to humans (Smith, 1991). *In vitro* testing, on the other hand, takes a reductionist approach by isolating and studying part of an organism in a controlled manner. Cell monocultures, cell co-cultures, and organ explant cultures are all used with varying degrees of success to analyze cell behavior and mechanisms of disease. Although monocultures of cells in polystyrene dishes, especially immortalized cells, are relatively straightforward, it has become apparent that these types of cells are morphologically and physiologically very different from their *in vivo* counterparts (Allen et al., 2005; Donato et al., 2008) and that continual passaging promotes further genetic drift (Yamasaki et al., 2009). On the opposite end of the

spectrum, organ explant cultures maintain the native cell and tissue architecture and are therefore more physiologically relevant; however, they can only be maintained in culture for several days and there is limited ability to deduce the spatial distribution of biomolecules, making it difficult to gain mechanistic insights into physiology and pathophysiology (Astashkina et al., 2012).

The middle ground between these two techniques is to spatially pattern co-cultures of cells; although reductionist in nature, this approach still maintains more complex heterocellular and cell-matrix interactions while also enabling researchers to more easily visualize and analyze cell responses, thereby providing mechanistic insights into cell responses. To this end, microcontact printing (Falconnet et al., 2006), surface topography (Lim et al., 2007), inkjet printing (Ringeisen et al., 2006), microfluidic laminar flow patterning (Takayama et al., 1999; Berthier et al., 2011), and stencil-based patterning (Wright et al., 2007) have all been used. However, these techniques require user expertise, specialized equipment, and may damage cells during the printing process, making them difficult to implement in many laboratory settings.

In contrast to other methods for cell patterning, ATPS cell patterning is easy to learn and only requires rudimentary knowledge about the polymers themselves and the ability to perform cell culture and use a micropipettor. To this end, we have utilized the interfacial properties and partitioning effects of ATPSs to pattern several types of cells (Frampton et al., 2011; Tavana et al., 2010; Tavana et al., 2011a; Tavana et al., 2011b). Here we report a detailed protocol for generating patterned cell cultures using the ATPSs described in our previously-published applications (Frampton et al., 2013). This approach enables the generation of arrays of cell exclusion zones or cell islands for high-throughput migration assays; these techniques can also be combined to rapidly generate co-cultures of cells such as liver-fibroblast cell co-cultures. Patterning methods, ATPS parameters and example results are described.

3.2 Materials and Methods

3.2.1 Construction of Binodal Curves and Cell Compatibility

Cell culture media were enriched with PEG 35 kDa and DEX 500 kDa to various starting concentrations of each in 50 ml conical tubes (Figure 3.1, red circles). Solutions were gently rocked to dissolve polymers, at which point solutions appeared cloudy, indicating that multiple phases were present in solution. Polymer solutions in conicals were then incubated in a vertical position at room temperature for 20 min to verify phase separation occurred and two phases co-existed. Additional media was incrementally added to the conicals and the process of mixing and equilibrating was repeated until the solution no longer appeared cloudy and no longer phase-separated when incubated in the vertical position, indicating that the threshold for phase separation had been reached. Based on the initial masses of the added polymers as well as the final mass of the solution after adding media, the weight percentage of each polymer at which phase separation no longer occurred was calculated. This process was repeated for various initial starting concentrations, and final weight percentages of DEX and PEG were plotted on the x- and y-axes and fit with a 3-parameter rational function to describe the binodal curves.

Based on the binodal curves that were achieved for PEG 35 kDa and DEX 500 kDa, the critical point concentrations (the combination of lowest concentrations of polymers that still enable the formation of an ATPS) of each polymer were determined. The critical point concentrations and 2x and 3x critical point concentrations were then tested for their effects on cell morphology, serum precipitation, and ability to robustly pattern cells.

3.2.2 Monoculture Patterning and Cell Migration Analysis

To demonstrate exclusion patterning (Figure 3.2, left), first, separate polymer solutions of 5.0% wt/wt PEG and 12.8% wt/wt DEX in DMEM were prepared. HeLa cells were labeled with CellTracker™ Green (C2925, Molecular Probes), pelleted, and resuspended in PEG solution to a concentration of 375,000 cells/ml. Using a micropipettor, 0.5 μl droplets of DEX were pipetted into the bottom of a 48-well plate in 2x2 array format and dehydrated at room temperature. Following dehydration, 200 μl cell suspension in PEG was pipetted into each well of a 48-well plate and incubated in a humidified 5% CO_2 incubator at 37 ˚C for 12 h to allow cell attachment. Following cell adherence, polymer solutions were aspirated from each well, wells were washed three times with PBS, and 400 μl fresh growth medium was added to each well. Cells were returned to the incubator and monitored over the course of 72 h and fluorescent images were acquired at 24 h intervals to analyze closure of the circular void area.

To demonstrate island patterning (Figure 3.2, middle), first separate polymer solutions of 5.0% wt/wt PEG and 12.8% wt/wt DEX in DMEM were prepared. HeLa cells were labeled with CellTracker™ Red (C34552, Molecular Probes), pelleted, and resuspended in DEX solution to a concentration of 10,000 cells/μl. Using a micropipettor, 0.5 μl droplets of cell suspension in DEX were pipetted into the bottom of a 48-well plate in 2x2 array format. To prevent dehydration, 200 μl PEG solution was immediately and gently added to each well so as not to disrupt the DEX droplets. Plates were then incubated in a humidified 5% CO_2 incubator at 37 ˚C for 12 h to allow cell attachment. Following cell adherence, polymer solutions were aspirated from each well, wells were washed three times with PBS, and 400 μl fresh growth medium was added to each well. Cells were returned to the incubator and monitored over the course of 72 h, with fluorescent images being acquired at 24 h intervals to analyze expansion of the cell area. In

each instance, fluorescent images were acquired using a Nikon TE300 microscope and images were analyzed using ImageJ.

3.2.3 Co-Culture Patterning and Hepatocyte Albumin Production

To demonstrate the ability to use ATPS to achieve robust co-cultures (Figure 3.2, right), the techniques for exclusion- and island-patterning were combined. Like before, separate polymer solutions of 5.0% wt/wt PEG and 12.8% wt/wt DEX in DMEM were prepared. For proof of concept, 1 group of HeLa cells was labeled with CellTracker^{TM} Green (C2925, Molecular Probes), pelleted, and resuspended in PEG solution to a concentration of 375,000 cells/ml, while a 2nd group was labeled with CellTracker^{TM} Red (C34552, Molecular Probes), pelleted, and resuspended in DEX to a concentration of 10,000 cells/µl. Using a micropipettor, 0.5 µl droplets of red-labeled cell suspension in DEX were pipetted into the bottom of a 48-well plate in 2x2 array format. Immediately thereafter, 200 µl green-labeled cell suspension in PEG was pipetted into each well of a 48-well plate and incubated in a humidified 5% CO_2 incubator at 37 ˚C for 12 h to allow cell attachment.

In a separate demonstration more relevant to cell functionality, the same approach as above was used with slight modifications. HepG2/C3A (HB8065, ATCC) hepatocytes were pelleted and resuspended in DEX to a concentration of 10,000 cells/µl. A second cell type, NIH 3T3 fibroblasts (CRL1658, ATCC), was growth arrested for 2 h with 10 µg/ml mitomycin C (M4287, Sigma); this step was necessary due to the rapid proliferation of this cell type to prevent it from overgrowing the HepG2/C3A cells. They were then pelleted and resuspended in PEG to a concentration of 750,000 cells/ml. Using a micropipettor, 0.5 µl droplets of hepatocyte cell suspension in DEX were pipetted into a 3x3 array in a 35 mm dish. Immediately thereafter,

either 1 ml fibroblasts in PEG or 1 ml PEG alone were added to the dish and incubated in a humidified 5% CO_2 incubator at 37 ˚C for 12 h to allow cell attachment. After 24, 48, and 96 h, cells were fixed in 4% paraformaldehyde (19943, Affymetrix) for 15 min at room temperature, washed, permeabilized with 0.1% Triton X-100 (T9284, Sigma) for 15 min at room temperature, incubated with horseradish peroxidase-conjugated goat anti-human albumin (E80-129, Bethyl Laboratories) for 2 h, washed, and finally incubated with diaminobenzidine (750118, Novex) to develop color. Dishes were then imaged with brightfield microscopy on a Nikon SMZ8000 stereomicroscope.

3.3 Results and Discussion

3.3.1 Construction of Binodal Curves and Cell Compatibility

Based on results from the cloud point method experiments, 6 binodal curves were constructed for the following common media: DMEM, DMEM+10% fetal bovine serum (FBS), F12, F12+10% FBS, RPMI, and RPMI+10% FBS (Figure 3.1). As can be seen, in this case the binodal curves were nearly the same for all media used; however, it is important to determine this experimentally since the characteristics of the binodal curve are dependent on polymer characteristics as well as temperature, pH and ionic content.

From previous work, it was determined that the critical concentrations for PEG 35 kDa and DEX 500 kDa were 2.5% w/w and 3.2% w/w, respectively. Based on these critical concentrations, we tested nine phase system combinations for patterning, as shown in Table 1. When combining separate solutions enriched with PEG and DEX, there is a small flux of each polymer to the opposite phase as the system equilibrates. Therefore, after some combinations of PEG and DEX were combined, they did not form stable ATPSs and were therefore not useful for

patterning (Table 1A, x). Other polymer combinations produced recognizable patterns of cells, but were not uniform enough for experimentation (Table 1A, x/√). Useful polymer formulations formed exclusion zones or islands that were nearly devoid of cells in the non-patterned regions (Table 1a, √).

In addition to patterning capabilities, polymer effects on cell morphology and serum precipitation were analyzed. At 10% PEG, cell morphology was abnormally spindle-like after 24 h, and cells had a diminished ability to attach to the culture surface (Table 1B, x); on the other hand, morphology and attachment were normal for 2.5% and 5% PEG (Table 1b, √). At 10% PEG, serum also precipitated from the culture medium (Table 1C, x), suggesting that abnormal cell morphology and attachment in 10% PEG may be related to problems with access to serum.

Based on these results, combinations of 5% PEG/6.4% DEX and 5% PEG/12.8% DEX were considered well suited for cell patterning; however, 12.8% DEX produced more uniform cell patterning and was therefore selected for further experiments.

3.3.2 Monoculture Patterning and Cell Migration Analysis

Using the aforementioned patterning techniques, patterned monocultures of cells were successfully achieved. Exclusion- and island-patterned cells were assessed for proliferation and migration over 3 d (Figure 3.3). After 3 d, HeLa cells closed exclusion zones to approximately 1/3 their initial size (Figure 3.3 A-C), while island-patterned HeLa cells expanded outward from their initial area by approximately 50% (Figure 3.3 D-F).

Although not performed here, it would be easy to extend these types of patterned cell cultures to screen for potential therapeutic compounds. For example, by patterning an array of a single cell type in the island format in a single well, it is possible to consider each of the islands

as an individual sample in the population and therefore increase the statistical power of the test. On the other hand, it would also be possible to pattern islands of cell colonies with different expression profiles. In this format, when a therapeutic compound is applied to a single well, each island would likely respond differently, and researchers could further investigate the cell sub-populations to explain the inconsistencies. This could be especially useful in studies involving rare primary patient samples such as lung cancers; due to the rare nature of these samples, it would be unreasonable to spread them across many wells. Furthermore, because of tumor heterogeneity, cells from different locations within the tumor will respond dissimilarly to therapeutics and biomolecules. By using an ATPS patterning technique, researchers could conserve samples and further investigate differences in responses of cell and/or tissue subpopulations to treatments.

3.3.3 Co-Culture Patterning and Hepatocyte Albumin Production

Island and exclusion patterning techniques were successfully combined to create patterned co-cultures of HepG2/C3A cells, a hepatocellular carcinoma cell line that is commonly used to model hepatocyte biology, and NIH 3T3 fibroblasts that were growth-arrested with mitomycin C (Figure 3.4). Over 4 d, hepatocytes maintain their localization and colony shape (Figure 3.4 A). By placing an array of DEX droplets in the same plate and surrounding them with fibroblasts, it is possible to grow these cells in a format that is potentially useful for multiplexed and/or high throughput studies (Figure 3.4 B). Staining for albumin, a marker of hepatocyte functionality, was performed for hepatocytes patterned in monoculture in the island format as well as hepatocytes island-patterned among a layer of fibroblasts (Figure 3.4 C). Although qualitative in nature, albumin staining suggests that the hepatocytes in the co-culture

format are healthier and more functional, which could be attributed to the more physiologic juxtacrine signaling and cellular organization within the dish.

This brief demonstration highlights the potential future capabilities of this technique in drug screening and tissue engineering. In terms of drug screening, co-culture patterning can be used to create better organ-mimetic systems with more physiologically relevant signaling and responses to external stimuli. By using such platforms early in the screening process, researchers can make more informed decisions regarding a compound's potential future efficacy and off-target effects, thereby enabling more successful translation in clinical trials. This method may also be effective in tissue engineering strategies to enable researchers to easily pattern multiple cell types in physiologically-relevant configurations that optimize cell-cell and cell-matrix interactions to promote regeneration and/or restore function in diseased tissues.

3.4 Conclusions

An ATPS of PEG 35 kDa and DEX 500 kDa was characterized in terms of binodal curves for 6 different media types; varying concentrations of these polymers in DMEM were used to analyze their ability to effectively pattern cells, their effect on cell morphology, and their effect on serum solubility and precipitation. It was determined that 10% PEG was not useful for patterning cells due to its negative impact on cell morphology and tendency to precipitate serum out of solution. On the other hand, 2.5% PEG was also not useful for patterning due to the fact that it often resulted in poorly-defined patterns of cells. Therefore, a polymer combination of 5% PEG and 12.8% DEX was selected for further patterning demonstrations, such as exclusion and island patterning of HeLa cells and co-culture patterning of HepG2/C3A and NIH3T3 cells. Patterned HeLa cells were analyzed for proliferation and migration over time and it was

demonstrated that for exclusion patterning, the void area decreases, while for island patterning the cell area increases. Co-cultures of HepG2/C3A hepatocytes and NIH3T3 fibroblasts seemed to result in greater albumin production by hepatocytes, suggesting that patterned co-cultures may be more physiologically relevant than hepatocytes patterned in monoculture.

Aqueous two-phase patterning of cells is simple and easily adapted to almost any biological laboratory setting. This method allows any researcher with access to a typical cell culture lab (access to a hood, CO_2 incubator, and micropipettes) and the aforementioned polymers to reproducibly pattern cells in monoculture and co-culture. This is in contrast to other patterning techniques, such as patterning of extracellular matrix (Johnson et al., 2011), inkjet printing (Moon et al., 2007), and patterning by laminar flow in microfluidic devices (Takayama et al., 1999), which are technically challenging, require expensive and specialized equipment, and also may necessitate access to cleanroom facilities, making them burdensome to adopt in many labs.

Although ATPS patterning can be easily performed using a micropipette (as presented here), it can also be implemented with automated printing equipment to facilitate rapid generation of more complex, more precise, and/or higher throughput arrays (e.g., liquid handling robots and acoustic droplet ejection). For example, researchers can add small molecules that modulate cell proliferation and/or migration to wells containing an array of island-patterned cells or an array of exclusion voids; in doing so, researchers would have a substantially larger sample size, thereby allowing them to reach statistical significance with fewer iterations of testing and less consumption of extremely expensive biologics and small chemical compounds. Furthermore, it is conceivable that many subpopulations of cells could be cultured with a common feeder layer to investigate the impact of paracrine and juxtacrine signaling of many cell types grown together

in a single cell culture setup. Finally, tissue engineering applications frequently required spatial localization of one or more cell types. It may be possible to adapt this technique for use in patterning cells in order to produce more physiologically relevant tissue engineered disease models or to pattern cells on implantable materials for clinical applications. This would be especially interesting in drug discovery, where researchers seek techniques and/or assays whose results translate to actual human physiological responses and could be used to make earlier go/no go decisions regarding the pursuit of potential therapeutic compounds.

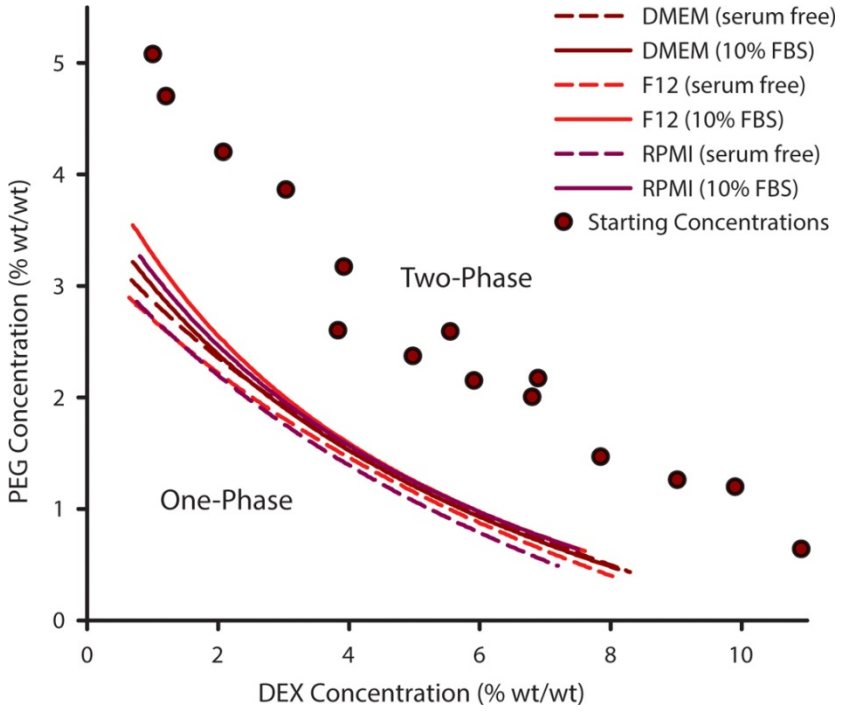

Figure 3.1: Binodal curves for serum-free and serum-enriched media. The polymer concentrations at which an ATPS can form can be extrapolated from experimentally determined binodal curves. Solutions with polymer concentrations above and to the right of the curves form two phases, while those below and to the left form one phase. These binodal curves were constructed using the cloud point method by preparing concentrated starting solutions of PEG and DEX (red circles) and diluting them with the appropriate media. Points on the binodal curve are determined when solutions no longer phase separate. Data points were fit with a 3-parameter rational function. N=3 for each data point.

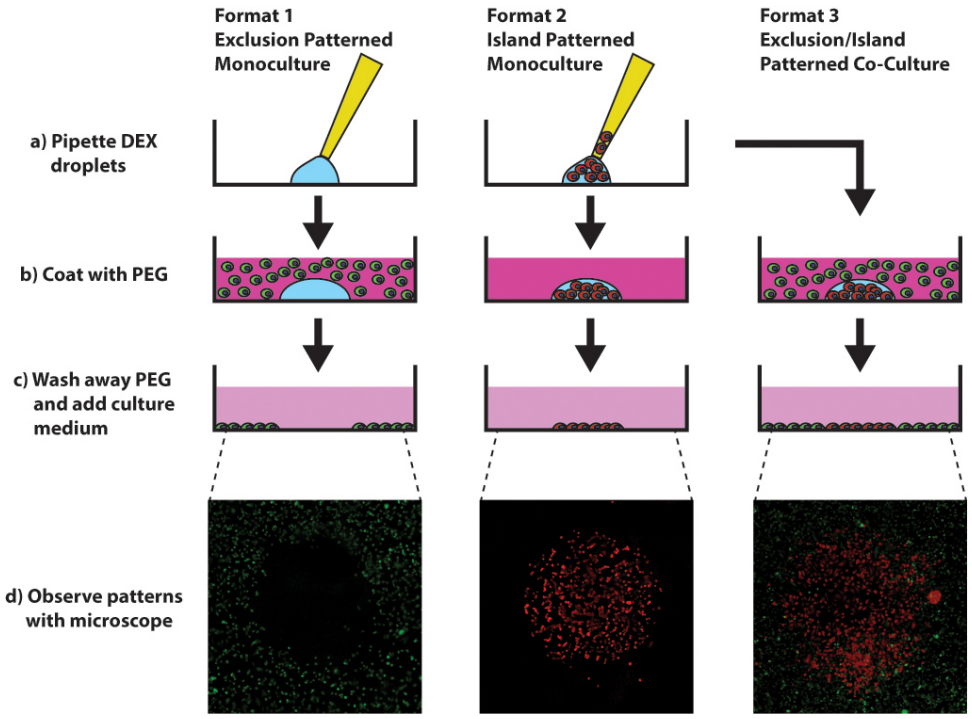

Figure 3.2: ATPS patterning techniques of cells. A) DEX droplets are pipetted onto the surface of a polystyrene dish without cells (left) or with cells (middle, right). B) PEG with cells (left, right) or without cells (middle) is then added over top of the DEX droplets. C) After overnight incubation, polymer solutions are washed away and dishes are filled with growth medium. D) Depending on the selected format, cells will be exclusion-patterned (left), island-patterned (middle), or combined into co-culture format (right). In these images, HeLa cells were stained with CellTracker dyes to track pattern formation.

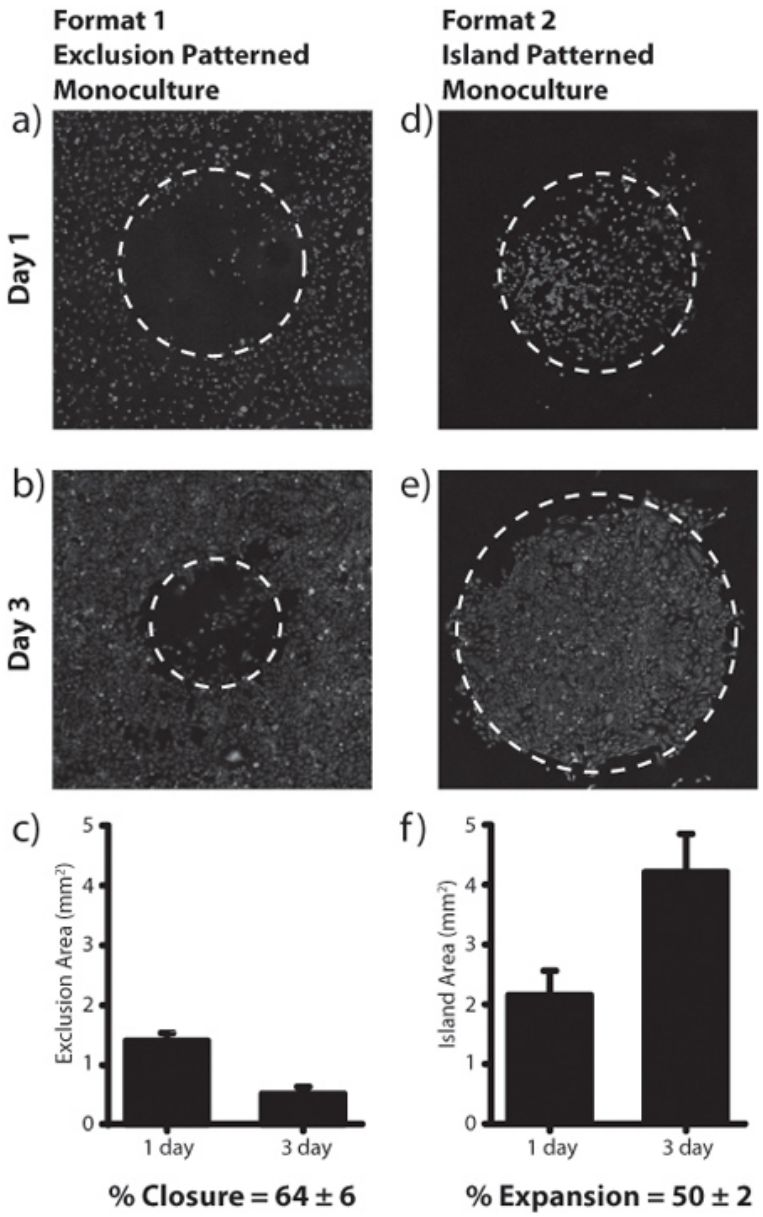

Figure 3.3: Migration and proliferation of monocultures of patterned cells. A) Exclusion-patterned HeLa cells 1 day after patterning. B) Exclusion patterned HeLa cells 3 days after patterning. C) Cells proliferate and migrate, significantly reducing the size of the exclusion zone. D) Island-patterned HeLa cells 1 day after patterning. E) Island-patterned HeLa cells 3 days after patterning. F) Cells proliferate and migrate outwards, significantly expanding the size of the island. Images were quantified using ImageJ software to measure the cell clearing and cell island areas before and after migration. Bars represent mean ± SEM of at least three independent observations.

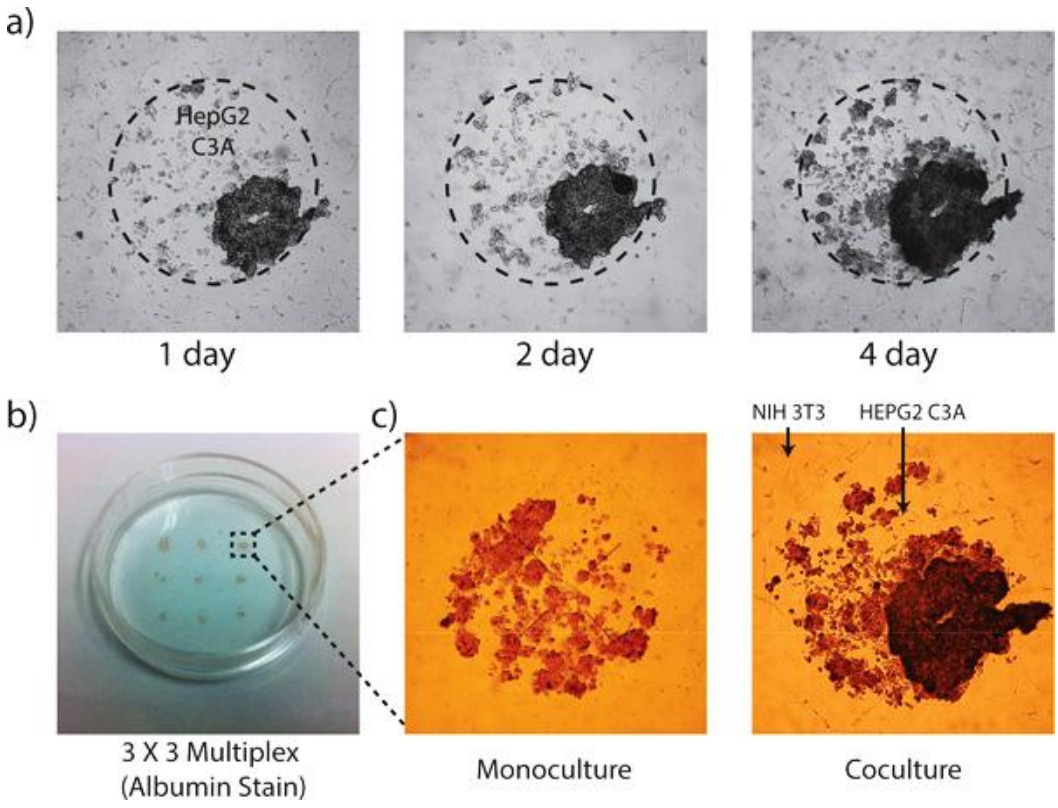

Figure 3.4: Albumin production from patterned hepatocytes in monoculture and co-culture. A) HepG2/C3A remain viable for at least 4 days in culture. B) A 3x3 array of hepatocyte islands were patterned among a sheet of growth-arrested NIH 3T3 fibroblasts. Multiple islands can be arrayed in a single dish with potential for multiplexed or high throughput assays. C) Compared to non-co-cultured island patterns, the co-cultured cells seem to display slightly higher levels of albumin production (brown staining), as evident from qualitative comparison of albumin staining of co-cultures versus monocultures.

a) Pattern Formed	DEX 3.2 %	DEX 6.4 %	DEX 12.8%
PEG 2.5%	x	x	x
PEG 5.0%	x/✓	✓	✓
PEG 10.0%	x/✓	✓	✓

b) Morphology	DEX 3.2 %	DEX 6.4 %	DEX 12.8%
PEG 2.5%	✓	✓	✓
PEG 5.0%	✓	✓	✓
PEG 10.0%	x	x	x

c) Serum Precipitation	DEX 3.2 %	DEX 6.4 %	DEX 12.8%
PEG 2.5%	✓	✓	✓
PEG 5.0%	✓	✓	✓
PEG 10.0%	x	x	x

Table 3.1: Patternability of ATPSs. A) ATPS formulations that can be used for patterning are indicated by √, those that cannot are indicated by x, and those that form poorly-defined patterns are indicated by x/√. B) Formulations that retain normal cell morphology and attachment properties are indicated by √, those that cannot are indicated by x. C) Formulations that resulted in precipitation of serum proteins are indicated by x.

3.5 References

Allen, D.D., R. Caviedes, A.M. Cardenas, T. Shimahara, J. Segura-Aguilar, and P.A. Caviedes. Cell lines as in vitro models for drug screening and toxicity studies. *Drug Dev. Ind. Pharm.* **31**, 757-768.

Astashkina, A., B. Mann, and D.W. Grainger. A critical evaluation of in vitro cell culture models for high-throughput drug screening and toxicity. *Pharmacol. Ther.* **134**, 82-106 (2012).

Berthier, E., J. Warrick, B. Casavant, and D.J. Beebe. Pipette-friendly laminar flow patterning for cell-based assays. *Lab Chip* **11**, 2060-2065 (2011).

Donato, M.T., A. Lahoz, J.V. Castell, and M.J. Gomez-Lechon. Cell lines: a tool for in vitro drug metabolism studies. *Curr. Drug Metab.* **9**, 1-11.

Falconnet, D., G. Csucs, H.M. Grandin, and M. Textor. Surface engineering approaches to micropattern surfaces for cell-based assays. *Biomaterials* **27**, 3044-3063(2006).

Frampton, J.P., D. Lai, H. Sriram, and S. Takayama. Precisely targeted delivery of cells and biomolecules within microchannels using aqueous two-phase systems. *Biomed. Microdev*., **13**, 1043-1051 (2011).

Frampton, J.P., J.B. White, A.T. Abraham, and S. Takayama. Cell co-culture patterning using aqueous two-phase systems. *J. Vis. Exp*. **73**, e50304, doi:10.3791/50304 (2013).

Johnson, D.M., N.A. LaFranzo, and J.A. Maurer. Creating two-dimensional patterned substrates for protein and cell confinement. *J. Vis. Exp.*, **55**, e3164, doi: 10.3791/3164 (2011).

Lim, J.Y. and H.J. Donahue. Cell sensing and response to micro- and nanostructured surfaces produced by chemical and topographic patterning. *Tissue Eng*., **13**, 1879-1891 (2007).

Moon, S., P.-A. Lin, H.A. Keles, S.-S. Yoo, and U. Demirci. Title cell encapsulation by droplets. *J. Vis. Exp.*, **8**, 316, doi: 10.3791/316 (2007).

Perkel, J.M. Animal-free toxicology: sometimes, in vitro is better. *Science Life Sci. Tech.* DOI: 10.1126/science.opms.p1200062 (2012).

Ringeisen, B.R., C.M. Othon, J.A. Barron, D. Young, and B.J. Spargo. Jet-based methods to print living cells. *Biotechnol. J.*, **1**, 930-948 (2006).

Smith, D.A. Species differences in metabolism and pharmacokinetics: are we close to an understanding? *Drug Metab. Rev.* **23**, 355-373 (1991).

Takayama, S., J.C. McDonald, E. Ostuni, M.N. Liang, P.J. Kenis, R.F. Ismagilov, and G.M. Whitesides. Patterning cells and their environments using multiple laminar fluid flows in capillary networks. *PNAS* **96**, 5545-5548 (1999).

Tavana, H., B. Mosadegh, and S. Takayama, Polymeric aqueous biphasic systems for non-contact cell printing on cells: engineering heterocellular embryonic stem cell niches. *Adv. Mater.*, **22**, 2628-2631 (2010).

Tavana, H., B. Mosadegh, P. Zamankhan, J.B. Grotberg, and S. Takayama, Microprinted feeder cells guide embryonic stem cell fate. *Biotechnol. Bioeng.*, doi: 10.1002/bit.23190 (2011a).

Tavana, H., K.K. Kaylan, T. Bersano-Begey, K.E. Luker, G.D. Luker, and S. Takayama. Rehydration of Polymeric, Aqueous, Biphasic System Facilitates High Throughput Cell Exclusion Patterning for Cell Migration Studies. *Adv. Func. Mat.*, **21**, 2920-2926 (2011b).

USDA Annual Report. Animal Usage by Fiscal Year (2010).

Wright, D., B. Rajalingam, S. Selvarasah, M.R. Dokmeci, and A. Khademhosseini. Generation of static and dynamic patterned co-cultures using microfabricated parylene-C stencils. *Lab Chip* **7**, 1272-1279 (2007).

Yamasaki, K., S. Kawasaki, R.D. Young, H. Fukuoka, H. Tanioka, M. Nakatsukasa, A.J. Quantock, and S. Kinoshita. Genomic aberrations and cellular heterogeneity in SV40-immortalized human corneal epithelial cells. *Invest. Ophthalmol. Vis. Sci.* **50**, 604-613.

Chapter 4

Aqueous-Two Phase Localization of Trypsin for *in vitro* Cell Migration Assays

This chapter describes the development and application of an ATPS for *in vitro* wound assays that is free of cell damage and can be implemented in a variety of cell culture settings. The process localizes trypsin to small regions on a monolayer of cells, and subsequent trypsin digestion and washing results in circular wound areas into which cells proliferate and migrate. A fluorescein isothiocyanate (FITC)-conjugated casein assay was utilized to detect trypsin activity and partition characteristics in various ATPSs. Although several ATPSs were investigated, a PEG/DEX ATPS was selected as the base system with which to perform subsequent *in vitro* trypsinization. *In vitro* wound assays were performed on A549 cells cultured in 6-well plates and 6-well transwells. The contact-free nature of the ATPS enables the system to be applied to new and more physiologically relevant substrates such as transwell inserts and potentially soft gels; furthermore, the flexibility with which the system can be implemented and its ease of use open the possibility for this system to be scaled to high-throughput screening applications.

4.1 Introduction

Cell migration is important in many physiological phenomena including developmental morphogenesis, immune response, and wound healing. During these processes, cells respond to extracellular directional stimuli in their environment and transduce those signals into intracellular responses that lead to migration. Single cell i*n vitro* assays, such as microfluidic gradient generators (Irimia et al., 2006) and constant-source micropipettes (Xu et al., 2005), often analyze rapid (seconds to minutes) cellular responses to changes in applied gradients of chemoattractants such as cell polarization and intracellular gradient formation of molecules involved in migration (Sawano et al., 2002; Williams et al., 2003). Although these types of assays provide useful information regarding the underlying signaling mechanisms of cell polarization and migration, *in vitro* collective cell migration assays may be better indicators of actual cell behavior *in vivo*.

In vitro collective cell migration assays, which are often monitored over hours or even days, create void areas in a monolayer of cells, which are then closed as cells migrate into the empty space. The *in vitro* scratch assay, which uses a pipette tip to scratch a cell monolayer and remove cells, is one of the most commonly used assays for this purpose (Liang et al., 2007). Because this approach kills cells, causing them to release unknown cytosolic factors into the surrounding medium (which can alter cell migration characteristics in an uncontrolled manner), and because this assay requires large numbers of cells and has limited reproducibility (Tavana et al., 2011), numerous other approaches that circumvent these problems have been developed: a circular invasion assay that removes cells with a rotating silicon tip (Kam et al., 2008), electroporation of a circular area of cells (Keese et al., 2004), mechanical stencil patterning

(Poujade et al., 2007), microfluidics patterning (Irimia and Toner, 2009) and laminar flow-based trypsin digestion (Murrell et al., 2011), and aqueous two-phase exclusion patterning (Tavana et al., 2011).

Although many of these approaches are useful, they are generally performed on polystyrene dishes or glass slides, which have elastic moduli values in the megapascal and gigapascal range (Lee et al., 2004). However, the only *in vivo* organ that has this type of stiffness is bone (Rho et al., 1993), while other organs such as skin, brain, muscle and lungs have elastic moduli values in the low kilopascal range (Kaster et al., 2011; Liu and Tschumperlin, 2011; Diridollou et al., 2000; Engler et al., 2004). The need to perform wound healing assays extends from soft surfaces to other non-conventional culture platforms such as transwells, which are used to culture epithelial cells at an air-liquid interface (ALI) to achieve polarization, ciliation, differentiation, and formation of tight junctions that best mimic *in vivo* environments (Ross et al., 2007; Dvorak et al., 2011; Wong et al., 2012); unfortunately, many of the aforementioned techniques cannot be incorporated into a transwell setup.

To overcome these limitations, we developed an *in vitro* wound assay that utilizes an aqueous two-phase system (ATPS) of polyethylene glycol (PEG) and dextran (DEX). The assay is based on the following principles: aqueous PEG and DEX solutions remain immiscible due to polymer incompatibility; when droplets of the denser DEX phase are pipetted into a dish containing PEG solution, they sink to the bottom of the dish where they are held in place by surface tension forces between the two aqueous solutions and the substrate; and trypsin is enriched into the DEX phase where it locally digests cell-cell and cell-substrate interactions, which, upon washing, creates a small circular void into which cells around the periphery can

migrate. This method is applied to traditional cell culture dishes and transwells to demonstrate its ability to be applied to multiple cell culture substrates.

4.2 Materials and Methods

4.2.1 Identification of ATPS for Localized Trypsinization

ATPS solutions were formulated from PEG 35 kDa (81310, Sigma), DEX 500 kDa (DEXT500, Pharmacosmos), and sodium citrate (CIT) (C7254, Sigma). Polymers and salts were added to PBS and mixed overnight on a rocking stage to fully dissolve the reagents into solution. For solutions consisting of PEG, DEX, or CIT alone, solutions were enriched to 5, 10, 20, and 30% w/w of individual reagents. For DEX+CIT, the 5% and 10% solutions consisted of 5% w/w and 10% w/w each of DEX and CIT in PBS, respectively. In a 96-well plate, 200 µl PEG solution was added to wells, followed by manual pipetting of 0.5 µl droplets of DEX or DEX+CIT solution. Wells were visualized with a Nikon ECLIPSE TE300 microscope over time to analyze droplet morphology and spreading.

4.2.2 FITC-Casein Assay to Analyze Trypsin Activity and Partitioning

A modified version of a previously described FITC-casein protocol was utilized to analyze trypsin activity and trypsin partitioning (Twining, 1984). First, assay performance was verified by testing PBS solutions with various pH values. FITC-casein (C2990, Molecular Probes) was reconstituted to 10 mg/ml in PBS and then further diluted to 2.5 mg/ml in PBS that was pH-adjusted with NaOH or HCl to values of 6, 7, 8, 8.5, and 9. Trypsin (T9935, Sigma) was reconstituted to 5 mg/ml in PBS with the same pH values as FITC-casein. In a 96-well U-bottom plate, 10 µl FITC-casein was added to 10 µl PBS and 5 µl trypsin solution (final trypsin concentration 1 mg/ml) (all with the same pH) (Figure 4.1 A). Wells were incubated for 0, 30, 60, 180, 300, and 600 s, at which point the trypsin-FITC-casein reaction was neutralized by

adding 5% trichloroacetic acid (TCA) (BP555, Fisher) (Figure 4.1 B). Liquid was transferred from the 96-well plate to 200 µl tubes, which were centrifuged for 10 min at 9,300 rcf to pellet the unreacted FITC-casein (Figure 4.1 C). From the tubes, 60 µl supernatant was diluted 1:10 in pH-matched PBS and stored at 4 ˚C overnight; the following day, 60 µl of this solution was added to a 96-well plate, which was analyzed at excitation and emission wavelengths of 485 nm and 535 nm, respectively, on a Biotek Synergy Neo HTS Multi-Mode Microplate Reader (Figure 4.1 D).

Trypsin partitioning was analyzed in a similar fashion to the calibration outlined above, with slight modifications. First, baseline trypsin activity was determined for 5%, 10%, and 15% solutions of the following solutions: PEG, DEX, CIT, and DEX+CIT. All solutions were prepared in PBS and pH values were adjusted to 7 using NaOH or HCl. In a 96-well plate, 25 µl test solution was added to each well: 15 µl appropriate polymer solution containing 0.2 mg/ml trypsin and 10 µl FITC-casein. Wells were again incubated for 0, 30, 60, 180, 300, and 600 s, neutralized with 5% TCA; liquid was transferred to 200 µl tubes, centrifuged, and supernatant was diluted 1:10, which was then analyzed at excitation and emission wavelengths of 485 nm and 535 nm, respectively. Once baseline values were determined, ATPS trypsin partitioning was measured. First, the following ATPSs were prepared: 5% PEG/DEX, 10% PEG/DEX, 5% PEG/DEX+CIT, 10% PEG/DEX+CIT, 15% PEG/DEX+CIT (percent refers to the weight percentage of each polymer/salt in solution), each of which were enriched with 0.2 mg/ml trypsin (Figure 4.2 A). Solutions were thoroughly mixed and then allowed to equilibrate at room temperature for 30 min, followed by centrifugation for 10 min at 9,300 rcf (Figure 4.2 B). From the phase separated ATPSs, 15 µl was pipetted from each phase and added to a 96-well plate with 10 µl FITC-casein (Figure 4.2 C). The remaining steps including incubation, neutralization,

centrifugation (Figure 4.2 D), and acquisition of fluorescent readouts (Figure 4.2 E) were the same as above.

4.2.3 Wound Closure by A549 Cells in Polystyrene Dishes and Transwell Inserts

A549 cells were maintained in F12 medium supplemented with 10% FBS (12306C, Sigma) and 1% anti-anti (15240-062, Gibco) in a 5% CO_2 37 ˚C incubator. Cells tested in 6-well polystyrene dishes were seeded at 20% confluence and grown to confluence over 5 days with medium changes every 48 h. Cells tested in 6-well transwell inserts were seeded at 2 different densities based on pre-wounding conditions. For cells maintained in submersion, cells were cultured in the same way as those in polystyrene dishes; however, for cells that were switched to ALI culture, cells were seeded at 75% confluence and grown to confluence over 2 days (Figure 4.3 A), at which point media was aspirated from the apical chamber of the transwell and cells were maintained for a further 3 days at ALI (Figure 4.3 B). For ALI-cultured cells, media was changed every 48 h, and once cells were switched to ALI culture, apical chambers were washed daily with PBS.

After 5 days of culture, wounding was performed by applying ATPS to localize trypsin to specific regions on the cell monolayer (Figure 4.3 C). First, wells were aspirated to remove media and then washed with PBS. Wells were then filled with 2 ml of solution consisting of PBS enriched with 10% w/w PEG 35 kDa and 10% v/v FBS; in the case of transwells, the basal chamber was filled with PBS. Next, 0.5 µl droplets of 10% w/w DEX 500 kDa enriched with 10 mg/ml trypsin (85450C, Sigma) were dispensed in a 3x3 array into wells using a Matrix MultiChannel Equalizer Pipette (Thermo Scientific), at which point they were incubated in a 5% CO_2 37 ˚C incubator to facilitate trypsin digestion. Upon removal from the incubator, 2 ml PBS

was vigorously added to each well to disrupt the ATPS and neutralize the localized reaction; this solution was quickly aspirated and 2 ml PBS was added back into each well and manually pipetted to facilitate the complete removal of cells from the locally digested areas (Figure 4.3 D). Wells were again aspirated to remove PBS, and for cells grown in polystyrene dishes, wells were either re-filled with growth medium or growth medium enriched with 50 ng/ml hepatocyte growth factor (HGF), while for cells grown in transwells, apical chambers were either re-filled with growth medium or maintained at ALI. Media were refreshed daily and wells maintained at ALI were rinsed every day with PBS. Subsequent cell proliferation and migration into the denuded areas were monitored over the course of 3 days (Figure 4.3 E).

Statistical testing was performed using Origin Pro 8.5.1. Student's t-tests were used to compare wound areas and wound closures; results were considered significant at $p<0.05$.

4.3 Results and Discussion

4.3.1 Identification of ATPS for Localized Trypsinization

To effectively create local wound areas in cell monolayers using ATPS, first it was necessary to identify a two-phase system that facilitated the formation of small localized droplet regions that retained their morphology over time. To this end, PEG/DEX, PEG/CIT, and PEG/DEX+CIT systems were tested at various concentrations. The PEG/CIT and PEG/DEX+CIT conditions were included based on a previously-published report that trypsin highly partitioned to CIT and maintained high activity in ATPSs with PEG formulations with molecular weights ranging from 0.6-8 kDa and CIT concentrations between 7 and 15.5% w/w (Tubío et al, 2007).

Although the previous report indicated high levels of trypsin activity and partitioning in a PEG/CIT system, the report utilized bulk solutions that did not require localized droplets to be patterned. Here, the CIT phase was denser than the PEG phase, which caused CIT droplets to sink to the surface of each well; however, after reaching the surface, CIT droplets lost their well-defined dome-like morphology as they continued to spread across the surface of the well (Table 1). As expected, all combinations of PEG/DEX resulted in well-defined formation of DEX droplets in the bottom of each well. Finally, 5% and 10% PEG/DEX+CIT solutions also formed and maintained droplets in wells, but their size was larger than the same weight percentage solutions of PEG/DEX. Based on these results, PEG/DEX and PEG/DEX+CIT solutions were further tested for trypsin activity and partitioning to achieve localize wounding.

4.3.2 FITC-Casein Assay to Analyze Trypsin Activity and Partitioning

A FITC-casein assay with PBS solutions with pH values of 6, 7, 8, 8.5, and 9 was used to verify the potential to use the assay in determining trypsin activity and partitioning. Trypsin has peak enzymatic activity at pH values between 7 and 9 (Bridson and Brecker, 1970), with the maximum occurring near a pH of 8.5 (Kasserra, 1969). The trypsin activity in the FITC-casein assay with different pH solutions follows this trend (Figure 4.4). As can be seen, trypsin incubated in pH 8.5 PBS produced the highest fluorescent signals over time, meaning that trypsin was the most enzymatically active and cleaved more FITC molecules from casein. At pHs of 7, 8, and 9, trypsin activity was slightly lower, while trypsin activity at pH 6 was greatly decreased, likely due to conformational alterations that make the enzymatic site less accessible.

After verifying the utility of the assay in analyzing trypsin activity, it was applied to determine trypsin partitioning in various ATPSs. Normally partitioning is determined by taking

the ratios of concentrations of a biomolecule of interest in the two phases according to the following equation:

$$K = \frac{C_{top}}{C_{bottom}}$$

where K is the partition coefficient and C_{top} and C_{bottom} are the concentrations of the biomolecule in the top and bottom phases, respectively. However, this measurement is generally obtained by directly measuring the biomolecule of interest. In the case of trypsin here, FITC is actually an indirect readout of trypsin concentration; the amount of FITC in solution is dependent on both the activity level of trypsin in solution as well as the amount of trypsin partitioned into the phase of interest:

$$K = \frac{I_{top}}{I_{bottom}} \cdot \frac{A_{bottom}}{A_{top}}$$

where I_{bottom} and I_{top} are the FITC signal intensities from the bottom and top phases, respectively, and A_{bottom}, and A_{top} are the baseline trypsin activities of the enzyme in a single solution of that phase. Using the basic FITC-casein protocol (Figure 4.1), trypsin activity was analyzed for 5%, 10%, and 15% solutions of PEG, DEX, CIT, and DEX+CIT (Figure 4.5 A). Trypsin incubated in PEG and DEX cleaves much less FITC (Figure 4.5 B), while trypsin in CIT or DEX+CIT releases much greater amounts of FITC into solution (Figure 4.5 C); this trypsin activity is quantified by finding the slopes of the linear fits to these data (Table 4.2).

The ATPS FITC-casein assay (Figure 4.2) produced similar plots of FITC vs. time compared to the basic FITC-casein assay (Figure 4.6 A). As can be seen from the magnified graphs of PEG and DEX ATPSs, fluorescent signals produced by PEG and DEX were still much lower than those produced from PBS (Figure 4.6 B). Interestingly, however, in the PEG and DEX+CIT systems, fluorescent signals produced by the PEG phase (green symbols) were

substantially higher than PBS (Figure 4.6 C), while their baseline values were much lower than PBS (Figure 4.5). This suggests that in this system trypsin actually partitions more to the PEG phase, which counteracts the low baseline trypsin activity to increase the signal. Fluorescent signal intensity (a function of trypsin partitioning and baseline activity in the polymer system of interest) was quantified by finding the slopes of the linear fits of these data (Table 4.3).

By combining ratios of fluorescent signal intensities and baseline trypsin activities, as seen in the equation above, partition coefficients were calculated for PEG and DEX and PEG and DEX+CIT ATPSs (Table 4.4). K was approximately 1 for PEG and DEX systems, meaning trypsin equally partitions between phases and essentially distributes based on diffusion alone. Interestingly, it was confirmed that ATPSs of PEG and DEX+CIT resulted in strong partitioning of trypsin into the PEG phase (K>1). Because the goal is to localize trypsin to small droplets of DEX or DEX+CIT that can be used to locally digest cell-cell and cell-matrix interactions to create *in vitro* wounds, it is apparent that these ATPSs cannot be used for this purpose as formulated. Instead, by using a work-around approach and enriching the PEG phase with FBS, droplets of DEX enriched with trypsin can still be dispensed and maintained in a solution of PEG; in this format, the DEX droplets act as a point source of trypsin that locally digests cell attachments in the DEX droplet, and trypsin that diffuses out of the DEX phase is saturated by proteins in FBS, thereby preventing it from digesting cell-cell and cell-matrix interactions in the PEG phase.

4.3.3 Wound Closure by A549 Cells in Polystyrene Dishes and Transwell Inserts

Although trypsin activity was highest in CIT and DEX+CIT solutions, because CIT did not form localized droplets with PEG and because DEX+CIT and PEG ATPSs actually favored

partitioning to the PEG phase, a PEG+DEX ATPS with FBS was pursued to achieve localized wounding. Both 5% and 10% ATPSs were tested with 10 mg/ml trypsin in the DEX phase and 10% FBS in the PEG phase, and both were able to produce wounds in a monolayer of cells (Figure 4.7). Figure 4.7 A shows representative images of cells exposed to a 10% ATPS; although 30 min is a reasonably long incubation time, it is clear that trypsin efficiently digests cell-cell and cell-matrix interactions during this time and that a series of gentle washes dislodges these cells to produce a clean wound area. The far right image is representative of a system in which FBS was not included in the PEG phase. In this case, due to the lack of trypsin partitioning and exclusion of FBS, trypsin digested cell-cell and cell-matrix interactions in the entire well and not just inside the DEX area. In terms of wound area, as expected, due to higher hydrophilicity and lower surface tension between the 5% DEX and PEG solutions, initial wound sizes were larger than their 10% counterparts (Figure 4.7 B). Because the wound areas were unreasonably large, and because the 5% ATPS produced more irregular (less circular) wound areas, the 10% ATPS was used for further testing.

Interestingly, wound areas were significantly different for cells cultured on polystyrene dishes and those cultured on transwell inserts for DEX volumes of 0.5 µl ($p=8.9x10^{-4}$) (Figure 4.7 C). As can be seen, wound areas for cells cultured in 6-well inserts and exposed to 0.5 µl droplets of trypsin-enriched DEX were approximately 2.59 mm^2, while wound areas for cells cultured on transwells were approximately 1.65 mm^2 for the same DEX volume. To achieve similar initial wound areas so as to be able to compare wound closure in transwells and 6-well dishes, it was therefore necessary to dispense 0.7 µl DEX droplets into transwells, which had an average wound area of 2.55 mm^2 and were therefore statistically similar to 0.5 µl droplets in polystyrene dishes ($p=0.56$). These results may be attributed to differences in cell morphology

caused by differences in cell-substrate binding and/or differences in cell surface (glyco)protein expression that modifies DEX interaction with the cell monolayer. However, at larger droplet volumes (1 and 2 µl), initial wound areas were not statistically different between polystyrene dishes and transwells ($p=0.71$, 1 µl; $p=0.10$, 2 µl). At larger volumes, the interactions between the polymer solutions are likely larger than interactions with the cell surface and therefore cause DEX droplets to spread equally across the cell monolayer and create similar wound areas.

After initial wounding, cells proliferate and migrate into the denuded wound area over the course of 72 h (Figure 4.8 A). At 24, 48, and 72 h, wound areas were imaged and later normalized against their respective initial wound areas (Figure 4.8 B). As expected, cells cultured in polystyrene dishes and exposed to 50 ng/ml HGF (+HGF), a chemokinetic and mitogenic factor (To et al., 2002; Skouteris and Schröder, 1996), proliferated and migrated significantly more into the wound area compared to cells cultured in growth medium (Control) ($p=4x10^{-8}$). Interestingly, all cells cultured on transwell inserts (Sub-Sub, Sub-ALI, ALI-Sub, ALI-ALI) closed their respective wound areas more significantly than cells cultured in polystyrene dishes ($p=2.7x10^{-7}$ HGF vs. Sub-ALI; all other $p<2.7x10^{-7}$). Even the cells that were cultured in submersion before wounding and returned to submersion culture after wounding (Sub-Sub), which is most like the conditions in the 6-well plate, closed their respective wound areas more rapidly than those in the 6-well plate (even when stimulated with HGF) ($p=1.3x10^{-9}$ vs. Control; $p=1.8x10^{-9}$ vs. HGF). Furthermore, cells that were cultured at ALI throughout the entire experiment (ALI-ALI) exhibited more complete closure compared to other transwell conditions ($p=0.0012$ Sub-Sub vs. ALI-ALI; all other $p<0.0012$). There are several possible explanations for this observation. First, epithelial cells may undergo phenotypic changes due to culture at ALI that improve their migratory and proliferative capabilities. Second, returning cells

to ALI after wounding means there is an extremely thin layer of fluid over cells; as cells secrete molecules into the apical chamber they become much more concentrated than when cells are returned to submersion culture where they secrete factors into 1 ml or more of culture medium in the apical chamber. Chemokinetic and mitogenic molecules such as trefoil factor family peptides (Oertel et al., 2001) and epidermal growth factor family proteins (Crosby and Waters, 2010) would then be more accessible to cells and more likely to stimulate their migration and proliferation into the wound space.

4.4 Conclusions

Cell migration plays an important role in many physiological processes, and to better understand the cellular mechanisms that underlie cell migration, researchers have developed numerous *in vitro* wound assays that mimic these *in vivo* responses. Unfortunately, many of these assays are performed in unphysiologic environments, such as polystyrene dishes, thereby limiting the conclusions that can be drawn from assay results. Other assays require the use of specialized equipment and skilled operators to perform, which limits their potential adoptability into traditional biological research settings. ATPSs, on the other hand, only require rudimentary knowledge of how to prepare solutions and the ability to use pipettors and can therefore be easily adopted and scaled.

A proof-of-concept for ATPS-based wounding was demonstrated with A549 cells cultured in polystyrene dishes and on transwell inserts. Transwells are important culture vessels in epithelial biology as they enable the differentiation of cells into functional and more physiologically relevant cell monolayers. Unfortunately, many traditional *in vitro* wounding techniques are not amenable to these types of cell culture dishes. Here, we used an ATPS of

trypsin-enriched DEX and FBS-enriched PEG to achieve efficient wounding of A549 cells cultured on transwells. Droplets of DEX applied to cells cultured in polystyrene dishes were larger than those dispensed onto cells cultured in transwells, suggesting that cell morphologies and/or cell surface protein expression may be different and cause differential spreading of DEX. Furthermore, after wounding, cells grown on transwells closed wound areas more rapidly than cells cultured in polystyrene dishes. Interestingly, cells exposed to ALI culture prior to wounding demonstrated faster wound closure compared to cells maintained in submersion culture, suggesting that culture at ALI may induce physiological changes that make cells more migratory and/or proliferative.

To better understand cell behavior and better predict cell responses to external stimuli, it is important to develop next-generation tools and assays that are more physiologically relevant such as transwells and soft gels. This localized ATPS-based trypsinization not only satisfies this criterion, but it is also easily adopted into labs and can be easily scaled to high-throughput formats by interfacing the technique with automated liquid handlers and imaging systems. It will be important to further validate this technique by utilizing primary cells, such as small airway epithelial cells, and by investigating *in vitro* wounding on soft gels so as to better mimic wounding and cell migration in soft environments such as the lungs. In doing so, this next-generation approach could be a potentially useful tool in better understanding cell migration and wound healing. Furthermore, as the technology is further validated and automated, one could envision this approach being a useful and informative tool in pre-clinical testing and high-throughput screening in the development of small molecules and biologics that modulate cell migration.

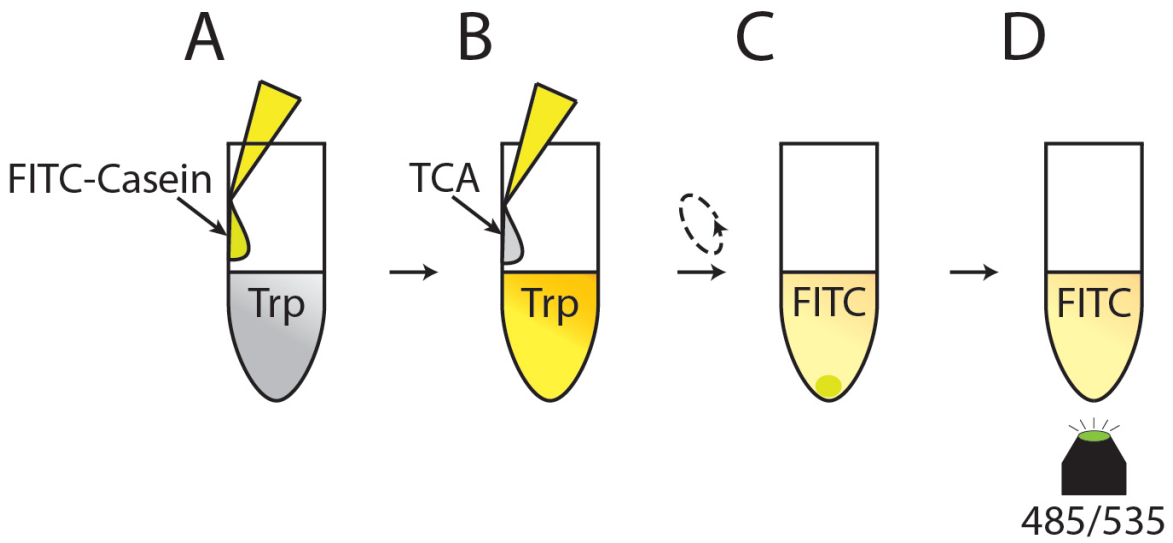

Figure 4.1: FITC-casein assay. A) A single solution of PBS or PBS with polymer is enriched with trypsin. A second solution of FITC-casein is added, mixed, and incubated for a prescribed amount of time. B) As time progresses, trypsin cleaves FITC from casein, thereby releasing it into solution. TCA is added to the solution to neutralize trypsin activity and stop the reaction. C) After centrifuging the reaction vials, unreacted FITC-casein is pelleted into the bottom of the vial, while FITC that was cleaved from casein remains soluble. D) An aliquot of solution containing solubilized FITC is diluted into another vial, which is read on a plate reader at excitation and emission wavelengths of 485 and 535 nm, respectively. The intensity of the fluorescent signal is proportional to the amount of FITC in solution, which is further dependent on the activity level of trypsin (higher trypsin activity results in greater amounts of cleaved FITC).

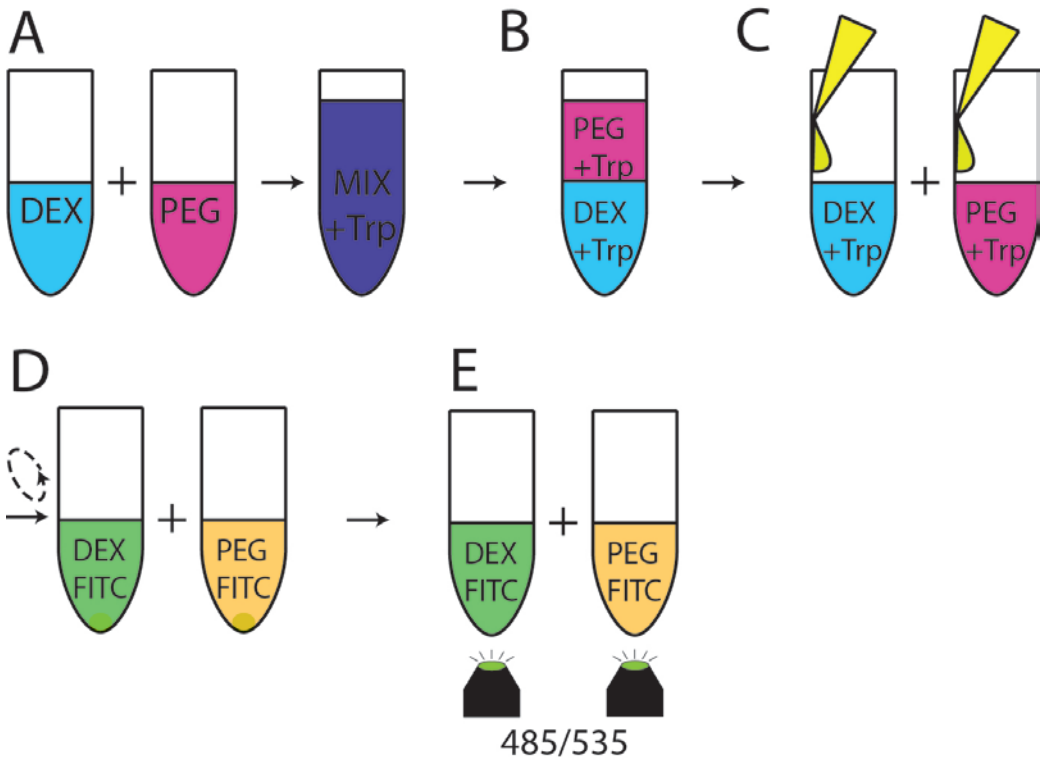

Figure 4.2: ATPS FITC-casein assay. A) In the ATPS FITC-casein assay, individual polymers and trypsin are first mixed together into a homogeneous solution. B) After centrifugation, the solution equilibrates into two distinct phases. Based on the physicochemical characteristics of the phase system and trypsin, trypsin may or may not partition to one phase over the other. C) Individual polymer solutions, which contain the partitioned trypsin, are separated into separate microcentrifuge tubes and each is further enriched with FITC-casein. As before, trypsin cleaves FITC from casein over time and releases it into solution; at the time point of interest, TCA is again added to neutralize the reaction (not shown). D) Centrifugation pellets the unreacted FITC-casein, leaving the reacted and solubilized FITC in solution. E) As before, aliquots containing solubilized FITC are diluted into another vial, which are read on a plate reader at excitation and emission wavelengths of 485 and 535 nm, respectively. Similar to the basic FITC-casein assay, the intensity of the fluorescent signal is proportional to the amount of FITC in solution. Unlike the basic FITC-casein, however, the amount of FITC in solution is dependent on both the activity level of trypsin in solution as well as the amount of trypsin partitioned into the phase of interest.

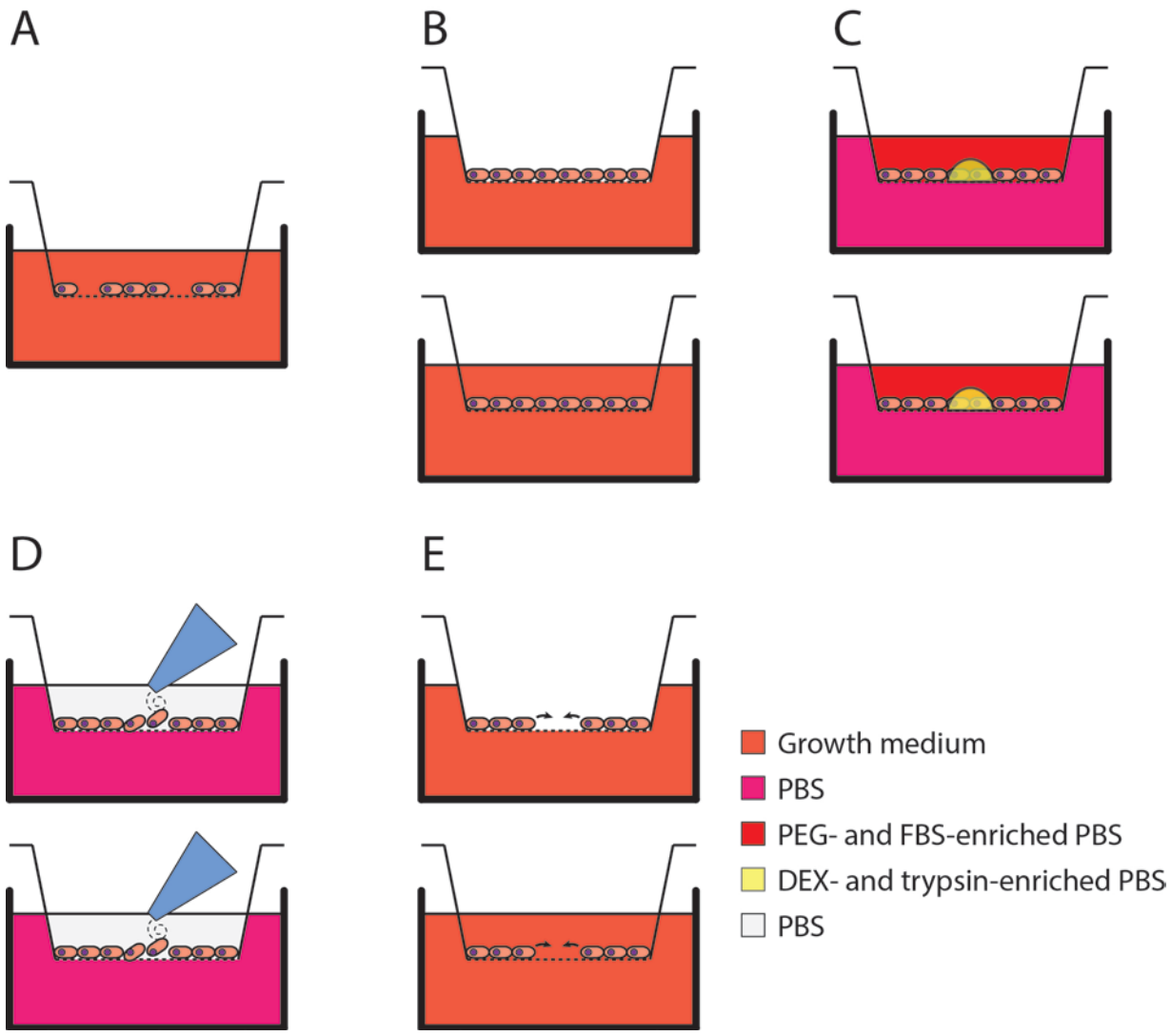

Figure 4.3: Schematic of ATPS-trypsin wound assay. A) Cells are seeded and maintained in submersion culture until they reach confluence. B) Upon reaching confluence, cells can be switched to ALI culture or maintained in submersion culture. C) After rinsing the dish with PBS, an ATPS of PEG and DEX is applied to locally digest cell-cell and cell-matrix interactions. In this case, the PEG phase is further enriched with FBS, while the DEX phase is enriched with trypsin. D) After incubating the ATPS to allow trypsin digestion, cell-cell and cell-matrix interactions are locally digested. By rinsing the chamber and pipetting PBS up and down several times, cells are released from the locally digested area, thereby leaving a denuded circular area. E) Cells can be further cultured in submersion or at ALI; over time, cells proliferate and migrate into the open area.

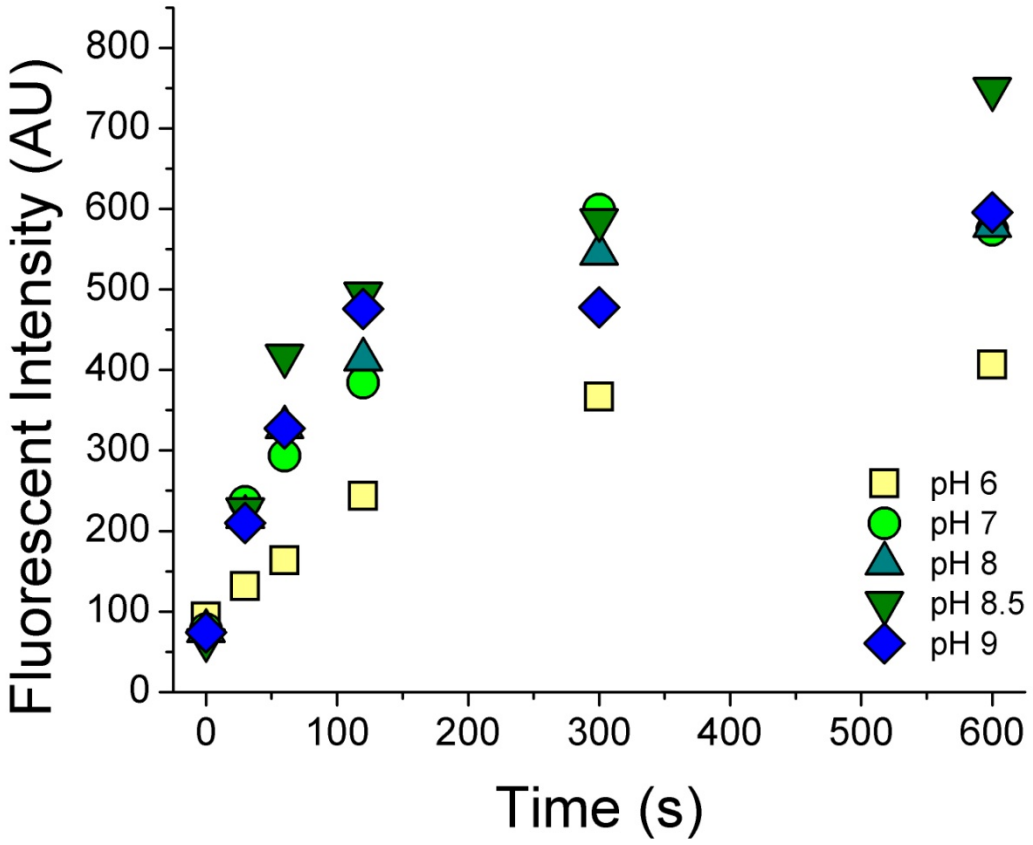

Figure 4.4: Trypsin activity in PBS with various pH values. Fluorescent signals from the FITC-casein assay for PBS solutions with pH values of 6, 7, 8, 8.5, and 9. The amount of fluorescent signal is proportional to the amount of FITC cleaved from casein.

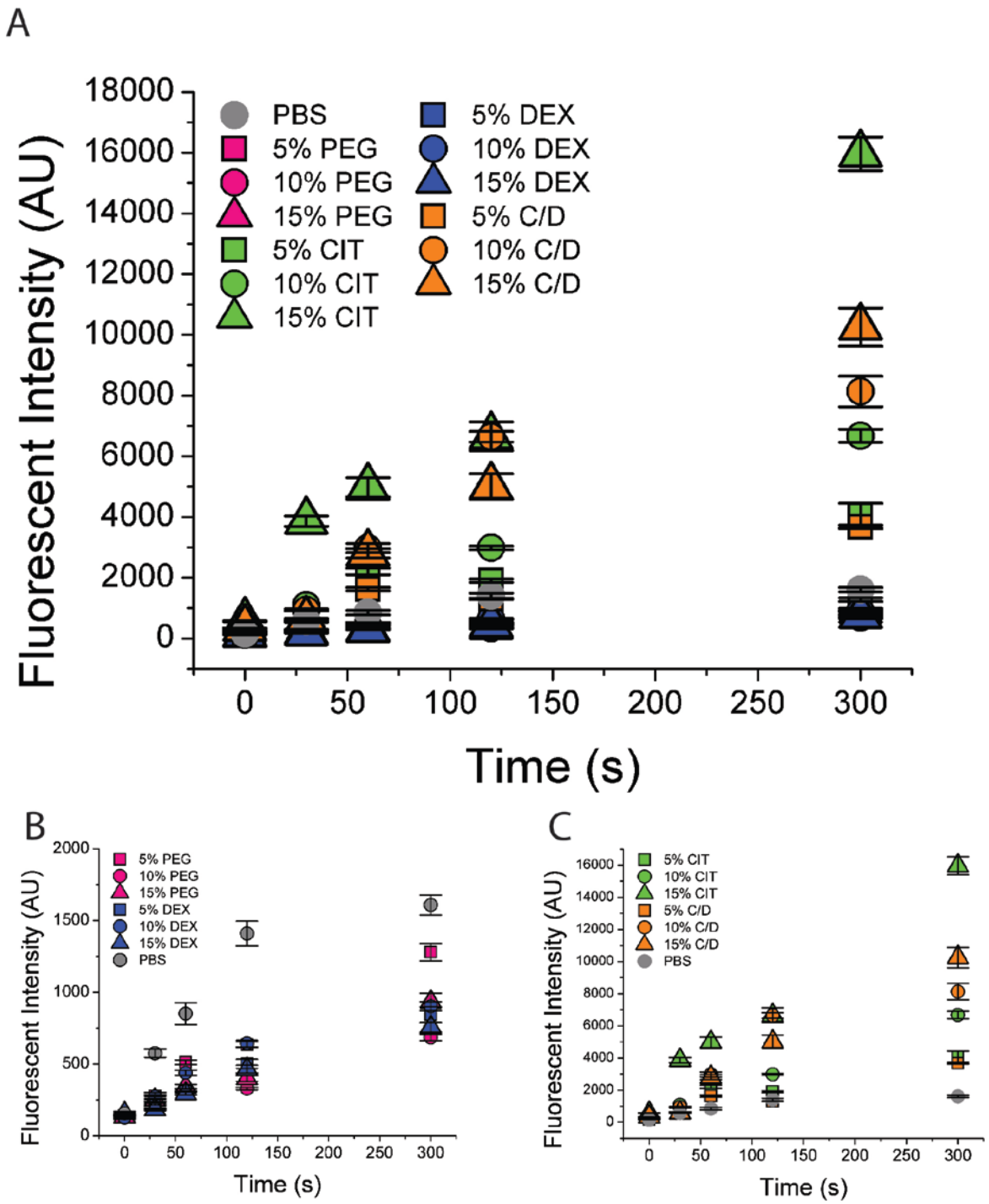

Figure 4.5: Trypsin activity in different polymer solutions at pH 7. A) Fluorescent signals from the FITC-casein assay for 5%, 10%, and 15% solutions of PEG, DEX, CIT, and DEX+CIT. B) Magnified view showing only PEG, DEX, and PBS solutions. C) Magnified view showing only CIT, DEX+CIT, and PBS solutions.

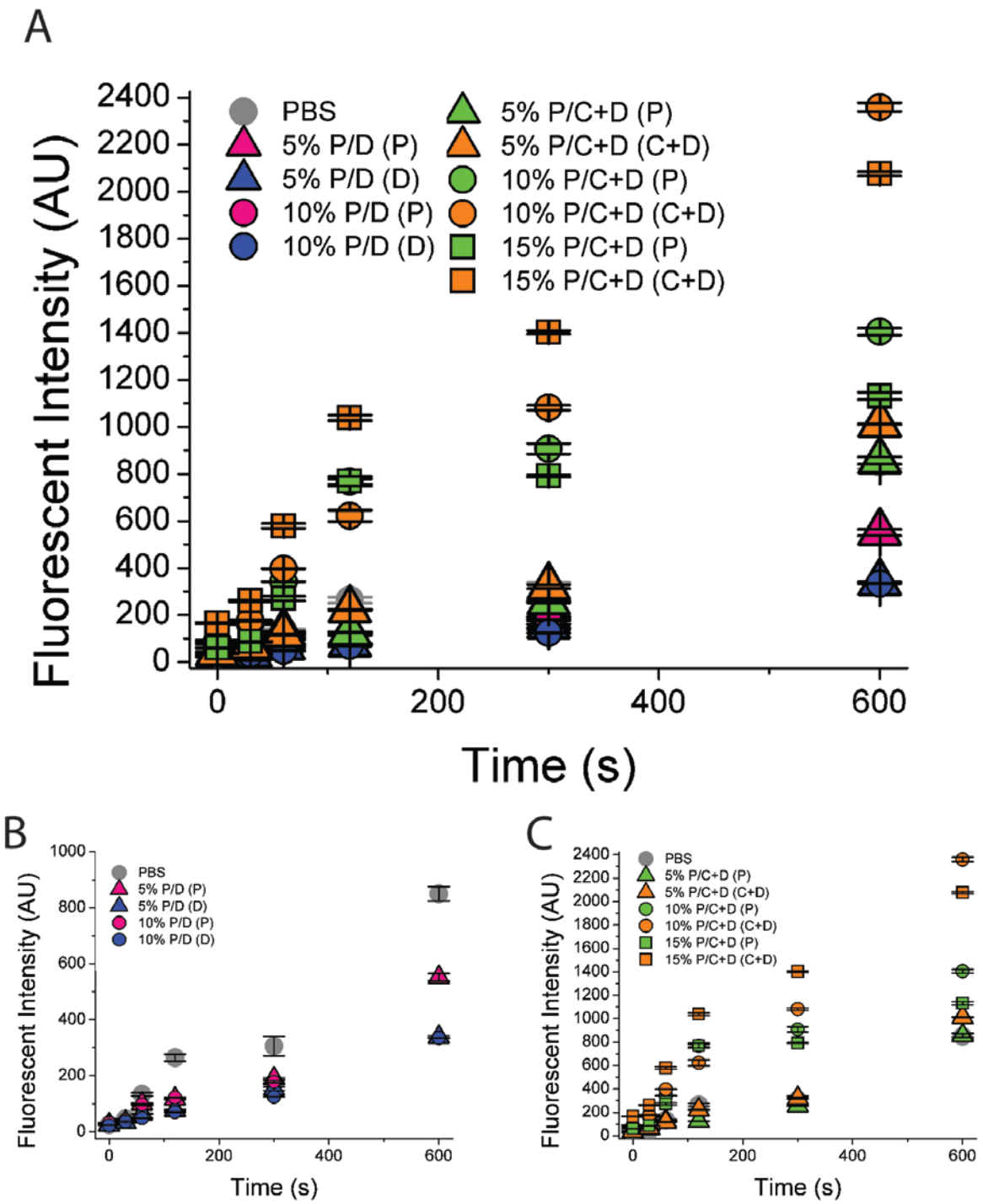

Figure 4.6: Trypsin activity in various ATPSs. A) Fluorescent signals from the FITC-casein assay for 5%, and 10% ATPSs of PEG and DEX and 5%, 10% and 15% ATPSs of PEG and DEX+CIT. B) Magnified view showing only PEG and DEX ATPSs and PBS. C) Magnified view showing only PEG and DEX+CIT ATPSs and PBS. In the graphs, the letter in parentheses refers to the phase from which sample was taken from the ATPS; e.g., 5% P/D (P) refers to a 5% PEG and DEX ATPS with a sample drawn from the PEG phase to be used in the FITC-casein assay.

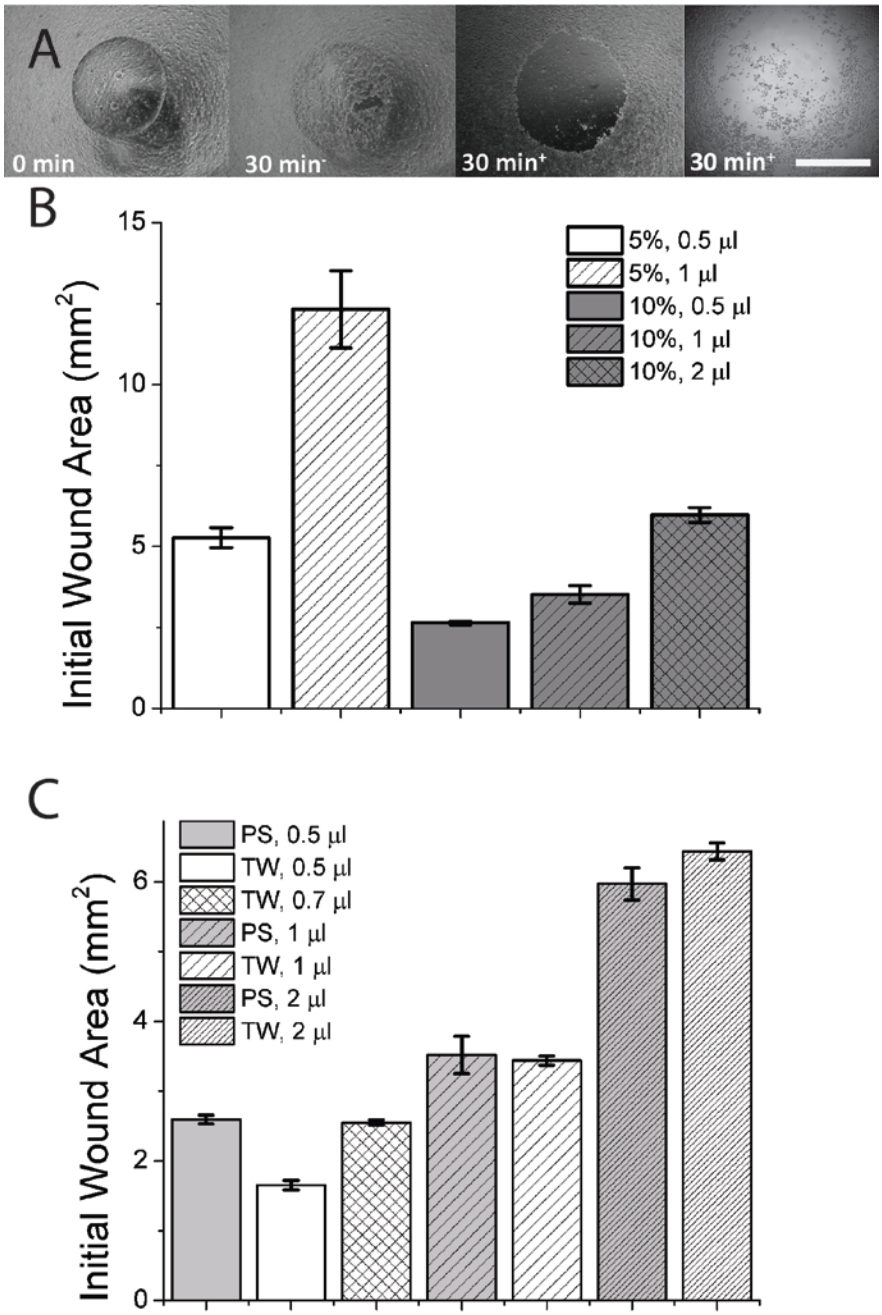

Figure 4.7: Initial wound characteristics of PEG and DEX ATPSs. A) Representative images of A549 cells cultured on transwell inserts and exposed to an ATPS of 10% PEG and DEX with 10 mg/ml trypsin; left: cells immediately after application of the ATPS, middle left: after 30 min incubation, middle right: after 30 min incubation and washes to dislodge trypsinized cells, and right: after 30 min in which the ATPS did not have FBS. Scale bar: 1mm. B) Initial wound areas were calculated for 5% and 10% PEG and DEX ATPSs for 0.5, 1, and 2 µl droplets applied to A549 cells cultured in polystyrene dishes. C) Initial wound areas were also analyzed for 0.5, 0.7, 1, and 2 µl droplets of DEX from a 10% PEG and DEX ATPS applied to A549 cells cultured on polystyrene dishes and transwell inserts. Wound areas were significantly different for 0.5 µl DEX droplets ($p=8.9x10^{-4}$), while they were statistically similar for 1 ($p=0.71$) and 2 ul ($p=0.10$) DEX droplets. Results represent averages ± SEM.

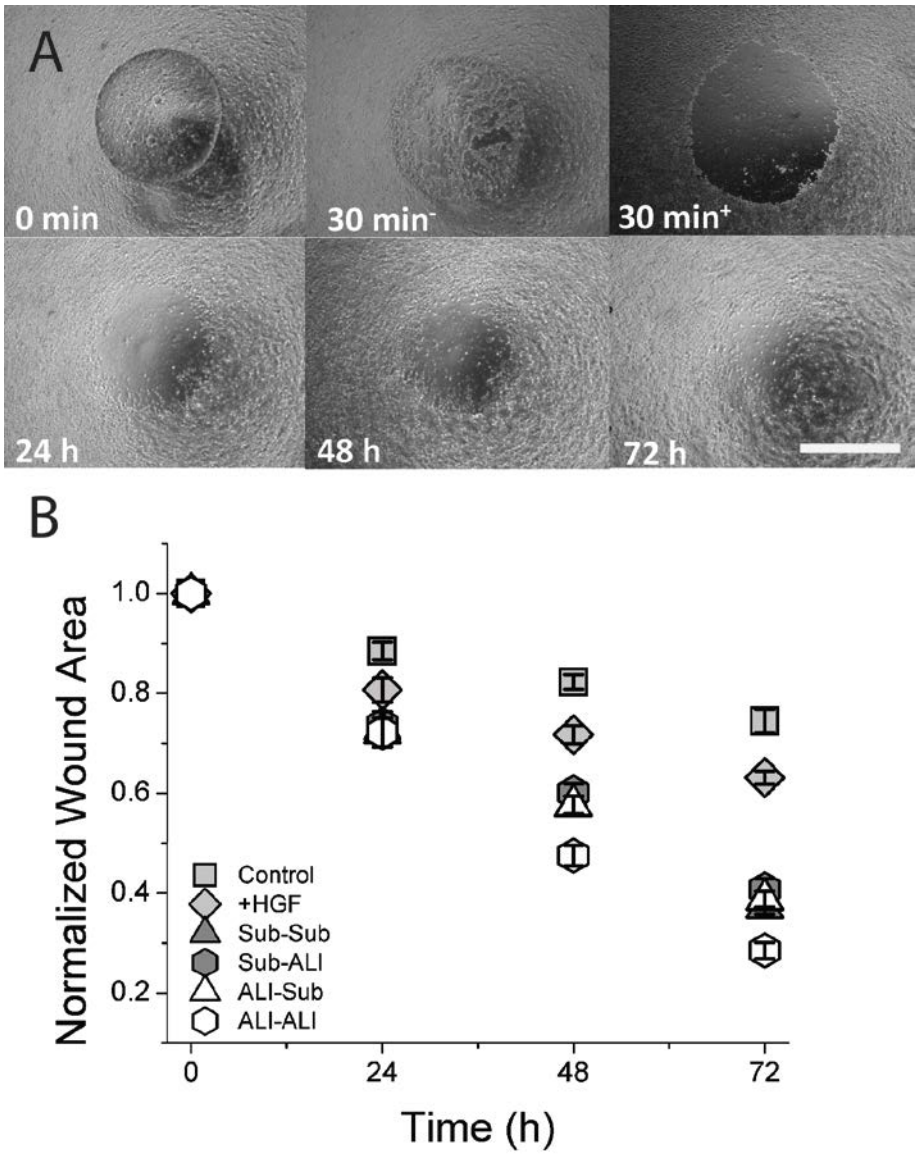

Figure 4.8: Wound closure by A549s in polystyrene dishes and transwell inserts. A) Representative images of A549 cells cultured on transwell inserts and exposed to an ATPS of 10% PEG and DEX in which the PEG was enriched with 10% FBS and DEX with 10 mg/ml trypsin; top left: cells immediately after application of the ATPS, top middle: after 30 min incubation, top right: after 30 min incubation and washes to dislodge trypsinized cells, bottom row: images taken at 24, 48, and 72 h time points. Scale bar: 1mm. B) Normalized wound areas of A549 cells over the course of 72 h: Control, F12 growth medium in a 6-well plate; +HGF, F12 growth medium enriched with 50 ng/ml HGF in a 6-well plate; Sub-Sub, cells grown to confluence and maintained in submersion culture prior to wounding, then returned to submersion culture after wounding; Sub-ALI, cells grown to confluence and maintained in submersion culture prior to wounding, then switched to ALI culture after wounding; ALI-Sub, cells grown to confluence and maintained at ALI prior to wounding, then switched to submersion culture after wounding; ALI-ALI, cells grown to confluence and maintained at ALI prior to wounding, then returned to ALI culture after wounding. Scale bar: 1 mm. Results represent averages ± SEM.

Droplet Formation	PEG/CIT	PEG/DEX	PEG/CIT+DEX
5%	N	Y	Y
10%	N	Y	Y
20%	N	Y	X
30%	N	Y	X

Table 4.1: Droplet formation by various ATPS combinations. ATPS formulations that produce well-defined droplets that retain their shape over time are indicated by Y, while those that do not are indicated by N. Cells marked with X were not tested due to the incomplete dissolution of reagents and/or inability to pipette the extremely viscous 20% and 30% w/w CIT+DEX solutions.

A	*PEG*	*DEX*	*CIT*	*DEX+CIT*
5%	3.696	2.384	48.085	33.855
10%	2.570	2.448	21.128	26.599
15%	1.730	2.053	11.957	10.897

B	*PEG*	*DEX*	*CIT*	*DEX+CIT*
5%	0.838	0.541	10.906	7.679
10%	0.583	0.555	4.792	6.033
15%	0.392	0.466	2.712	2.472

Table 4.2: Trypsin activity in various polymer solutions. A) Slopes of the linear fits applied to the plots shown in Figure 4.5. B) Trypsin activity normalized against the activity in PBS (4.409).

A	*P/D (P)*	*P/D (D)*	*P/D+C (P)*	*P/D+C (D+C)*
5%	0.837	0.514	1.303	1.556
10%	0.478	0.504	2.187	3.688
15%			1.825	3.081

B	*P/D (P)*	*P/D (D)*	*P/D+C (P)*	*P/D+C (D+C)*
5%	0.644	0.396	1.004	1.199
10%	0.368	0.388	1.685	2.841
15%			1.406	2.374

Table 4.3: Slopes of linear fits to fluorescent signals for various ATPSs. A) Slopes of the linear fits applied to the plots shown in Figure 4.6. B) Values normalized against PBS (1.298).

	$\frac{I_{PEG}}{I_{DEX}}$	$\frac{A_{DEX}}{A_{PEG}}$	$K\left(\frac{PEG}{DEX}\right)$	$\frac{I_{PEG}}{I_{DEX+CIT}}$	$\frac{A_{DEX+CIT}}{A_{PEG}}$	$K\left(\frac{PEG}{DEX+CIT}\right)$
5%	$\frac{0.644}{0.396}$	$\frac{0.541}{0.838}$	1.050	$\frac{1.004}{1.199}$	$\frac{7.679}{0.838}$	4.623
10%	$\frac{0.368}{0.388}$	$\frac{0.555}{0.583}$	0.903	$\frac{1.685}{2.841}$	$\frac{6.033}{0.583}$	6.138
15%	n/a		n/a	$\frac{1.406}{2.374}$	$\frac{2.472}{0.392}$	3.432

Table 4.4: Trypsin partitioning in various ATPSs. Partition coefficients were determined for various ATPSs by dividing the ratios of fluorescent intensities (I), as determined in Table 4.3, and by multiplying by the inverse ratios of baseline trypsin activity (A), as determined in Table 4.2.

4.4 References

Bridson, E.Y. and A. Brecker. Design and Formulation of Microbial Culture Media. *Methods in Microbiology Vol. 3A*. Ed. J.R. Norris and D.W. Robbins (1970).

Crosby, L.M. and C.M. Waters. Epithelial repair mechanisms in the lung. *Am. J. Physiol. Lung Cell Mol. Physiol*. **298** L715-L731 (2010).

Diridollou, S., F. Patat, F. Gens, L. Vaillant, D. Black, J.M. Lagarde, Y. Gall, and M. Berson. In vivo model of the mechanical properties of the human skin under suction. *Skin Res. Technol.* **6**, 214-221 (2000).

Dvorak, A., A.E. Tilley, R. Shaykhiev, R. Wang, and R.G. Crystal. Do airway epithelium air-liquid cultures represent teh in vivo airway epithelium transcriptome? *Am. J. Respir. Cell Mol. Biol*. **44**, 465-473 (2011).

Engler, A.J., M.A. Griffin, S. Sen, C.G. Bonnemann, H. Lee Sweeney, and D.E. Discher. Myotubes differentiate optimally on substrates with tissue-like stiffness: pathological implications for soft or stiff microenvironments. *J. Cell Biol*. **166**, 877-887 (2004).

Irimia, D. and M. Toner. Spontaneous migration of cancer cells under conditions of mechanical confinement. *Int. Biol.* **1**, 506-516 (2009).

Irimia, D., S.-Y. Liu, W.G. Tharp, . Saamadani, M. Toner, and M.C. Poznansky. Microfluidic system for measuring neutrophil migratory responses to fast switches of chemical gradients. *Lap Chip* **6**, 191-198 (2006).

Kam, Y., C. Guess, L. Estrada, B. Weidow, and V. Quaranta. A novel circular invasion assay mimics *in vivo* invasive behavior of cancer cell lines and distinguishes single-cell motility *in vitro*. *BMC Cancer* **8**, 198 (2008)

Kasserra, H.P. Kinetics and mechanism of trypsin catalysis. Diss. University of Ottawa (1970).

Kaster, T., I. Sack, and A. Samani. Measurement of the hyperelastic properties of *ex vivo* brain tissue slices. *J. Biomech.* **44**, 1158-1163 (2011).

Keese, C.R., J. Wegener, S.R. Walker, and I. Giaever. Electrical wound-healing assay for cells *in vitro*. *PNAS* **101**, 1554-1559 (2004).

Lee, J.N., X. Jiang, D. Ryan, and G.M. Whitesides. Compatibility of mammalian cells on surfaces of poly(dimethylsiloxane). *Langmuir* **20**, 11684-11691 (2004).

Liang, C.C., A.Y. Park, and J.L. Guan. In vitro scratch assay: a convenient and inexpensive method for analysis of cell migration in vitro. *Nat. Protoc.* **2**, 329-333 (2007).

Liu, F. and D.J. Tschumperlin. Micro-mechanical characterization of lung tissue using atomic force microscopy. *J. Vis. Exp*. **54**, doi: 10.3791/2911 (2011).

Murrell, M., R. Kamm, and P. Matsudaira. Tension, free space, and cell damage in a microfluidic wound healing assay. *PLoS ONE* **6**, E24283 (2011).

Oertel, M., A. Graness, L. Thim, F. Bühling, H. Kalbacher, and W. Hoffman. Trefoil factor family-peptides promote migration of human bronchial epithelial cells. *Am. J. Respir. Cell Mol. Biol.* **25** 418-424 (2001).

Poujade, M., E. Grasland-Mongrain, A. Hertzog, J. Jouanneau, P. Chavrier, B. Ladoux, A. Buguin, and P. Silberzan. Collective migration of an epithelial monolayer in response to a model wound. *PNAS* **104**, 15988-15993 (2007).

Rho, J.Y., R.B. Ashman, and C.H. Turner. Young's modulus of trabecular and cortical bone material: ultrasonic and microtensile measurements. *J. Biomech.* **26**, 111-119 (1993).

Ross, A.J., L.A. Dailey, L.E. Brighton, and R.B. Devlin. Transcriptional profiling of mucociliary differentiation in human airway epithelial cells. *Am. J. Respir. Cell Mol. Biol.* **37**, 169-185 (2007).

Sawano, A., S. Takayama, M. Matsuda, and A. Miyawaki. Lateral propagation of EGF signaling after local stimulation is dependent on receptor density. *Dev. Cell* **3**, 245-257 (2002).

Skouteris, G.G. and C.H. Schröder. The hepatocyte growth factor receptor kinase-mediated phosphorylation of lipocortin-1 transduces the proliferating signal of the hepatocyte growth factor. *J. Biol. Chem.* **271**, 27266-27273 (1996).

Tavana, H., K. Kaylan, T. Bersano-Begey, K.E. Luker, G.D. Luker, and S. Takayama. Rehydration of polymeric, aqueous, biphasic system facilitates high throughput cell exclusion patterning for cell migration studies. *Adv. Funct. Mat.* **21**, 2920-2926.

To, Y., M. Dohi, K. Matsumoto, R. Tanaka, A. Sato, K. Nakagome, T. Nakamura, and K. Yamamoto. A two-way interaction between hepatocyte growth factor and interleukin-6 in tissue invasion of lung cancer cell line. *Am. J. Resp. Cell Mol. Biol.* **27**, 220-226 (2002).

Tubío, G., B. Nerli, and G. Picó. Partitioning features of trypsin and alpha-chymotrypsin in polyetheyleneglycol-sodium citrate aqueous two-phase systems. *J. Chromatog. B* **852**, 244-249 (2007).

Twining, S.S. Fluorescein isothiocyanate-labeled casein assay for proteolytic enzymes. *Anal. Biochem.* **143**, 30-34 (1984).

Williams, H.P. and A.J. Harwood. Cell polarity and *Dictyostelium* development. *Curr. Opin. Microbiol.* **6**: 621-627 (2003).

Wong, A.P., C.E. Bear, S. Chin, P. Pasceri, T.O. Thompson, L.-J. Huan, F. Ratjen, J. Ellis, and J. Rossant. Directed differentiation of human pluripotent stem cells into mature airway epithelia expressing functional CFTR protein. *Nat. Biotech.* **30**, 876-882 (2012).

Xu, X., M. Meier-Schellersheim, X. Jiao, L.E. Nelson, and T. Jin. Quantitative imaging of single live cells reveals spatiotemporal dynamics of multistep signaling events of chemoattractant gradient sensing in *Dictyostelium*. *Mol. Biol. Cell* **16**, 676-688 (2005).

Chapter 5

Aqueous-Two Phase Patterning of Detection Antibodies for Multiplexed and Crosstalk-Free ELISA

This chapter describes the use of a PEG/DEX ATPS for patterning detection antibodies in a multiplexed and crosstalk-free enzyme-linked immunosorbent assay (ELISA). First, polymers were tested in several ELISA formats to verify their compatibility with ELISA. Next, PEG and DEX polymers were tested for antibody partitioning characteristics in various formats including timelapse immunofluorescence, spatially patterned antibody diffusion studies, and ATPS equilibration and dot blot. After verifying polymer compatibility with ELISA and antibody partitioning, PEG/DEX ATPS signal outputs were characterized for several polymer molecular weights and concentrations, blocking conditions, and spotting parameters. A 20% w/w PEG/DEX system with casein blocking was selected to achieve the highest fidelity signal output in an array-based planar immunoassay. A customized dimpled plate was developed in conjunction with the assay to facilitate manual patterning of antibody solutions and effective washing. Finally, samples of patients with graft-versus-host-disease (GVHD) were tested with the ATPS-ELISA; results show that ATPS-ELISA achieves better limits of detection, has broader linear dynamic range, has less background signal, and can be used to better stratify patients based on multiple biomarker readouts when compared to single ELISA.

5.1 Introduction

The enzyme-linked immunosorbent assay (ELISA) is used to accurately and reproducibly quantify levels of soluble proteins. The first ELISA that was developed involved the immobilization of proteins on an assay plate; these proteins were then detected by antibodies specific to an epitope on the protein of interest, and a signal was produced by way of an enzyme conjugated to a second antibody that created a chromogenic, fluorescent or chemiluminescent signal (Engvall and Perlman, 1971). This approach, now known as a direct ELISA, still exists today. Since this initial ELISA was developed, the technology has been modified to facilitate a greater range of functionality and applications. One common variation to the technique involves the immobilization of a capture antibody on the assay plate, known as a sandwich ELISA, which generally improves sensitivity and selectivity of the assay (Crowther, 2001). Owing to their versatility and reliability, ELISAs have been used to detect and/or diagnose a range of pathologies including HIV/AIDS (Halbert et al., 1986), malaria (Voller et al., 1975), cancer (Paul et al., 2005; Kim et al., 2002), and autoimmune diseases (Levine et al., 2012; Paczesny et al., 2010), among others.

Due to their effectiveness, commercial ELISAs with standardized protocols are widely used in clinical, drug development, and biomedical research settings. ELISAs, however, are not without their limitations, such as high reagent costs, long assay incubation times, inefficient use of patient samples, and inability to prevent antibody cross-reactivity in multiplexed formats (Moody et al., 2002; Wiese et al., 2001). With increasing demand for greater amounts of data to aid in more complete patient stratification and diagnosis, as well as to explain patient response to therapeutic regimes, there has been a significant push to develop efficient multiplex platforms and assays. To this end, several multiplexed technologies have been developed that spatially

segregate capture antibodies to many individual spots or beads within an assay (MacBeath 2002; Ellington et al., 2009). These planar and bead-based technologies have been further developed by numerous companies into standardized and commercially available equipment that facilitate the multiplex detection of soluble proteins in ELISA format (Table 5.1). Although these methods can greatly increase ELISA throughput, they still often suffer problems associated with cross-reactivity of detection antibodies applied as a cocktail. The interactions among detection antibodies or between detection antibodies and inappropriate capture antibodies or antigens can lead to false positive or false negative readouts.

We eliminate the problem of cross-reactivity in multiplexed ELISA by using a PEG/DEX ATPS to confine detection antibodies to regions where their corresponding capture antibodies are immobilized on the surface of a polystyrene plate (Frampton et al., 2013). This method, referred to as ATPS-ELISA, works on the three following principles: (1) droplets of the denser DEX solution sink in the PEG solution and remain in contact with the assay plate during incubation; (2) interfacial tensions between DEX-PEG and DEX-assay plate cause the DEX droplets to form domes that remain in place; and (3) detection antibodies are retained, without diffusive dispersion, in the DEX phase due to partitioning effects. We combine the ATPS-ELISA technology with a customized polystyrene assay plate that helps further localize DEX droplets while also enabling efficient washing and signal detection. We demonstrate that this approach is effective at simultaneously detecting four different antigens associated with acute graft-versus-host disease (GVHD), a disease that benefits from multiple biomarker analysis for definitive diagnosis and prognosis (Paczesny et al., 2009a). In addition to resolving the problem associated with antibody cross-reactivity in multiplexed ELISAs, our assay also consumes less antibody and patient sample than conventional single biomarker ELISA. These attributes, as well as the

potential for automation, make ATPS-ELISA a promising next-generation technique for clinical diagnostics and drug development by enabling better early-stage biomarker validation and later in clinical trials for improved patient stratification and to explain patient response to treatments.

5.2 Materials and Methods

5.2.1 PEG and DEX Polymer Compatibility with ELISA

In developing the ATPS-ELISA, it was first necessary to determine the compatibility of the different polymers with traditional ELISA workflow. To do so, a commercially available IL-8 ELISA kit was tested (KAC1301, Life Technologies). This kit is a direct sandwich ELISA (Figure 5.1 A) that has the surfaces of 96-well plates pre-coated with capture antibodies directed against human IL-8, lyophilized human protein to be used as a protein standard, and prepared solutions of horseradish peroxidase (HRP)-conjugated detection antibodies and chromogen to produce signal. These types of pre-packaged kits decrease the amount of work required by the end user but can also decrease flexibility in tailoring the ELISA to suit each researcher's needs.

First, three separate assays were performed side-by-side to determine the compatibility of PEG and DEX with the kit: (1) following manufacturer's instructions with slight modifications for producing signal, (2) the same as (1) but also enriching each solution with DEX, and (3) the same as (1) but also enriching each solution with PEG. For example, in (2) when the assay calls for adding a solution of IL-8 antigen, instead of adding a pure solution of reconstituted protein, the IL-8 solution was enriched with DEX. Finally, whereas the manufacturer's protocol called for the addition of tetramethylbenzidine to produce a colorimetric readout proportional to the amount of IL-8 in each well, the modified protocol used SuperSignal ELISA Femto Maximum

Sensitivity Substrate (PI37074, Fisher Scientific) to produce chemiluminescent signal, which was detected on x-ray film instead of on a plate reader.

Further tests to determine polymer compatibility were conducted with R&D Systems ELISA DuoSet kits (DY208, R&D Systems). Whereas the previous ELISA was a direct sandwich ELISA with pre-coated well plates, the DuoSet kit is an indirect sandwich ELISA (Figure 5.1 B) that provides all reagents in a lyophilized form; although this format generally requires more work by the end-user, it also enables greater flexibility in developing assays. Based on the incompatibility of the polymers with the direct sandwich ELISA, a series of experiments was performed to determine which step of the process was incompatible with the polymers. That is, by eliminating the polymer from only 1 step in each experiment, the reagent that was incompatible with the polymer-enriched version of the assay could be determined.

5.2.2 Antibody Partitioning

Antibody partitioning was determined with 3 separate methods: timelapse fluorescence, antibody co-localization analyses, and ATPS equilibration and dot blot.

To perform timelapse microscopy, separate solutions of PBS were enriched with 20% w/w 500 kDa DEX (Dextran T500, Pharmacosmos) and 20% w/w 35 kDa PEG (81310, Sigma). Phycoerythrin-conjugated mouse anti-human CD184 IgG2a (555974, BD Pharmingen) and 500 kDa fluorescein-dextran (D7136, Molecular Probes) were added to the stock solution of DEX at dilutions of 1:200 and 1:100, respectively. PEG was added to a 35 mm dish and 0.5 µl droplets of DEX were dispensed into the dish and imaged over the course of 2 h.

Two separate antibody co-localization studies were performed. The first test analyzed the potential for cross-reactive antibodies to produce signal when spotted in proximity using ATPS.

First, a spot of mouse anti-ST2 and a spot of anti-goat antibody were placed within 1 mm proximity on a polystyrene dish and incubated at 4 ˚C overnight to allow antibody adsorption. Following blocking and ST2 antigen incubation, a DEX droplet containing biotinylated goat anti-ST2 was localized to the area where mouse anti-ST2 had been spotted and incubated for 2 h. Plates were then incubated with streptavidin-conjugated HRP (Strep-HRP) and signal was produced using chemiluminescent substrate. In the second test, mouse anti-TNFR was spotted onto a polystyrene dish as in the first test. After blocking and TNFR antigen incubation, a DEX droplet containing biotinylated goat anti-TNFR was spotted using ATPS so as to only partially overlap the capture antibody spot in a Venn diagram configuration. As in the first tests, plates were incubated with Strep-HRP and signal was developed with chemiluminescent substrate. In each test, images were acquired using a FluorChem M Digital Imager (ProteinSimple).

ATPS equilibration and dot blot was performed by diluting biotinylated detection antibodies from ELISA kits (DY225, DY294, DY523, DY1747, R&D Systems) to 500 ng/ml in Eppendorf tubes containing 1 ml total 10% w/w PEG 35 kDa and 10% w/w DEX 500 kDa in PBS. Control tubes contained only PEG and DEX and were not enriched with antibodies. The contents of each Eppendorf tube were thoroughly mixed by rocking at room temperature for 10 min. The tubes were then centrifuged at 400 rcf at 4° C for 15 min, which facilitated the complete phase separation and equilibration of the PEG and DEX phases. Polyvinylidene fluoride (PVDF) membranes (10413052, Whatman) were soaked in methanol for 15 s, water for 2 min and finally PBS for 5 min. Six 0.5 µl samples each of the PEG and DEX phases were then dispensed onto the PVDF. The membranes were blocked in 1% BSA for 1 h and washed 4 times with PBS containing 0.05% Tween-20. Membranes were then incubated with streptavidin-conjugated horseradish peroxidase for 1 h, washed 4 times, and incubated with SuperSignal

ELISA Femto Maximum Sensitivity Substrate. Chemiluminescent signal was detected using a FluorChem M Digital Imager. Partition coefficients, defined as the reagent concentration in the PEG phase divided by the reagent concentration in the DEX phase, were calculated by taking the ratios of chemiluminescent signals from the PEG and DEX spots on the PVDF membranes.

5.2.3 ATPS-ELISA Characterization

Spatial control over ATPS-ELISA-based signal outputs was optimized for types of blocking conditions, molecular weights of polymers, and concentrations of polymers. For blocking conditions, bovine serum albumin (BSA) and casein buffers were tested at concentrations ranging from 0.1% to 5%. For polymer molecular weight, PEG was held constant at 35 kDa, while DEX molecular weights of 3.5, 10, and 500 kDa were investigated. Polymer concentrations of 5, 10, 20, and 30% were investigated for each of the combinations of PEG and DEX.

To test how each of the above parameters affected the size of the signal spot generated by the assay, a modified ATPS-ELISA was performed. Briefly, a polystyrene dish was coated with TNFR capture antibody at 4 ˚C overnight. Plates were washed and blocked for 1 h with the appropriate blocking buffer. Plates were washed again and then incubated with TNFR antigen for 2 h. Following another wash, ATPSs with various combinations of polymer molecular weights and concentrations were used to dispense DEX droplets containing biotinylated TNFR detection antibody into PEG and incubated for 2 h. Next, plates were washed, incubated for 1 h with Strep-HRP, washed, and finally incubated with chemiluminescent substrate to generate signal, which was detected using a FluorChem M Digital Imager.

5.2.4 Customized Dimpled Plate

A mold for the production of a customized dimpled-well plate was designed in AutoCAD (AutoDesk) and SolidWorks (Dassault Systems), which was then machined from aluminum at Protomatic, Inc. (Dexter, MI). Using the aluminum mold, plates were hot embossed from square polystyrene dishes by melting the plates above their glass transition temperature and then inducing an abrupt temperature change to harden the dishes and release them from the aluminum mold.

5.2.5 Multiplexed and Crosstalk Free Detection of 4 Biomarkers from Patient Samples

Standard curves for four GVHD biomarkers (HGF, elafin, ST2, and TNFR1) were generated in multiplexed ATPS-ELISA format in the customized dimpled plate by modifying the singleplex ELISA workflows for their corresponding commercially available kits (DY225, TNFR; DY294, HGF, DY523, ST2; and DY1747, elafin, R&D Systems). Briefly, monoclonal capture antibodies were reconstituted in PBS to their recommended concentrations and 3 µl of each was dispensed into one of the small dimples in the customized plate. Plates were incubated at 4 ˚C overnight in dishes containing saturated KimWipes to prevent evaporation of the droplets. After overnight incubation, plates were washed (all wash buffer contains PBS with 0.05% Tween20) 5 times and then blocked for 1 h with 3% casein in PBS. During blocking, multiplex antigen ladders were prepared by mixing single antigens into a common standard diluent of 10% healthy pooled plasma and 1% FBS in PBS to maximum concentrations of 10,000 pg/ml for each antigen. A quarter-log serial dilution was then performed to obtain concentrations ranging from 1.78 pg/ml-10,000 pg/ml. After blocking, plates were again washed 5 times and antigen solutions were added to the appropriate larger common wells of the

customized plate and incubated for 2 h. Following another 5 washes, ATPS (10 µl 20% w/w PEG 35 kDa containing 0.1% casein added to each well) was used to spot DEX droplets (3 µl, 20% w/w DEX 500 kDa) containing the appropriate detection antibody to the same dimple containing its corresponding capture antibody and incubated for 2 h. Next, plates were washed 8 times to thoroughly remove polymer, incubated for 1 h with Strep-HRP, washed 5 times, and finally incubated with chemiluminescent substrate to generate signal, which was detected using a FluorChem M Digital Imager.

Heparinized plasma samples were also collected from patients who received allogeneic bone marrow transplantation at the University of Michigan between 2000 and 2010 for testing. Plasma samples were collected under protocols approved by the University of Michigan Institutional Review Board and stored at the University of Michigan. This group, which contained samples from patients that received allogeneic bone marrow transplants and did not manifest symptoms of GVHD, as well as patients that received allogeneic bone marrow transplants and were diagnosed with acute GVHD, was compared with healthy controls. The workflow for performing ATPS-ELISA of patient samples was the same as outlined above, except the test solution applied to each well contained 10% patient plasma and 1% FBS in PBS. We were blind to the GVHD status of the samples during the experiment and image quantification.

All plots and statistical analyses were carried out in Sigmaplot with Sigmastat (Systat Software). Standard curves were fit using a four parameter logistic function. The limit of detection (LoD) was determined from the equation $LoD = LoB + 1.645*(SD_{low\ concentration\ sample})$, where SD is the standard deviation and LoB is the limit of blank. LoB was calculated from $LoB = mean_{blank} + 1.645*(SD_{blank})$ (Armbruster and Pry, 2008). Linear dynamic range (LDR) was

determined using LDR = maximum linear response/ LoD. To compare ATPS-ELISA values with conventional ELISA values, a Pearson product-moment correlation test was used.

5.3 Results and Discussion

5.3.1 PEG and DEX Polymer Compatibility with ELISA

Using a direct sandwich ELISA format (Figure 5.1 A), we found that PEG and DEX were both incompatible with at least a portion of the ELISA (Figure 5.2). In this figure, X-ray film was exposed to chemiluminescent signal that was produced from individual wells in a 96-well plate. Signal intensity, i.e., the density of the black region, is proportional to the amount of antigen that was present in the individual wells; therefore, signal intensity should be greatest in the top well where the concentration of IL-8 was highest (200 pg/ml), decrease by ½ in each subsequent well due to the serial dilution of IL-8, and be 0 in the bottom well, where wells were left unexposed to IL-8.When following the prescribed instructions from the manufacturer's protocol (with the aforementioned modifications to the signal generation step), we obtained the expected results (Figure 5.2 #1). However, when PEG (Figure 5.2 #2) or DEX (Figure 5.2 #3) were added to the ELISA, signal intensity was not only much higher than expected, but in the case of PEG the signal was uniform across conditions and in the case of DEX the level of background staining was exceptionally high (as demonstrated by the large amount of signal in the bottom well, where no signal should be present).

Due to these results, we switched to an indirect sandwich ELISA kit because all reagents are provided in a lyophilized format. This format gives us more control over each step and allows us to use known solutions instead of pre-packaged reagent solutions that contain an unknown mixture of preservatives, dyes, and other reagents. Using the indirect sandwich ELISA,

we performed a series of experiments in which PEG and DEX were omitted from just one step of the assay. In doing so, we determined that incubation of PEG and DEX with an HRP-conjugated reagent led to non-specific binding that produces signals seen in Figure 5.2 #2-3. By omitting PEG and DEX from the step that includes HRP, we again obtain the expected results (Figure 5.2 #5). This is an important result in the development of the assay because the end goal is to develop technology in which detection antibodies can be spatially patterned. Many commercially available kits have detection antibodies that are directly conjugated to HRP; as can be seen from our results, however, we cannot use these HRP-conjugated antibodies because they will nonspecifically bind and produce signal that is not proportional to the amount of protein in solution, thereby yielding false positive readouts. Therefore, indirect sandwich ELISA workflow, where detection antibodies are either unconjugated or biotinylated, must be used and another enzyme-conjugated antibody must be applied in bath solution without PEG or DEX to generate the appropriate signals.

5.3.2 Antibody Partitioning

After demonstrating that PEG and DEX are compatible with indirect sandwich ELISAs as long as they are not applied with HRP, and keeping in mind the end goal of creating a multiplexed ELISA that eliminates antibody crossreactivity by patterning detection antibodies, we sought to demonstrate that antibodies partition to the DEX phase in an ATPS.

First, timelapse microscopy was used to visualize DEX droplet stability and antibody diffusion characteristics when dispensed into a solution of PEG. As can be seen in Figure 5.3, the DEX droplet, which is visualized using FITC-DEX, initially forms a circular cross-sectional area that slightly decreases in size over 2 h but is still stable and distinct from the surrounding PEG

phase. Furthermore, PE-IgG is colocalized to the same region as DEX and does not show diminishing signal intensity, suggesting that antibodies stably partition to the DEX phase.

Although timelapse microscopy suggests that antibodies partition to DEX, there is a possibility that antibodies diffuse out of the DEX droplet and the signal is not sufficiently detected by microscopy. To this end, we performed 2 antibody co-localization experiments. In the first, a mouse anti-ST2 capture antibody was spotted within 1 mm of an anti-goat antibody (Figure 5.4 A). After blocking and incubating with ST2 antigen, ATPS was used to spot biotinylated goat anti-ST2 detection antibody on top of the capture antibody area (Figure 5.4 B) and incubated for 2 h. Plates were then washed, incubated with Strep-HRP, washed and developed using chemiluminescent substrate. If detection antibodies stay retained within the DEX droplet, signal will only be localized to the ST2 signal area; however, if detection antibodies diffuse away from the droplet, the anti-goat antibody will react with the goat-derived detection antibody and produce a second signal spot (Figure 5.4 C). As can be seen from the readout (Figure 5.4 D), antibodies were retained and signal was localized to a single spot.

The second antibody co-localization experiment was a further verification of the results of the previous assay. After spotting TNFR capture antibody (Figure 5.5 A), blocking and incubating with antigen, ATPS was used to partially overlap a spot of detection antibody to the initial capture antibody area (Figure 5.5 B). Following the same washing and chemiluminescent development steps, signal was only produced in the overlapping region, much like a Venn diagram (Figure 5.5 C).

Finally, ATPS equilibration and dot blot was used to quantify antibody partitioning. After thoroughly mixing solutions of PEG and DEX enriched with biotinylated detection antibodies, solutions were equilibrated into two distinct phases (Figure 5.6 A). During this process,

antibodies naturally partition based on molecular characteristics and phase system properties. We sampled aliquots from each phase and detected chemiluminescent signals from the aliquots on a FluorChem M Digital Imager. In this format, chemiluminescent signal intensity is proportional to the amount of antibody in solution. By dividing signal intensity of the PEG phase by that of the DEX phase, we obtained partition coefficients for several different ATPS concentrations (Figure 5.6 B). As can be seen, partition coefficients were < 0.45 for all antibodies in the phase system tested; for elafin, this means there is approximately a 2:1 ratio of antibodies in the DEX:PEG phases, and that in all other phases the ratio is higher. Although this number is high for partitioning, when analyzed in combination with other partition results, it seems that antibodies do strongly partition. Unfavorable partition coefficients found by dot blot are likely due to high background and/or low signal intensity. This low signal-to-noise ratio would lead to the calculation of larger partition coefficients, even when signal is visually predominantly produced from the DEX phase.

5.3.3 ATPS-ELISA Characterization

After demonstrating ATPS compatibility with ELISA and effective antibody partitioning, we characterized the signals generated by various combinations of ATPS molecular weights and concentrations as well as blocking schemes. To do so, we modified the conventional ELISA (Figure 5.7 A); instead of bath applying detection antibodies, we used ATPS to manually pipette detection antibodies into small localized regions on a plate uniformly coated with capture antibodies. Using this approach, the signal that was generated was proportional to the area over which the DEX droplet containing the detection antibody was applied.

When considering blocking conditions, casein tended to outperform BSA (Figure 5.7 B). As can be seen, when analyzing the signals generated by various concentrations of 500 kDa DEX ATPSs, there seems to be a higher degree of background staining when BSA is used. Although this staining could result from insufficient washing, BSA also tends to form phase systems with PEG and DEX and could therefore interfere with the localization of detection antibodies. We also evaluated the effects of polymer molecular weights and concentrations (Figure 5.7 C). As expected, signal areas were smaller for higher molecular weights and higher concentrations of polymers due to higher surface tensions between the phases that minimized the amount of droplet spreading on the surface.

Because the end goal is to optimize an ATPS that can be utilized for multiplex ELISA, it is necessary to be able to create multiple small signal areas in a single well of a multi-well plate. Casein, which demonstrated cleaner signals with less background staining, was therefore selected as the blocking buffer for future experiments. When selecting concentrations and molecular weights of polymers to achieve small signal areas, we had more flexibility. As can be seen in Figure 5.7 C, signal area decreases for higher concentrations of all polymer molecular weights, and in the case of BSA, signal area is approximately the same for ATPSs with 20% w/w DEX 500 kDa, 25% w/w DEX 40 kDa, and 30% DEX 10 kDa. However, at these very high concentrations, solutions become exceedingly viscous and difficult to handle. Therefore, the 20% w/w DEX 500 kDa/PEG 35 kDa ATPS was chosen because its signal areas were small enough to enable 4-plex ELISA in a well the size of a 96-well plate and because it had sufficiently low viscosity to enable easy handling of the assay.

5.3.4 Customized Dimpled Plate

Although 96-well plates are common laboratory supplies and can be used with automated equipment, they are more difficult to use with the ATPS-ELISA format because their high walls make it difficult to thoroughly wash and remove the ATPS solutions. To facilitate easier washing and manual pipetting and localization of antibodies, several iterations of customized plates were designed and tested. One approach utilized wax pencils to "draw" hydrophobic well walls on a planar surface and a second approach used a xurographer to cut circular holes into tape, which was then stuck to a polystyrene dish so that the holes acted as sample wells.

These first attempts, although capable of creating multiple wells on a single planar surface, were not robust. For example, wax often detached from the surface, thereby removing all "wells" from the surface; furthermore, if the tape stencil was not applied perfectly to the polystyrene dish, liquid from individual wells would seep underneath the tape and mix with adjacent wells. Due to these problems, and because we sought to facilitate easier manual co-localization of capture and detection antibody spots, we designed a new customized plate in AutoCAD and SolidWorks (Figure 5.8). The negative of the plate shown in Figure 5.8 A was machined from aluminum at Protomatic, Inc. and was used as a mold with which to hot emboss square polystyrene dishes. A magnified view (Figure 5.8 B) shows the distinct features of the plate that optimize its use for ATPS-ELISA. First, a 9x9 array of 6.5 mm diameter wells are used for incubating samples. Second, 4 1.5 mm diameter dimples (colored green, red, blue, and purple) are included in each larger well, which are used as sub-wells for 4 different capture and detection antibody pairs. These small dimples, in addition to helping to localize DEX, also act as a physical feedback that help guide manual pipetting. Finally, the shallow well and dimple features facilitate rapid and thorough washing of the plate. The resulting plate after hot

embossing is shown in Figure 5.8 C; although the exterior plate walls are not retained in the final plate, they do not actually play a role in the assay workflow and their absence does not affect its performance.

5.3.5 Multiplexed and Crosstalk Free Detection of 4 Biomarkers from Patient Samples

Using the customized plates, the following 4 biomarkers were detected in multiplex ATPS-ELISA format in standard diluent: elafin, HGF, ST2, and TNFR (Figure 5.9 A). As can be seen, although each protein was spiked into standard diluent at the same concentrations in each well, their corresponding signals displayed different characteristics (Figure 5.9 B). Using the signals produced from each antigen at concentrations ranging from 0-10,000 pg/ml, standard curves were generated for each biomarker (Figure 5.9 C-F). As can be seen, the single and ATPS-ELISA formats produced standard curves with similar sigmoidal shapes. However, by inspecting the graphs and by calculating LoD and LoB for each biomarker, it is apparent that ATPS-ELISA tends to outperform single standard ELISA. For elafin, HGF, and ST2, ATPS-ELISA has lower LoD, meaning protein can be detected and quantified at lower concentrations, and higher LDR, meaning there is a broader range of protein concentrations that can be quantified. Although traditional ELISA outperformed ATPS-ELISA for TNFR, the LoD and LDR were very similar between the two formats.

Next, we used traditional single ELISA and ATPS-ELISA to analyze plasma samples from three patient groups: healthy controls (n=20), allogeneic bone marrow transplant patients who did not manifest symptoms of GVHD (GVHD –; n=19, median 28 days post-transplant) and allogeneic bone marrow transplant patients who had been diagnosed with acute GVHD (GVHD+; n=32, median 28 days post-transplant) (Figures 5.10-5.11). ATPS-ELISA was well-

correlated with individual sandwich ELISAs by Pearson product-moment correlation, demonstrating the robustness of this technique (Figure 5.12). As expected, the GVHD+ patient group had higher levels of HGF, elafin, ST2 and TNFR1 than the GVHD– group and the healthy donor group. Furthermore, owing at least partially to the lower LoD and greater LDR in multiplexed ATPS-ELISA compared to traditional single ELISA, we were able to more effectively assess the GVHD status of the samples. These observations are consistent with observations from others that suggested that small spot sizes and assay volumes produce superior LoD and LDR values (Ekins, 1989; Hartmann et al., 2009). It is also possible that ATPS-ELISA benefits from microscale surface localization effects that enhance detection antibody binding, more effective washing due to the shallow well profiles, and less depletion of chemiluminescent substrate, all of which can affect LoD and LDR. Finally, receiver operating characteristic (ROC) analysis indicated that our test was sensitive and specific, as determined by measuring the area under the ROC curve (Figure 5.13).

5.4 Conclusions

In our assay, capture antibody spots can be arranged in a variety of plate formats similar to other array-based multiplexed ELISAs. Importantly, the resulting assay signals can be read with a range of plate readers and chemiluminescence imagers, making it easy to adopt and scale. We demonstrated that the ATPS-ELISA method works with proteins contained in buffered solutions as well as with human plasma. Our assay offers several advantages over conventional single biomarker ELISAs including use of small plasma volumes (≤1 μL/well of plasma for four biomarkers), cost savings (orders of magnitude less detection antibody consumption) and use of

conventional plate materials and detection systems. Most importantly, it eliminates antibody cross-reactivity in the multiplexed format.

While many biomarkers have been discovered, there are multiple barriers (especially for multiplexed biomarker assays) to biomarker verification, qualification and FDA approval. One technological barrier has been the lack of multiplexed immunoassays that are efficient in usage of precious samples (consume less per run), robust in providing quantitative data without an increase of background or cross-reactivity, rapidly customizable and free from reliance on difficult to access reagents, plates and hardware (HTStec 2010; Master et al., 2006). In addition, poor antibody specificity is problematic for immunoassays in general. Even with the best antibodies, high background and loss of linearity occur with multiplexing due to higher total antibody concentrations. Our assay addresses these key areas and removes a bottleneck to clinical translation by utilizing a customized dimpled plate to localize (and therefore eliminate cross-reactivity) capture and detection antibody droplets as well as consuming small amounts of patient samples. Because antibody pairs are co-localized to small defined areas, our multiplexed signals are cleaner due to lack of cross-reactivity. This also aids in the multiplex validation procedure because each biomarker in the multiplex panel is independent of the others. Therefore, if reagents change or one assay does not work, the remaining biomarkers are still valid. This reduces time and cost associated with development and validation of new panels of multiplexed immunoassays.

In addition, a single biomarker is often not sufficient for conclusive diagnosis, patient stratification, or definitive explanation of patient response to drugs. In the context of GVHD diagnosis and biomarker qualification, for example, it is important to use a panel of multiple biomarkers (Paczesny et al., 2009a). Once diagnosed with GVHD, patients are usually

administered immunosuppressant drugs such as corticosteroids, or in the case of corticosteroid-resistant GVHD, patients are given anti-IL2Rα, anti-TNFR1 or anti-thymoglobulin therapy (Paczesny et al., 2009b). These drugs are effective at controlling the T-cell mediated immune response associated with GVHD, but they may cause serious side effects. In addition, suppression of the immune response, which is required for GVHD treatment, may increase the risk of cancer relapse and serious infections. To highlight the importance in our study, one of the GVHD– patients had high levels of HGF (6615 pg/mL), as well as slightly elevated levels of TNFR1 (990 pg/mL). Based only on the levels of these two biomarkers, this patient could have been diagnosed with GVHD and could have potentially received unnecessary treatment. However, with the inclusion of ST2 and elafin measurements that were both below the limit of detection, this patient can be considered GVHD– and avoid unnecessary treatments that may cause dangerous side effects. This issue is further underscored by the fact that overall GVHD patient cohort survival rate does not always improve, even after "successful" diagnosis and treatment. This indicates that some patients may be stratified based on incomplete biomarker data, which leads to inappropriate treatment with immunosuppressant drugs and further complications and mortality. In the context of drug development, in clinical trials it would be more useful to analyze levels of multiple biomarkers to more fully understand patient responses (both on-target and off-target) and to use the information to optimize dosages and/or delivery characteristics. In either case, however, the only way to confidently make decisions based on multiplex assays is to use tests with very low probabilities of false positive signals, which is effectively achieved in our assay.

Because our method is simple and requires few (if any) fabrication steps or customized materials, we expect that it is more easily translatable into clinical, research, and drug

development settings than other multiplexing technologies. The multiplexing capabilities offered by this assay, in addition to the minimal potential for false positive signals, make this assay a potentially exciting tool to aid in biomarker analysis to better explain patient responses to therapeutic regimes and optimize treatment protocols.

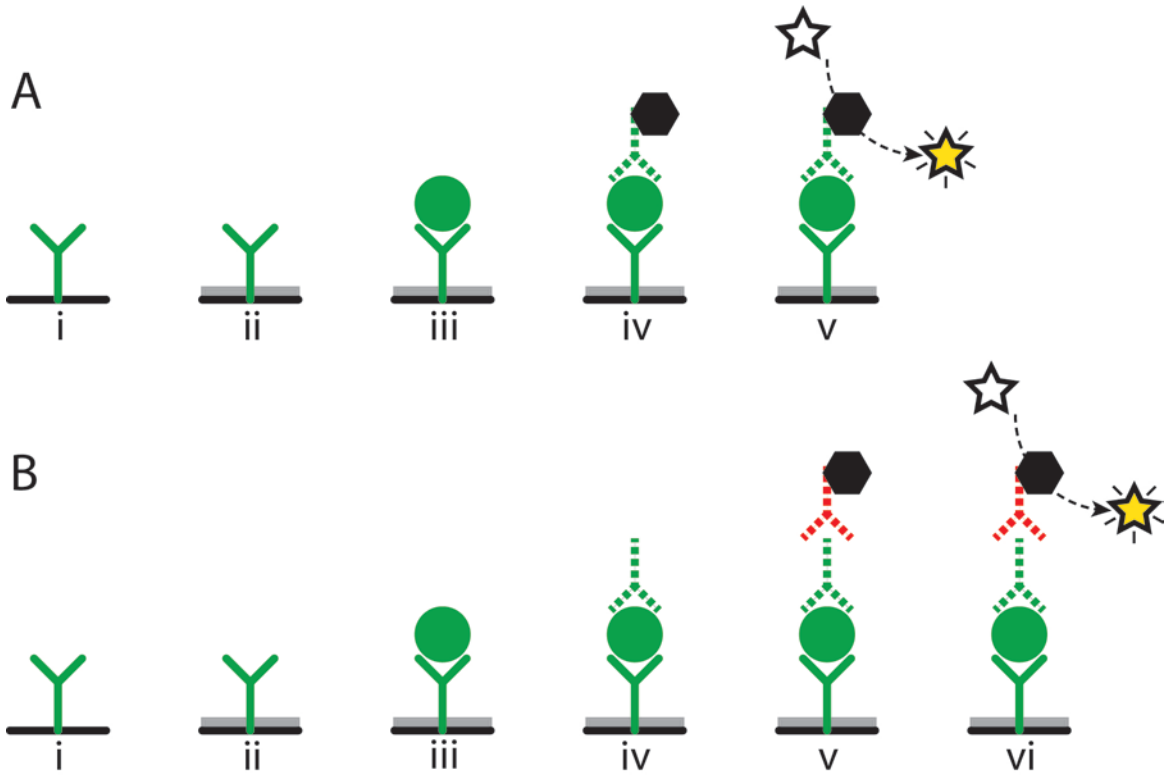

Figure 5.1: Direct and indirect sandwich ELISA formats. A) In the direct sandwich ELISA, capture antibodies are bound to the surface (i). After washing away excess capture antibody in solution, plates are blocked (ii) and then incubated with test solution. Capture antibodies bind to specific antigens from the test solution (iii). Following another wash, wells are incubated with detection antibodies, which are directly conjugated to signal-generating enzymes such as horseradish peroxidase (iv). Following another wash, a final solution is added that contains a substrate that reacts with the enzyme to produce a colorimetric, fluorescent, or chemiluminescent signal (v). B) In the indirect sandwich ELISA, the format is very similar (i-iii), except the detection antibody is either unlabeled or biotinylated (iv). An additional incubation is required where an enzyme-conjugated molecule is added; this molecule is generally either an antibody directed against the species of the corresponding detection antibody or conjugated to streptavidin (v). The final step also requires incubation of a solution containing substrate that reacts with the enzyme on the signal-producing molecule to produce a colorimetric, fluorescent, or chemiluminescent signal (vi).

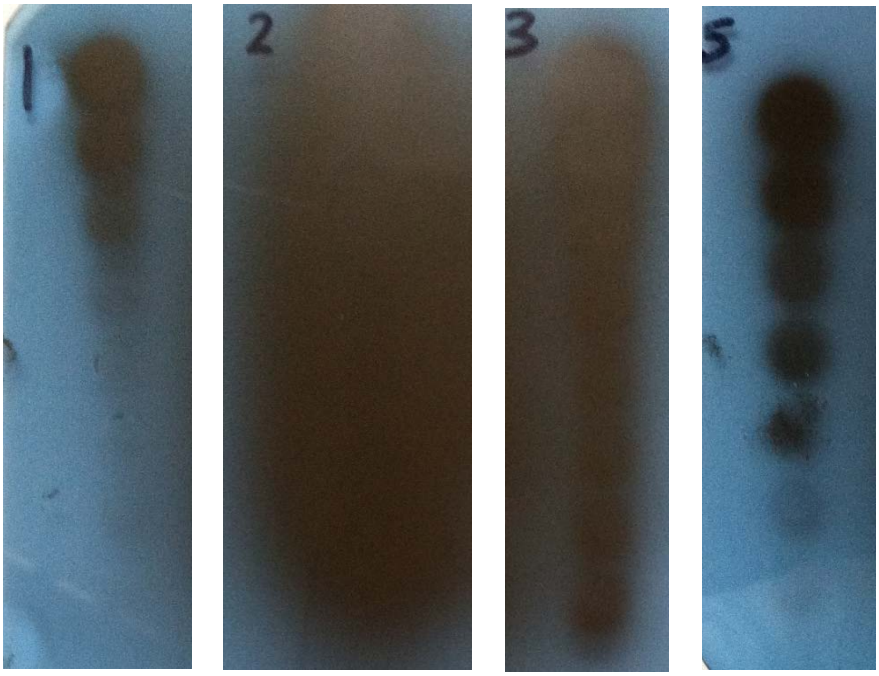

Figure 5.2: X-ray film readouts of an IL-8 ELISA to test PEG and DEX compatibility. 1) Results from the standard direct ELISA protocol where the only step in the protocol that was changed was switching the enzyme substrate from a colorimetric substrate to a chemiluminescent substrate. 2) Results from the same protocol used in (1) except all solutions were enriched with PEG. 3) Results from the same protocol used in (1) except all solutions were enriched with DEX. 5) Results from a standard indirect ELISA protocol in which PEG was added to the solutions for all steps except the addition of Strep-HRP; the HRP is precipitated onto the surface by both polymers, resulting in the intense non-specific signals seen in (2) and (3).

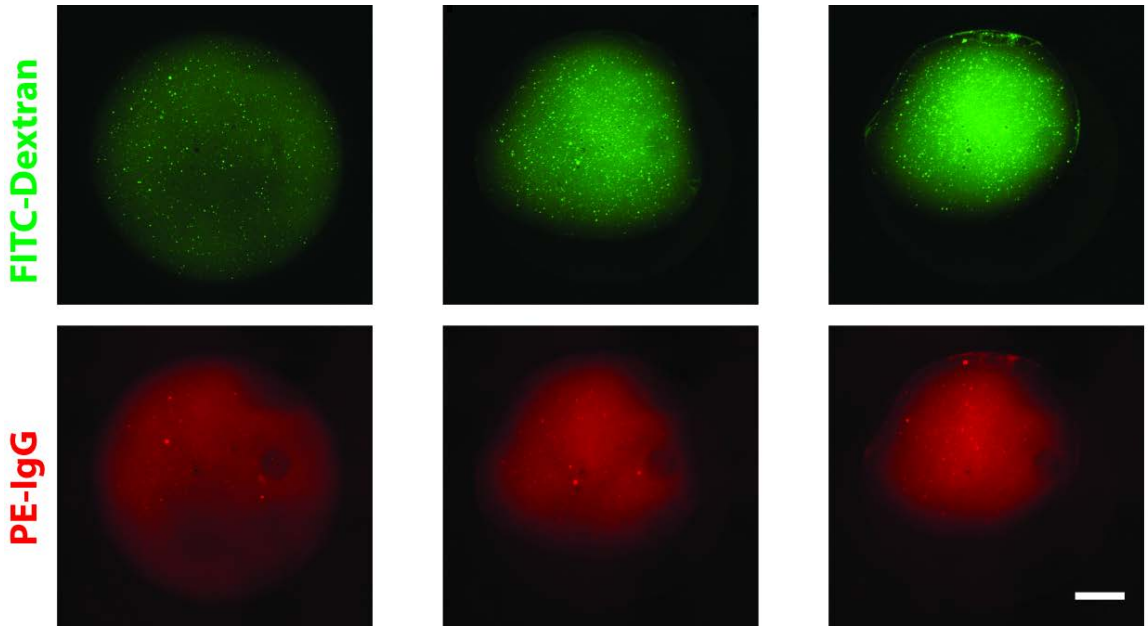

Figure 5.3: Fluorescent timelapse of a DEX droplet containing fluorescently-labeled antibody. A 20% w/w solution of DEX 500 kDa was enriched with a 1:100 dilution of FITC-DEX 500 kDa and 1:200 dilution of phycoerythrin-conjugated antibody. After initially dispensing the droplet into a solution of 20% PEG 35 kDa (left), the droplet slightly spreads on the surface. Over the course of 30 (middle) and 120 min (right), the droplet slightly shrinks in size but it is clear that antibody is retained within the droplet as shown by the overlap of fluorescent signals. Scale bar: 1 mm.

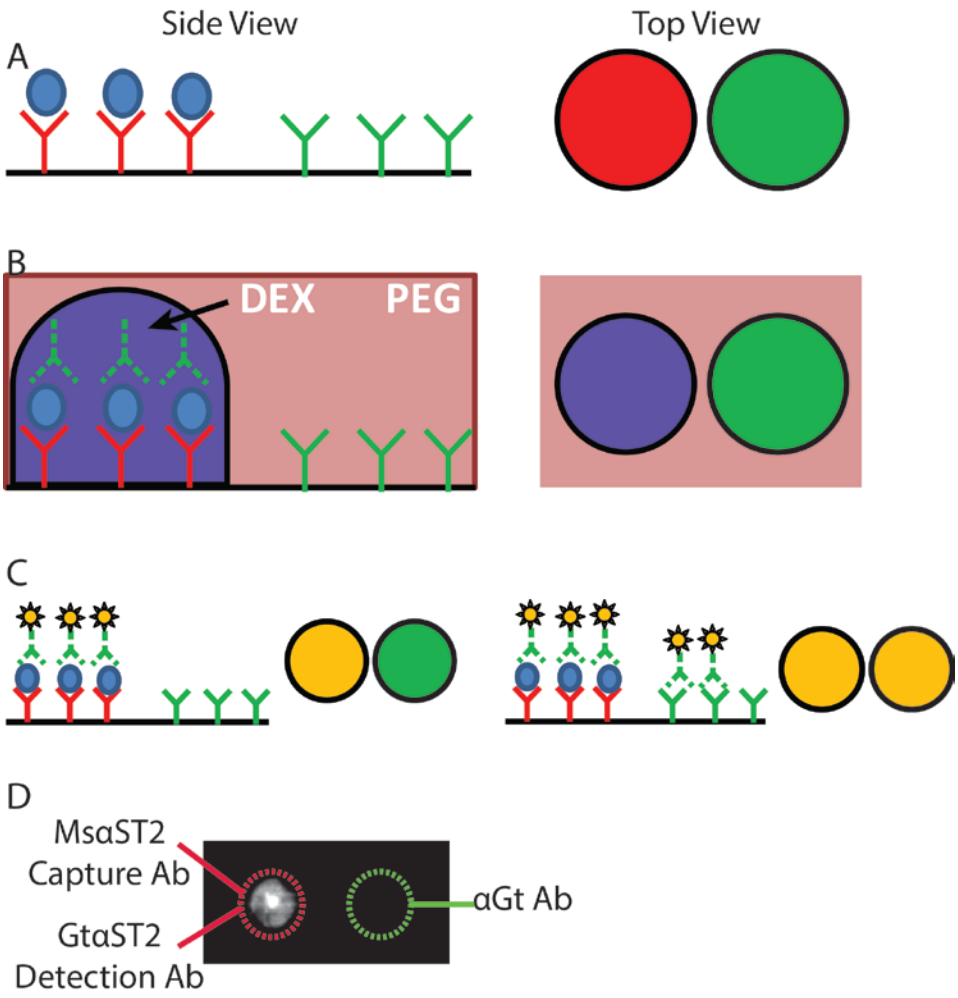

Figure 5.4: Co-localization study of cross-reacting antibodies. A) Mouse anti-ST2 and anti-goat antibodies were spotted within 1 mm of each other. Plates were then washed to remove unbound antibodies, blocked, and incubated with ST2, which was bound by the capture antibodies. B) Following another wash to remove unbound antigen, ATPS was used to dispense a DEX droplet containing biotinylated goat anti-ST2 to the same area as its capture antibody. C) If the detection antibodies are retained within the DEX droplet, subsequent incubation with Strep-HRP and chemiluminescent developer will only produce signal where the detection antibody was spotted (left). If, however, antibodies do not partition to the DEX droplet, they will diffuse outward and will be bound by the anti-goat antibodies located adjacently (right). D) Results show that chemiluminescent signal is indeed only produced in the location where both capture and detection antibodies were localized.

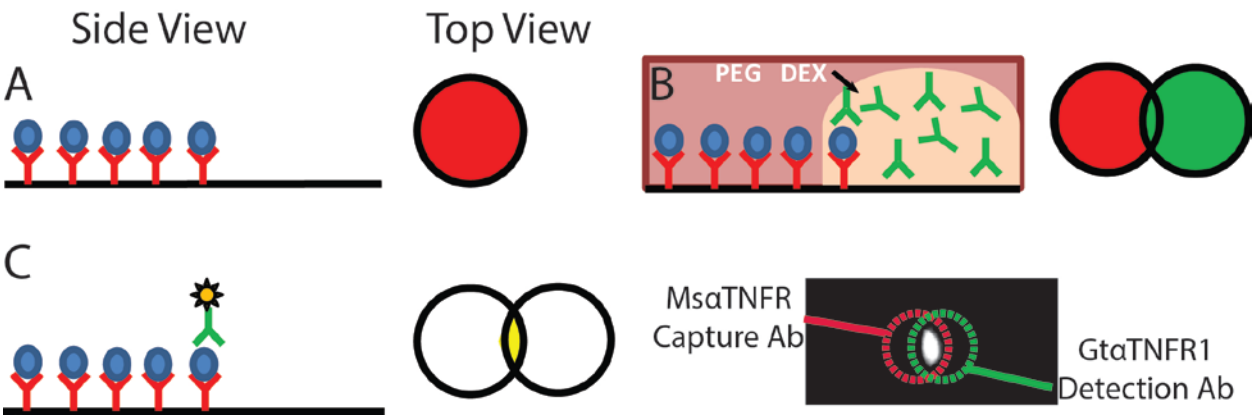

Figure 5.5: Co-localization of antibodies in a Venn diagram configuration. A) Mouse anti-TNFR antibodies were localized to a small region on a dish. B) Following washing, blocking, and incubation with TNFR antigen, ATPS was used to spot a DEX droplet containing biotinylated goat anti-TNFR so that only a small portion of the DEX droplet overlapped the capture antibody region. C) Assuming detection antibodies are retained within the DEX phase, subsequent incubation with Strep-HRP and chemiluminescent substrate should only produce signal in the overlapping region of the Venn diagram. Results show that signal is indeed only produced in the overlapping region, further confirming that antibodies are retained within the DEX droplet.

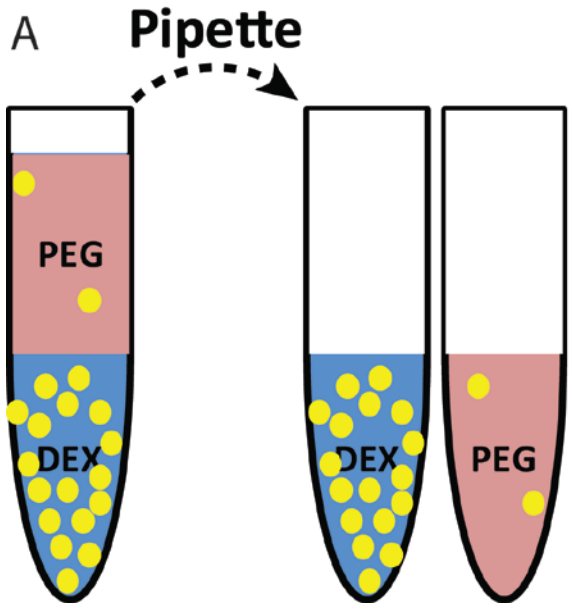

B

Antibody	K
Biotin goat anti-Elafin	0.45
Biotin goat anti-ST2	0.18
Biotin goat anti-TNFR	0.22
Biotin goat anti-mouse	0.11

Figure 5.6: ATPS equilibration and quantification of antibody partitioning. A) Solutions of PEG and DEX were enriched with fluorescently-labeled antibodies. Microcentrifuge tubes were thoroughly mixed and then allowed to naturally phase separate over the course of 2 h. Following phase separation (and natural partitioning of antibodies), aliquots were removed from each phase and fluorescent signals were detected using a plate reader. B) Partition coefficients were calculated by dividing fluorescent signal intensity of the PEG phase by fluorescent intensity of the DEX phase.

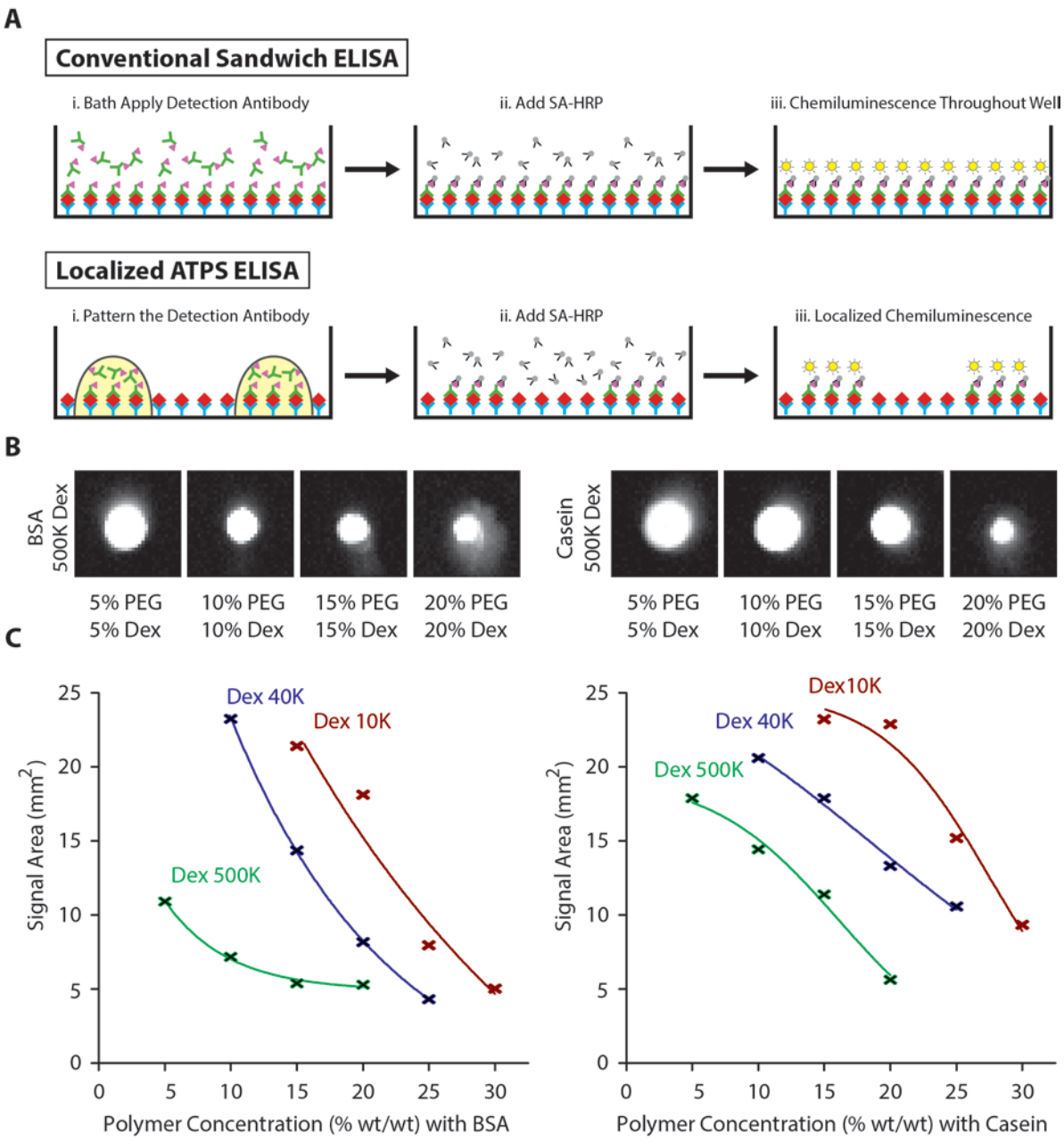

Figure 5.7: ATPS-ELISA signal characterization. A) In traditional ELISA, the entire surface of a polystyrene well is coated with capture antibody that binds antigen; a bath solution of detection antibodies is then applied, which also binds antigen across the entire surface. Therefore, when Strep-HRP and chemiluminescent substrate are added, signal is produced in the entire well. To characterize signal spot size in ATPS-ELISA, the entire surface of a polystyrene well is coated with capture antibody that binds antigen; ATPS localizes detection antibodies in drops of DEX. Therefore, when Strep-HRP and chemiluminescent substrate are added, signal is produced in small discrete areas. B) BSA and casein blocking conditions were tested in ATPS-ELISA; representative images from 500 kDa DEX show that casein blocked more effectively than BSA and had less background signal. C) Signal area size was characterized for various combinations of blocking conditions and molecular weights of DEX.

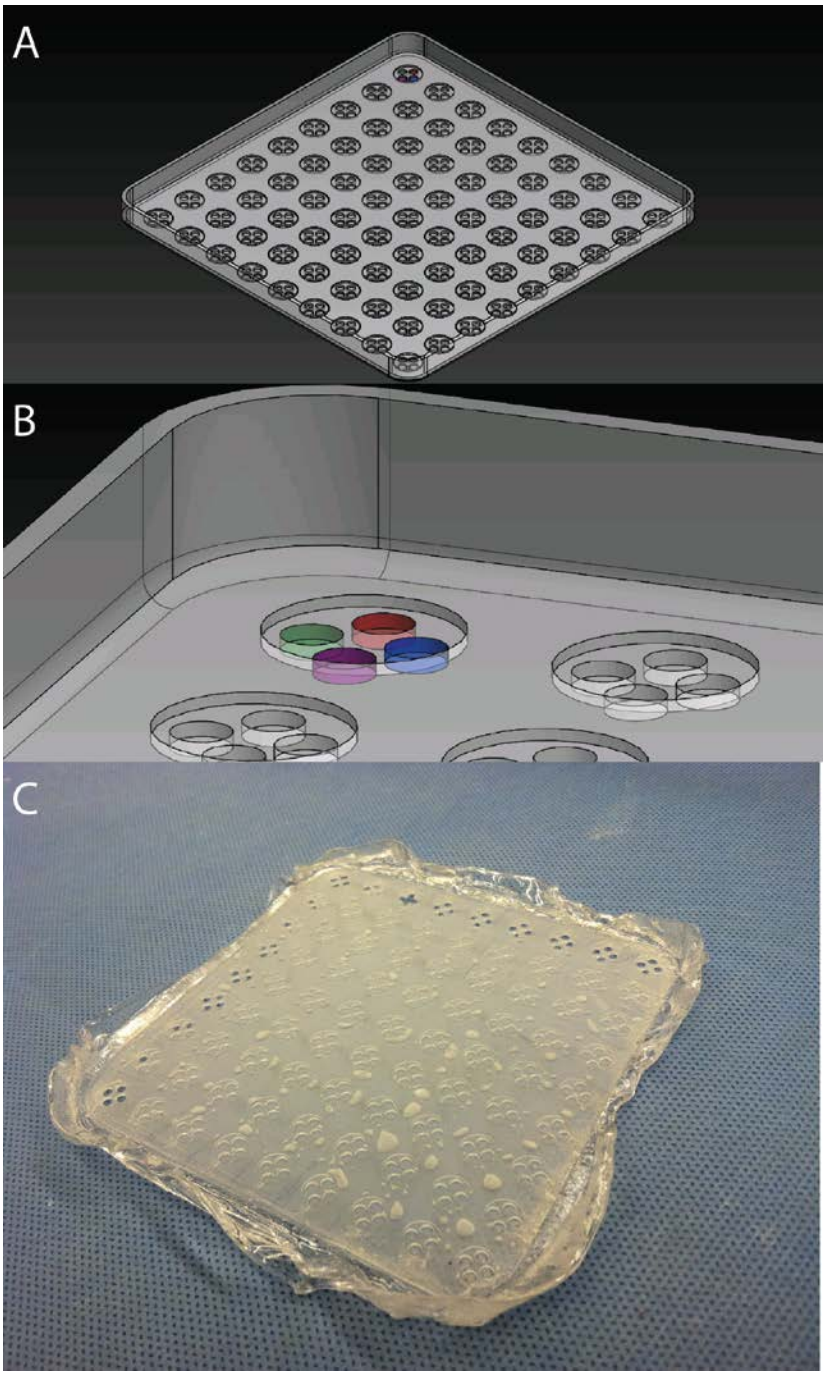

Figure 5.8: Customized ATPS-ELISA plate. A) SolidWorks representation of the final version of the customized plate; the negative of the plate was machined into aluminum to act as a mold with which to emboss a polystyrene dish. B) Magnified view of the plate; the plate contains a 9x9 array of larger 6.5 mm wells for incubating samples. The 4 smaller dimples in each larger well (falsely colored to highlight the ability to localize 4 different antibody pairs) are used to localize capture and detection antibodies and to provide physical feedback for manual pipetting. Wells and dimples have shallow well features that facilitate washing. C) Example of a final customized plate after hot embossing a polystyrene dish.

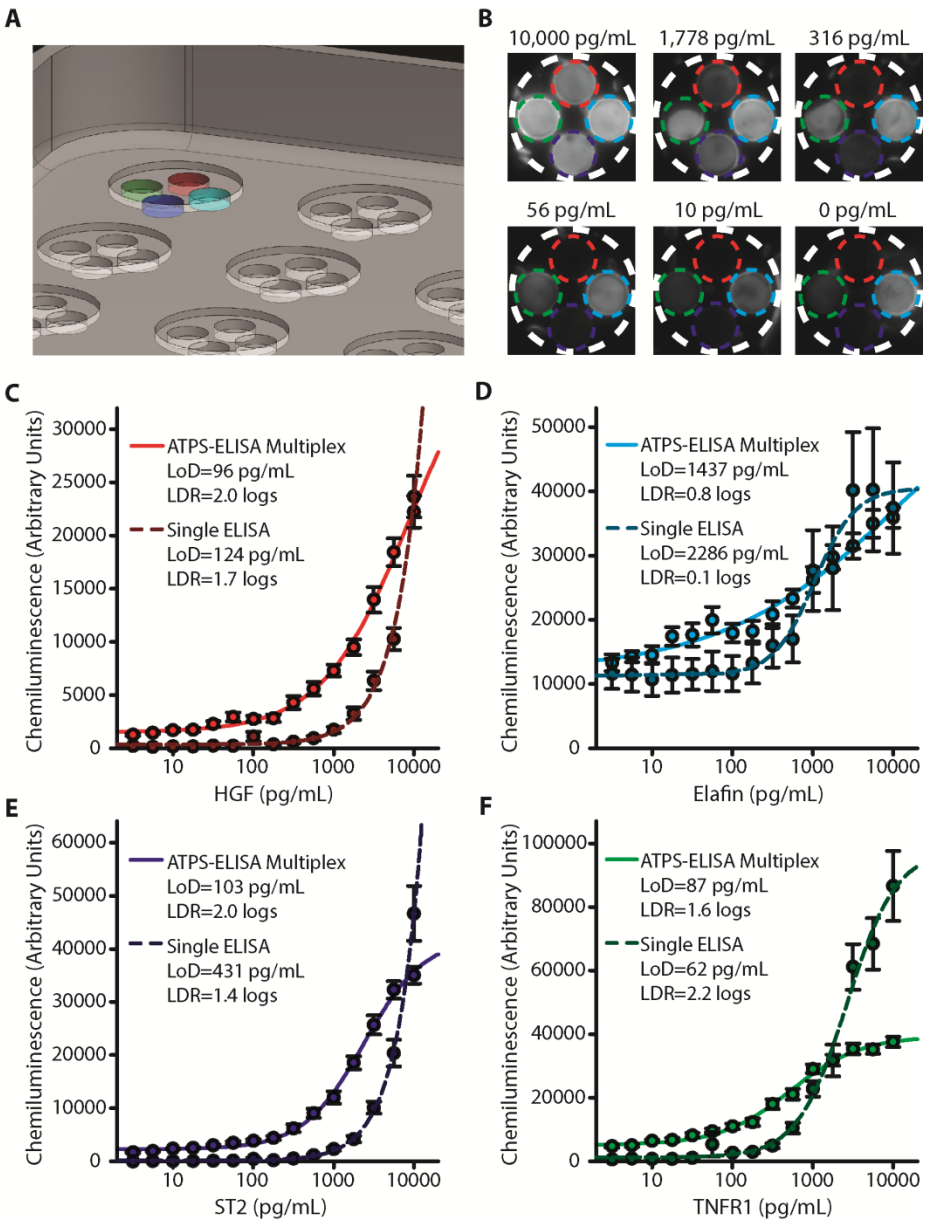

Fig. 5.9: Standard curves for ELISA and ATPS-ELISA. A) Close up view of the customized plate with false color added to show the areas where the various biomarkers were detected (red, HGF; cyan, elafin; blue, ST2; green, TNFR). B) Representative images of a multiplexed readout from ATPS-ELISA for various concentrations of elafin, HGF, ST2, and TNFR. C) Single ELISA and ATPS-ELISA standard curves for HGF. D) Single ELISA and ATPS-ELISA standard curves for elafin. E) Single ELISA and ATPS-ELISA standard curves for ST2. F) Single ELISA and ATPS-ELISA standard curves for TNFR. Curves for all four GVHD biomarkers were generated by densitometric quantification of chemiluminescence images. Error bars represent standard error of the mean.

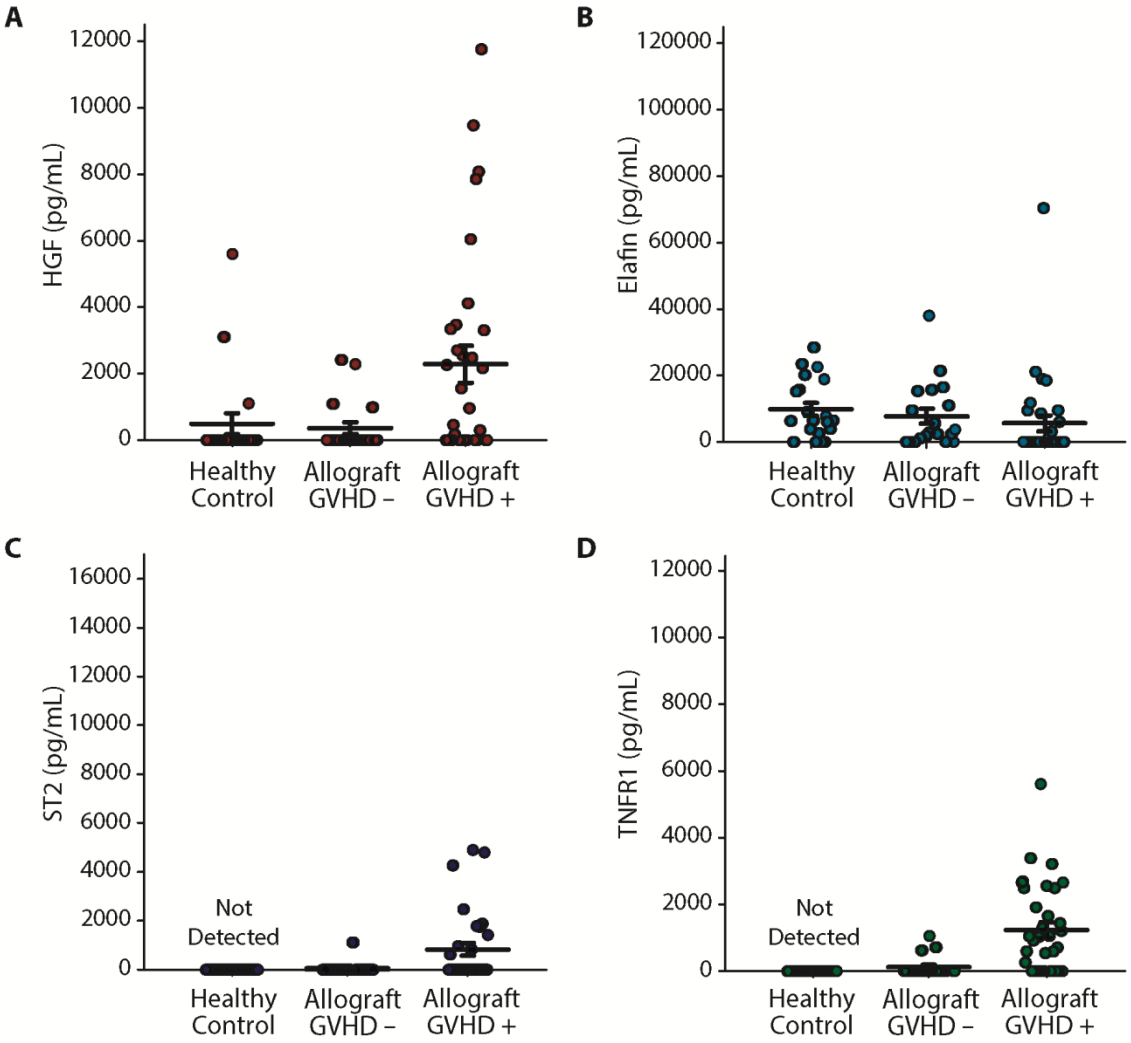

Figure 5.10: Patient levels of biomarkers for GVHD using single ELISAs. A) Quantification of levels of HGF. B) Quantification of levels of elafin. C) Quantification of levels of ST2. D) Quantification of levels of TNFR. Levels were determined by comparing densitometric signal intensity of patient samples to their respective standard curves. Significance between the GVHD+ group and the GVHD- and healthy control groups was obtained for HGF and TNFR1 ($p<0.05$ by one-way ANOVA with Dunn's multiple comparison test), but not for elafin or ST2, although ST2 values for the GVHD+ group tended to be higher than the other groups. Error bars represent standard error of the mean.

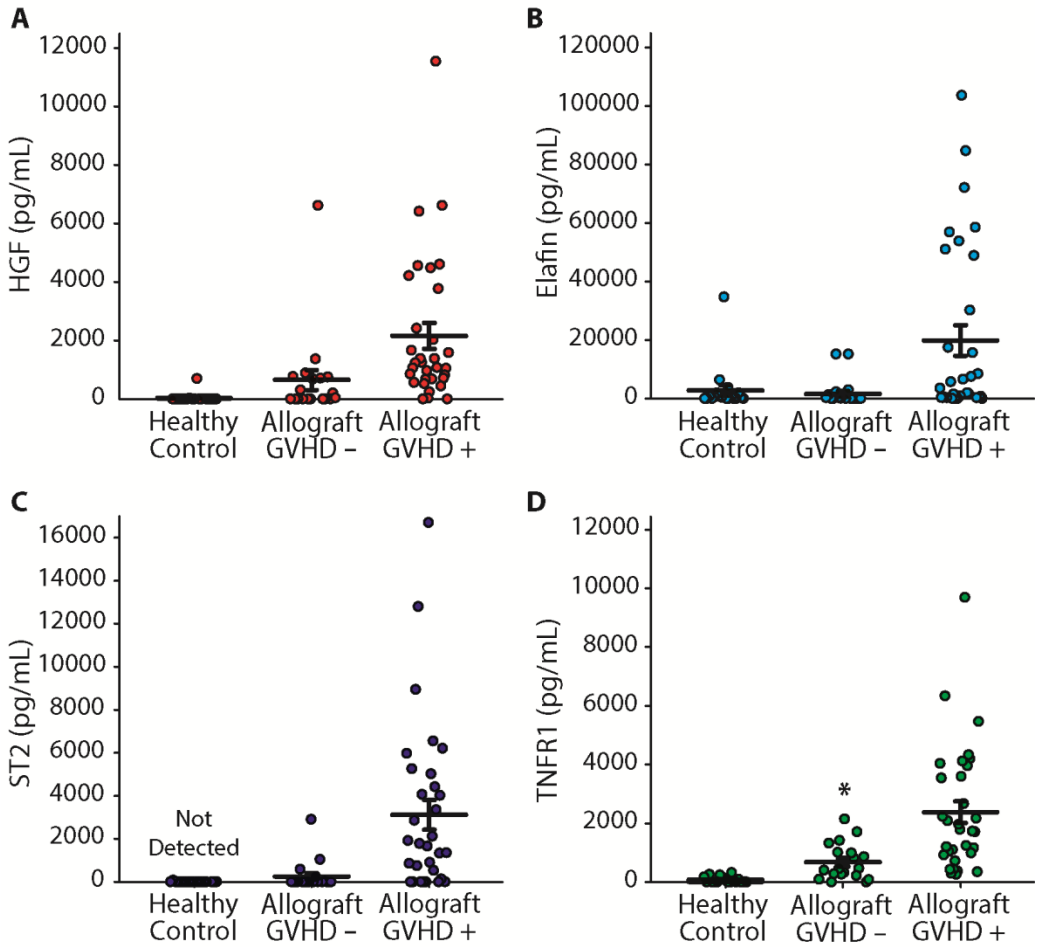

Figure 5.11: Patient levels of biomarkers for GVHD using ATPS-ELISAs. A) Quantification of levels of HGF. B) Quantification of levels of elafin. C) Quantification of levels of ST2. D) Quantification of levels of TNFR. Levels were determined by comparing densitometric signal intensity of patient samples to their respective standard curves. Significance between the GVHD+ group and the GVHD- and healthy control groups was obtained for HGF and TNFR1 ($p<0.05$ by one-way ANOVA with Dunn's multiple comparison test), but not for elafin or ST2, although ST2 values for the GVHD+ group tended to be higher than the other groups. Error bars represent standard error of the mean.

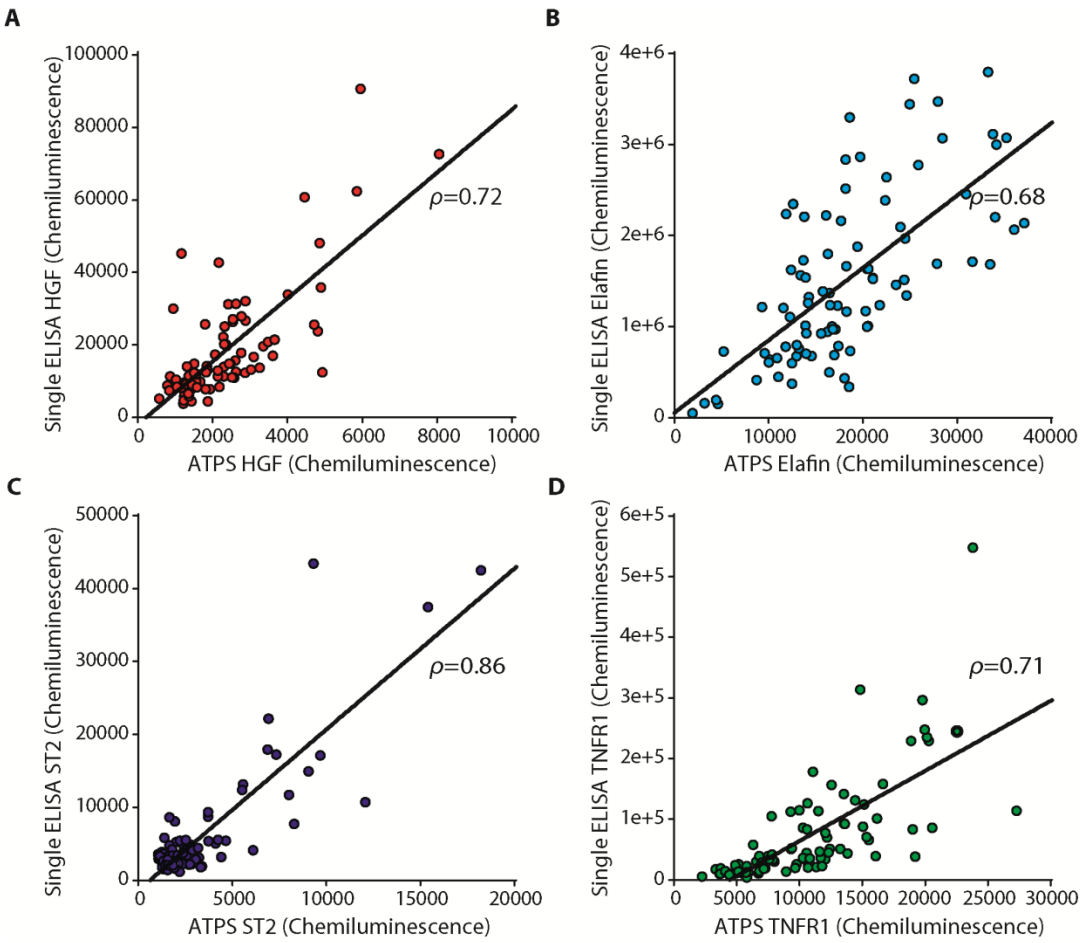

Figure 5.12: Pearson correlation of single ELISA and ATPS-ELISA. A) Scatter plot showing correlation between patient sample measurements for ATPS-ELISA (x-axis) and single sandwich ELISA (y-axis) for HGF. B) Scatter plot showing correlation between patient sample measurements for ATPS-ELISA and single ELISA for elafin. C) Scatter plot showing correlation between patient sample measurements for ATPS-ELISA and single ELISA for ST2. D) Scatter plot showing correlation between patient sample measurements for ATPS-ELISA and single ELISA for TNFR. Pearson's coefficient (ρ) is listed next to each linear regression fit.

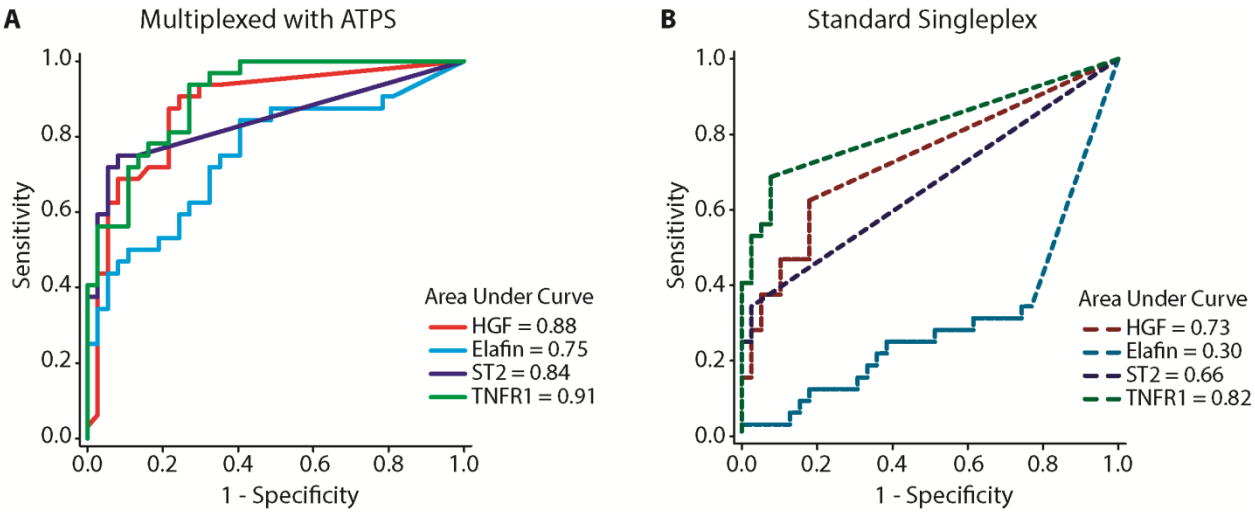

Fig. 5.13. ROC curves for standard single ELISA and ATPS-ELISA. A) ROC curves for multiplexed ATPS-ELISA. The nearly right angle feature, and therefore the high areas under the ROC curves (maximum possible area of 1), show that ATPS-ELISA is highly specific and sensitive. B) ROC curves for standard single ELISA. ROC curves with lower areas under their respective curves show that single ELISAs are less sensitive and specific.

Company and Platform	Type of ELISA (Planar array or bead-based)	Publicized maximum degree of plexing
Luminex xMAP	Bead-based	100
Meso Scale Discovery MULTI-ARRAY and MULTI-SPOT	Planar array	100
Ray Biotech Quantibody	Planar array	40
R&D Systems Proteome Profiler	Planar array	16
Quansys Q-Plex	Planar array	16
BD Biosciences Cytometric Bead Array	Bead-based	30

Table 5.1. Commercially available multiplex platforms. Numerous companies have entered the multiplex ELISA technology space. Planar arrays have capture antibodies fixed to the surface of a 96-well plate, glass slide, or membrane, while bead-based assays have capture antibodies fixed to the surface of micron-sized beads in suspension.

5.5 References

Armbruster, D. A. and T. Pry. Limit of blank, limit of detection and limit of quantitation. *Clin. Biochem. Rev.* **29 Suppl 1**, S49-S52 (2008).

Boja, E.S. and H. Rodriguez. Regulatory considerations for clinical mass spectrometry: multiple reaction monitoring. *Clin. Lab. Med.* **31**, 443-453 (2011a).

Boja, E.S., S.A. Jortani, J. Ritchie, A.N. Hoofnagle, Ž. Težak, E. Mansfield, P. Keller, R.C. Rivers, A. Rahbar, N.L. Anderson, P. Srinivas, and H. Rodriguez. The journey to regulation of protein-based multiplex quantitative assays. *Clin. Chem.* **57**, 560 (2011b).

Crowther, J.W. The ELISA Guidebook. Humana Press (2001).

Ekins, R.P. Multi-analyte immunoassay. *J. Pharm. Biomed. Anal.* **7**, 155-168 (1989).

Ellington, A.A., I.J. Kullo, K.R. Bailey, and G.G. Klee, Measurement and quality control issues in multiplex protein assays: a case study. *Clin. Chem.* **55**, 1092-1099 (2009).

Engvall, E. and P. Perlman. Enzyme-linked immunosorbant assay of immunoglobulin G. *Immunochemistry* **8**, 871-874 (1971).

Frampton, J.P., J.B. White, A.B. Simon, M. Tsuei, S. Paczesny, and S. Takayama. Aqueous two-phase system patterning of detection antibody solutions for cross-reactivity-free multiplexed ELISA. *Sci. Transl. Med.* **Submitted.**

Halbert, S.P., B. Poiesz, A.E. Friedman-Kien, R. Montagna, W.A. Blattner, and M. Anken. Quantitative estimation by a standardized enzyme-linked immunosorbent assay of human T-cell lymphotropic virus type I antibodies in adult T-cell leukemia and acquired immune deficiency syndrome. *J. Clin. Microbiol.* **23**, 212-216 (1986).

Hartmann, M., J. Roeraade, D. Stoll, M.F. Templin, and T.O. Joos. Protein microarrays for diagnostic assays. *Anal. Bioanal. Chem.* **393**, 1407-1416 (2009).

HTStec. ELISA Trends 2010. (2010).

Kaiser, J. Biomarker tests need closer scrutiny, IOM concludes. *Science* **335**, 1554 (2012).

Kim, J.H., S.J. Skats, T. Uede, K.K. Wong, J.O. Schorge, C.M. Fltmate, R.S. Berkowitz, D.W. Cramer, and S.C. Mok. Osteopontin as a potential diagnostic biomarker for ovarian cancer. *JAMA* **287**, 1671-1679 (2002).

Levine, J.E., B.R. Logan, J. Wu, A.M. Alousi, J. Bolanos-Meade, J.L. Ferrara, V.T. Ho, D.J. Weisdorf, and S. Paczesny. Acute graft-versus-host disease biomarkers measured during therapy can predict treatment outcomes: a Blood and Marrow Transplant Clinical Trials Network study. *Blood* **119**, 3854-3860 (2012).

MacBeath, G. Protein microarrays and proteomics. *Nat. Genet.* **32 Suppl**, 526-532 (2002).

Master, S.R., C. Bierl, and L.J. Kricka. Diagnostic challenges for multiplexed protein microarrays. *Drug Discov. Today* **11**, 1007-1011 (2006).

Moody, M.D., S.W. Van Arsdell, K.P. Murphy, S.F. Orencole, and C. Burns. Array-based ELISAs for high-throughput analysis of human cytokines. *BioTechniques* **31**, 186-190 (2001).

Paczesny, S., O.I. Krijanovski, T.M. Braun, S.W. Choi, S.G. Clouthier, R. Kuick, D.E. Misek, K.R. Cooke, C.L. Kitko, A. Weyand, D. Bickley, D. Jones, J. Whitefield, P Reddy, J.E. Levine, S.M Hanash, and J.L. Ferrara. A biomarker panel for acute graft-versus-host disease. *Blood* **113**, 273-278 (2009a).

Paczesny, S., S.W. Choi, and J.L. Ferrara. Acute graft-versus-host disease: new treatment strategies. *Curr. Opin. Hematol.* **16**, 427-436 (2009b).

Paczesny, S., T.M. Braun, J.E. Levine, J. Hogan, J. Crawford, B. Coffing, S. Olsen, S.W. Choi, H. Wang, V. Faca, S. Pitteri, Q. Zhang, A. Chin, C. Kitko, S. Mineishi, G. Yanik, E. Peres, D. Hanauer, Y. Wang, P. Reddy, S. Hanash, and J.L. Ferrara. Elafin is a biomarker of graft-versus-host disease of the skin. *Sci. Transl. Med.* **2**, 13ra2 (2010).

Paul, B., R. Dhir, D. Landsittel, M.R. Hitchens, and R.H. Getzenberg. Detection of prostate cancer with a blood-based assay for early prostate cancer antigen. *Cancer Res.* **65**, 4097-4100 (2005).

Voller, A., G. Huldt, C. Thors, and E. Engvall, New serological test for malaria antibodies. *Br. Med. J.* **1**, 659-661 (1975).

Wiese, R., Y. Belosludtsev, T. Powdrill, P. Thompson, and M. Hogan. Simultaneous multianalyte ELISA performed on a microarray platform. *Clin. Chem.* **47**, 1451-1457 (2001).

Chapter 6

Conclusions and Future Directions

The drug development process has become increasingly inefficient as biotech and pharmaceutical companies have invested billions of dollars in their drug development pipelines, only to see an overwhelming majority of drug compounds fail in clinical trials. There are many contributing factors to this trend that include biological and physiological complexities of the diseases being targeted, strategic business portfolio management to pursue high risk and potential high reward projects, and difficult regulatory requirements that make it challenging to successfully navigate clinical trials, to name a few.

New technological advances should enable these companies to become more successful; for example, increased knowledge of the human genome and microbiome, better biostatistical analysis and epidemiological understanding of diseases, and the implementation of next-generation technologies that increase the amount and quality of data generated and better model *in vivo* pathophysiology will improve all aspects of drug development from initial compound screening to clinical trials. Unfortunately, to date many of these so-called enabling technologies have yet to cause paradigm shifts and/or drastic changes in the way biotech and pharmaceutical companies conduct drug development. The disconnect in excitement surrounding these technologies and their actual impact can be attributed to difficulties in adoptability, reproducibility, manufacturability, and scalability, to name a few. For example, cutting edge research is often performed in academic settings or labs heavily geared toward basic science.

While many of these labs do make significant contributions to the understanding of diseases and technological capabilities, there has been a lack of translation into commercially viable entities. Until this gap is closed, potentially fruitful technologies will continue to flounder.

ATPS assays may be able to overcome the limitations associated with many of these previously-developed technologies. For example, ATPSs are highly biocompatible and can be implemented with tissue, cells (including plant, bacterial, and mammalian), proteins, and nucleic acids, thereby enabling the development of assays to test the biological material of interest. Furthermore, these systems are very easy to adopt as they only require the formulation of solutions and dispensing with pipettors or liquid handlers. Finally, due to the patternability of ATPSs, it is easy to achieve high-throughput arrays for various types of tests.

Included in this dissertation are four concrete examples of ways in which ATPSs were used in the early development of next-generation *in vitro* assays. First, localized and multiplexed immunocytochemistry was used to show that antibodies partition to DEX in a PEG/DEX ATPS and that this approach can be used to stain for multiple biomarkers in parallel from a single cell monolayer; furthermore, this technique enables faster antibody binding and higher signal intensity (likely due to greater antibody binding) than traditional staining formats. An ATPS of 5% polyethylene glycol (PEG) and 12.8% dextran (DEX) was then determined to be the optimal system with which to perform cell monoculture patterning for high-throughput screening analysis of cell migration and to perform co-culture patterning to achieve more physiologically relevant cell behavior that can be used as a toxicological and/or functional screening assay. An ATPS was further used to create an assay that localizes trypsin to achieve reproducible and high-throughput *in vitro* wounding on transwell inserts (which to this point has not been possible). Finally, an ATPS-enzyme-linked immunosorbent assay (ELISA) was developed to pattern

detection antibodies and quantify 4 biomarkers of graft-versus-host-disease without antibody cross-reactivity and with greater sensitivity compared to traditional ELISA. These proofs-of-concept demonstrate ways in which ATPS assays can be implemented at various points in the drug development process to improve the likelihood of generating an FDA-approved compound.

Future work will still be needed to validate and translate these technologies to the point where they can be implemented on a large scale. Multiplexed immunocytochemistry will need to be expanded upon to achieve staining and multiplexed protein detection of histological samples; although the process will be essentially the same in this format, it will be crucial to demonstrate this capability to make it amenable to eventual users. Furthermore, in terms of using the technology for diagnosis and/or biomarker discovery, it will be necessary to develop a scoring system in which researchers and/or clinicians can assign grades to samples based on the amount and/or intensity of staining. To this end, it would also be useful to develop image analysis software or other methodology that could quantify protein expression levels based on staining intensity.

With regards to multiplex cell patterning, it will be important to demonstrate cell patterning in a 96-well plate as opposed to large dishes to show its utility in a format more likely to be used in screening. Furthermore, although we qualitatively demonstrated improved hepatocyte function in a patterned co-culture format, it will be important to extend co-culture patterning to primary cells and with quantitative readouts. These patterned primary cell co-cultures could be very useful in drug screening; for example, by using patterned primary hepatocytes and support cells it could be possible to develop a platform that better predicts off-target hepatic toxicity *in vitro* at early stages. This would enable scientists to make more

informed decisions about whether or not to pursue a potential compound and potentially save billions of dollars in downstream optimization and clinical trials expenses.

The ATPS *in vitro* wound assay will also require further development that is similar to the co-culture patterning technique. We demonstrated the utility of this assay with A549 cells cultured on transwell inserts; however, it will be more instructive to demonstrate this assay with primary cell lines that undergo more pronounced differentiation when maintained at ALI. Furthermore, it would be interesting to combine this assay with compounds that interact with mucins and other biological molecules present with cells cultured at ALI to monitor their effects on wound closure (which could not be done with cells in submersion culture). It would also be interesting to modify the wounding technique so that instead of locally delivering trypsin to achieve a denuded cell area, small particulate and/or biological matter were delivered locally to model inspired particles depositing on small areas of the lung to monitor subsequent cell signaling and repair that occurs *in vivo*. Finally, it would be interesting to expand the application of this technology to other non-traditional cell culture settings such as soft polyacrylamide, which better models tissue stiffness of organs such as the lungs.

Lastly, the ATPS-ELISA technique was significantly validated for its use with patient plasma in a completely hydrated format. Although this approach is easy in the regard that it only requires pipetting and does not require any extra complicated instrumentation, it still requires user skill and knowledge to be able to reproducibly perform the assay. Therefore, to be able to use ATPS-ELISA on a large scale, it will be necessary to modify the assay so as to minimize user handling and potential for error due to pipetting mistakes. In this regard, creating a plate with pre-dehydrated (or lyophilized) and spotted capture and detection antibody pairs could be a viable solution. In this format, the only steps the end user would have to perform would be to

enrich their sample of interest with PEG and add the PEG-enriched solution to wells, thereby making it much easier to adopt into lab settings. Furthermore, we have only validated the technology for a 4-plex panel of biomarkers from patient plasma. The capability of this assay should also be investigated for higher degrees of multiplex detection and with other sample matrices such as urine.

The ATPS assays described here are exciting first steps in their development as next-generation technologies that can increase throughput and provide better physiological relevance compared with other *in vitro* assays. Further technological advancements and biological proofs-of-concept will enable them to be implemented as useful screening tools in the drug development process.